C 51.17/12:988/7

Tech Notes

JULY 1988

PB88-925907

NTIS

U.S. DEPARTMENT OF COMMERCE
National Technical Information Service
Center for the Utilization of Federal Technology

U.S. DEPARTMENT OF COMMERCE
C. William Verity, Secretary of Commerce

National Technical Information Service
Joseph F. Caponio, Director

ISSN 0889-8464

COPYRIGHT WARNING
International Copyright © National Technical Information Service, 1988. All portions of this publication are protected against copying or other reproduction outside of the United States under the provisions of Article II of the Universal Copyright Convention. United States copyright is not asserted under the United States Copyright Law, Title 17, United States Code.

The Secretary of Commerce has determined that the publication of this periodical is necessary in the transaction of the public business required by law of this department. Use of funds for printing this periodical has been approved by the Director of the Office of Management and Budget through 1988.

Tech Notes

Highlighting Selected U.S. Government Technology & Resources

JULY 1988

Contents

Agriculture & Food 544
Computers 547
Electrotechnology 553
Energy 563
Engineering 567
Environmental Science & Technology 583
Manufacturing, Machinery & Tools 585
Materials 595
Medicine & Biology 611
Natural Resources Technology & Engineering 615
Physical Sciences 617
Transportation & Components 628

Published monthly by the National Technical Information Service (NTIS), Tech Notes bring together individual one to two page fact sheets prepared by Federal agencies, their laboratories, or contractors. These fact sheets highlight current Federal technology determined to have commercial or practical application. Topics cover new processes, materials, techniques, software, instrumentation, and resources.

Some of the current sources are the Department of the Navy, Department of the Army, NASA, Department of Energy, Environmental Protection Agency, Department of the Interior, and the Department of Agriculture.

Special assistance is provided by the Federal Laboratory Consortium.

Change of address or questions concerning subscriptions should be sent to:
Subscriptions Department
National Technical Information Service
Springfield, VA 22161
(703) 487-4630

Suggestions, comments, or questions concerning Tech Notes should be directed to:
Tech Notes Editor
Room 300B F
National Technical Information Service
Springfield, VA 22161
(703) 487-4805

U.S. Depository Copy

How to Use Tech Notes

Every Tech Notes fact sheet lists a source for additional information. The source of this information may be a special support package from the originating agency, a personal contact, a licensing opportunity, or a backup report available from NTIS.

Each fact sheet also is perforated to allow for easy removal for those subscribers who may wish to keep a special fact sheet file or route to others in their organization

Sources of Further Backup Information

Below are two representative examples of how each Tech Note fact sheet provides you with a source of further information. In most cases, this information is provided directly by the agency or its laboratory.

However, there are cases where NTIS is the source for backup documentation. In these cases, use the order form at the end.

Examples:

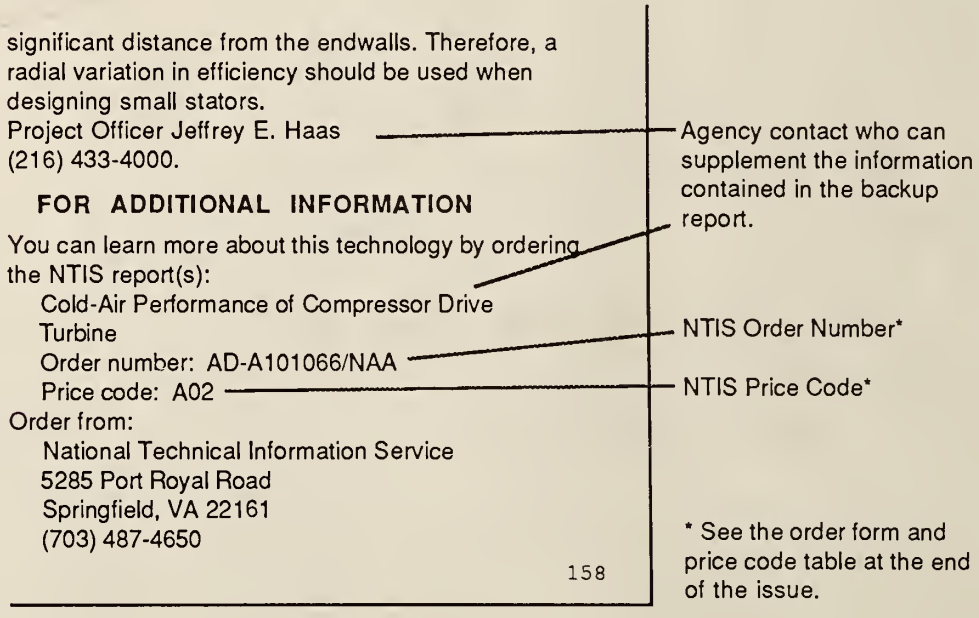
significant distance from the endwalls. Therefore, a radial variation in efficiency should be used when designing small stators.
Project Officer Jeffrey E. Haas
(216) 433-4000.
FOR ADDITIONAL INFORMATION
You can learn more about this technology by ordering the NTIS report(s):
Cold-Air Performance of Compressor Drive Turbine
Order number: AD-A101066/NAA
Price code: A02
Order from:
National Technical Information Service
5285 Port Royal Road
Springfield, VA 22161
(703) 487-4650
158
Agency contact who can supplement the information contained in the backup report.
NTIS Order Number*
NTIS Price Code*
* See the order form and price code table at the end of the issue.

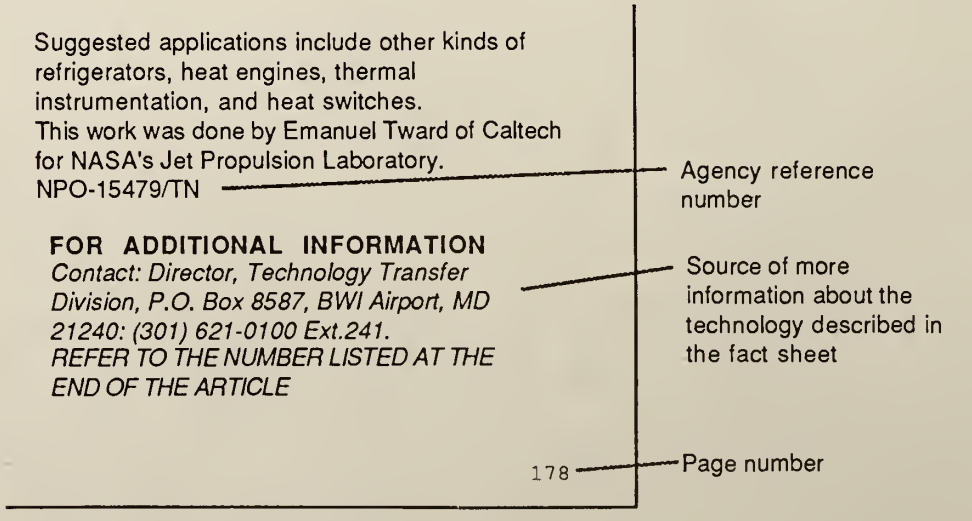
Suggested applications include other kinds of refrigerators, heat engines, thermal instrumentation, and heat switches.
This work was done by Emanuel Tward of Caltech for NASA's Jet Propulsion Laboratory.
NPO-15479/TN
FOR ADDITIONAL INFORMATION
Contact: Director, Technology Transfer Division, P.O. Box 8587, BWI Airport, MD 21240: (301) 621-0100 Ext.241.
REFER TO THE NUMBER LISTED AT THE END OF THE ARTICLE
178
Agency reference number
Source of more information about the technology described in the fact sheet
Page number

Tech Notes Title List for July 1988

Agriculture & Food

544 New Plow Saves Soil, Harnesses Microbe Power

545 Protecting Chickens Against Marek's Disease (Licensing Opportunity)

Testing & Instrumentation

546 Screening for Alcohol-Producing Microbes — A dye reaction rapidly identifies alcohol-producing microbial colonies.

Computers

547 Data-Acquisition System for Rotor Vibrations — A new system trades hardware for software to reduce cost.

548 Digital-Difference Processing for Collision Avoidance — The difference in frequency between two signals is tracked digitally. (Licensing Opportunity)

549 Handling Flight-Research Data in Real Time — Researchers at widely separated locations will be able to participate in tests and analyze data immediately. (Licensing Opportunity)

550 Real-Time Processor for Synthetic-Aperture Radar — Images are formed aboard the airplane. (Licensing Opportunity)

551 Research in Optical Processing of Data — Potential advantages include high speed and low cost. (Licensing Opportunity)

552 Signal Generator Compensates for Phase Shift in Cable — A stabilized reference signal is delivered to a remote unit.

Electrotechnology

553 Navy's VHSIC Program Proceeds on Course

554 Surface-Mount Technology at Fermilab

555 Coding Strategy for Critical Data — Repetition preserves the most critical data during severe attenuation.

556 Arc-Jet Power Sup[ply and Starting Circuit — Power efficiency is high, current is regulated, and starting is automatic. (Licensing Opportunity)

557 Diffractively Coupled, Refractively Guided Lasers — Semiconductor-laser arrays would be more reliable, more powerful, and easier to make. (Licensing Opportunity)

558 Improved Tracking of Square-Wave Subcarrier — The variance of the phase error is reduced.

559 Optical Rotary Joint for Data Transfer — A proposed joint would increase bandwidth and reduce errors.

560 Temperature-Controlling Circuit — Operational amplifiers control large current to a resistance heater. (Licensing Opportunity)

561 Wide-Band, Wide-Scan Antenna for Circular Polarization — Circular polarization is generated by linearly polarized elements.

Testing & Instrumentation

562 Difference-Equation/Flow-Graph Circuit Analysis — Solutions are reached quickly on small computers.

Other Items of Interest

597 Ultralow-Loss Infrared Optical Fibers Developed

Energy

563 Horizontal Ground-Coil Heat Exchangers

564 Energy and Economic Efficiency Alternatives for Electric Lighting in Commercial Buildings

565 Systems Analysis of Advanced Coal-Based Power Plants — Fuel-cell technologies are evaluated and compared with advanced non-fuel-cell alternatives.

566 Testing Parabolic-Dish Concentrators — Experience at a solar-energy test site is described.

Engineering

567 Motor Current Signature Analysis Process

568 Acoustical Measurement of Mine-Shaft Length — The length is calculated from the measured resonant frequency. (Licensing Opportunity)

569 Adaptive-Wall Wind Tunnel — Side vents are controlled automatically to compensate for interference by walls. (Licensing Opportunity)

570 Analysis of Flow Across Cylinders — Despite its importance in engineering, the flow/cylinder interaction is understood poorly.

571 Minimum-Time Control Robotic Manipulators — Current Theories are examined critically.

572 Heat Exchanger for Rotating Modular Structures — Heat is transferred efficiently across plates without interstitial fillers. (Licensing Opportunity)

573 Television-and-Laser Range-Measuring System — Triangulation enables the measurement of distances from 1 to 200 ft (0.3 to 60 m). (Licensing Opportunity)

574 Simplified Analysis of Shock Waves — Semiempirical expressions and conventional analyses agree within about 3 percent.

Software

575 Calculating Flows in Multiple-Blade-Element Cascades — Blade shapes and spacings can be varied.

576 Computer Analysis of High-Speed Roller Bearings — Performance of highly stressed bearings are predicted.

577 Computer Program Predicts Turbine-Stage Performance — Complicated three-dimensional and dissipative effects are taken into account.

578 Strain-Energy-Release Rates in Delamination — Failures of composite laminates are analyzed under a variety of loads.

579 Software for Tomographic Reconstruction from Neutron Radiographs

Engineering (cont.)

580 REAL-OPS: Real-Time Expert System Control

Testing & Instrumentation

581 Calibrating Nonremovable Pressure Transducers — Units are calibrated en masse in a large pressure chamber. (Licensing Opportunity)

582 Laminar-Boundary-Layer Crossflow Sensor — Crossflow vorticity is detected with nonintrusive electronic sensor elements. (Licensing Opportunity)

Other Items of Interest

607 Super Grip

629 New Acoustic Treatment for Aircraft Sidewalls — Cabin noise is reduced with minimal addition of weight.

631 Unducted-Fan Engine — Counterrotating propellers are directly connected to turbines. (Licensing Opportunity)

632 Aerodynamic-Analysis Programs fr Microcomputers — Lifts, drags, and moments can be calculated for subsonic and supersonic speeds.

Environmental Science & Technology

583 Vibrating Mesh Screen Conveyor Solves Solid Waste Disposal Needs

584 Manual for Preventing Spills of Hazardous Substances at Fixed Facilities

Manufacturing, Machinery, & Tools

585 High Disposition Welding Process

586 Transpiration Cooled Combustor Liner

587 Flexible Protective Shield for Newly Welded Joints — A simple device promotes defect-free welds in oxidation-prone metals. (Licensing Opportunity)

588 Computer-Graphical Simulation of Robotic Welding — Limitations on equipment can be investigated in advance to prevent expensive mistakes.

589 Micromachining of Silicon — Diffusion and preferential etching make new structures possible.

590 Portable Horizontal-Drilling and Positioning Device — This portable device drills horizontal holes in irregularly shaped objects.

591 Rotation Control in a Cylindrical Acoustic Levitator — A second driver introduces net circulation around the levitated sample. (Licensing Opportunity)

Testing & Instrumentation

592 Checking Fits with Digital Image Processing — Computer-aided video inspection of mechanical and electrical connectors if feasible. (Licensing Opportunity)

593 Optical-Fiber Temperature Sensor — Temperature could me measured in rotating machinery without speed-limiting mechanical sliprings. (Licensing Opportunity)

594 Real-Time X-Ray Inspection — An x-ray imaging instrument is adapted to continuous scanning. (Licensing Opportunity)

Other Items of Interest

567 Motor Current Signature Analysis Process

571 Minimum-Time Control Robotic Manipulators — Current Theories are examined critically.

579 Software for Tomographic Reconstruction from Neutron Radiographs

Materials

595 Bainite Hardenability of ASTM A723 Steel

596 Properties of Pulse-Electrodeposited Alloys

597 Ultralow-Loss Infrared Optical Fibers Developed

598 Contamination Barrier for Contour-Molding Material — A release agent prevents the molding compound from adhering to or contaminating the surface.

599 Carboranylmethylene-Substituted Cyclophosphazene Polymers — A new synthesis produces unusual electrical and chemical properties. (Licensing Opportunity)

600 Calculating Percent Gel for Process Control — The reaction state of a thermosetting resin is tracked to assure desired properties. (Licensing Opportunity)

601 Evaluating Solid-Lubricant Films — The pin-on-disk tribometer provides valuable information when used properly.

602 Investigation of Epoxy Curing — A kinetic model describes major features of the curing process. (Licensing Opportunity)

603 Microstructure of MnBi/Bi Eutectic Alloy — The effect of convection is examined.

604 Molding Compound for Inspection of Internal Contours — This material is clean, sets rapidly, and is easy to use.

605 Nonisothermal Crystallization in PEEK/Fiber Composite — Several features of the crystallization process are attributable to the fibers.

606 Stress-and-Strain Analysis of Hot Metal/Fiber Composites — Macroscopic mechanical properties are derived from micromechanics.

Testing & Instrumentation

607 Super Grip

608 Automatically Inspecting Thin Ceramics for Pinholes — Flaws would be located and marked.

609 Checking Nickel Plate for Porosity — A porosity test goes for a free ride with a cryogenic adhesion test.

610 Fast Measurements of Thermal Diffusivities of Ceramics — The temperature rises of samples are compared with that of a reference sample. (Licensing Opportunity)

Other Items of Interest

586 Transpiration Cooled Combustor Liner

Medicine & Biology

611 Protein in Diet Affects Excretion of Drugs

612 Heavy-Duty Rescue Straps for Coveralls — Straps enable rescuers to move injured people.

Software

613 Modeling Human Behavior During a Fire

Testing & Instrumentation

614 Blood Test Predicts Clinical Recurrence to Ovarian Cancer — The test uses CA125 radiometric assay.

Other Items of Interest

546 Screening for Alcohol-Producing Microbes — A dye reaction rapidly identifies alcohol-producing microbial colonies.

Natural Resources Technology & Engineering

615 Computer Architecture for Research in Meteorology and Atmospheric Chemistry

Testing & Instrumentation

616 Ultraviolet Lidar Would Measure Wind Velocity — Incoherent Doppler-shifted scattering from aerosols will reveal important weather data.

Other Items of Interest

568 Acoustical Measurement of Mine-Shaft Length — The length is calculated from the measured resonant frequency. (Licensing Opportunity)

Physical Sciences

617 Electrochemical Growth of Crystals in Gels — Nucleation and growth rates are readily controlled. (Licensing Opportunity)

618 Equations for Fading-Memory Filters — Simplified solutions are based partly on the exponential decay of effects of previous states.

619 Mechanical Properties of Large Sodium Iodide Crystals — For the first time, data on large thallium-doped samples are available.

620 Slow Release of Reagent Chemicals from Gel Matrices — A simple technique enables the slow diffusion of chemicals into solutions. (Licensing Opportunity)

Testing & Instrumentation

621 Preconcentrating Air Sampler—PAS-100 — Enhancing analysis with a simple first step.

622 Portable, Surface-Enhanced Raman Spectroscopy System

623 Crystal Laser Monitor

624 Measuring Incorporation of Arsenic in Molecular-Beam Expitaxy — Changes in surface layers cause oscillations in RHEED measurements.

625 Pressure-Sealing Optical Coupling — Light signals are passed out of a high-pressure cryogenic environment.

626 Optical Temperature Sensor for Gas Turbines — The new design promises accuracy even in the presence of contamination. (Licensing Opportunity)

627 Probing Polymer-Segment Motions by ESR — Molecular origins of mechanical properties and aging processes can be studied.

Other Items of Interest

599 Carboranylmethylene-Substituted Cyclophosphazene Polymers — A new synthesis produces unusual electrical and chemical properties. (Licensing Opportunity)

Transportation & Components

628 Landing-Time-Controlled Management of Air Traffic — A conceptual system would control aircraft with old and new guidance equipment. (Licensing Opportunity)

629 New Acoustic Treatment for Aircraft Sidewalls — Cabin noise is reduced with minimal addition of weight.

630 Study of Helicopter-Tail-Rotor Noise — Impulsive noise and blade loads in blade/vortex interactions are discussed.

631 Unducted-Fan Engine — Counterrotating propellers are directly connected to turbines. (Licensing Opportunity)

Software

632 Aerodynamic-Analysis Programs fr Microcomputers — Lifts, drags, and moments can be calculated for subsonic and supersonic speeds.

Agriculture & Food

544 New Plow Saves Soil, Harnesses Microbe Power

545 Protecting Chickens Against Marek's Disease (Licensing Opportunity)

Testing & Instrumentation

546 Screening for Alcohol-Producing Microbes — A dye reaction rapidly identifies alcohol-producing microbial colonies.

United States Department of Agriculture

Research Technology
Agricultural Research Service

New Plow Saves Soil, Harnesses Microbe Power

An underground plow originally designed to pulverize hard, thin planes of soil in dryland wheat-growing regions may become a boon to conservation tillage farmers, says an Agricultural Research Service scientist.

The new tillage tool, invented by soil scientist Lloyd N. Mielke and colleagues at the University of Nebraska, should benefit producers of rain-fed row crops such as corn and soybeans by saving soil and water and exploiting microbial activity. Mielke is patenting a sweep plow he modified by attaching four steel shanks underneath to break up the soil.

Since the great drought of the 1930's, the sweep plow has been a mainstay of Great Plains wheat growers for subsurface tillage of fallow or bare fields. A sweep is a flat V-shaped blade with a "wingspan" up to 5-1/2 feet. In operation, the blade is pulled horizontally through the soil, point first, about 3 to 4 inches below the surface.

The sweep plow undercuts emerging weeds and loosens the soil layer above the blade. It does this without greatly disturbing a surface layer of crop residue maintained to slow evaporation of scarce rainfall. On the negative side, the blade's bottom edge "shears off the soil," Mielke says. "The sheared soil plane looks as though someone smeared it with a giant putty knife, closing up root and worm holes and similar cracks and openings."

Eventually the shear plane may become a virtually impenetrable barrier. It curbs infiltration of water, deprives beneficial microbes of oxygen, forces roots to grow sideways, and may cut crop yields.

To remedy these problems, Mielke attached 6-inch-long steel shanks to the underside of the sweep blade. After many trials involving positioning and bending of the shanks, he came up with a workable system.

In Mielke's design, two shanks are attached under each side of the V-blade. The shanks incline toward the center so that as they travel forward their geometry of bends and twists thoroughly breaks up the soil to a depth of 8 to 10 inches, leaving it porous, well aerated, and mellow.

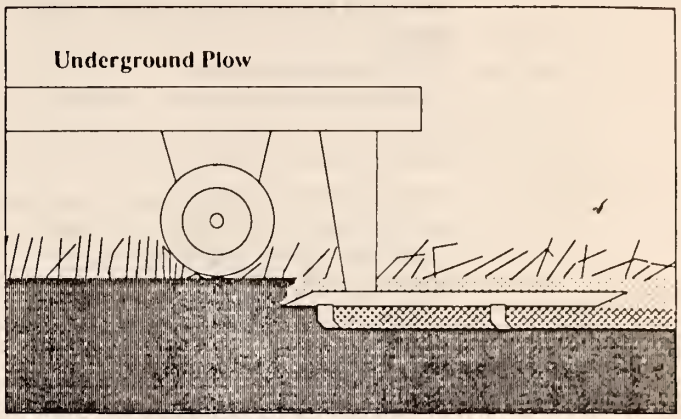

Modified from existing sweep plows, the underground plow loosens soil and increases water-holding capacity, yet leaves crop residues on the surface to cut erosion. (Not to scale.)

"Basically, the modified sweep plow does what a moldboard plow does, except it keeps crop residue where it belongs, on the surface," Mielke says.

That noninversion feature could make Mielke's plow useful for corn and soybean production in regions of heavier rainfall. Farmers practicing conservation tillage (also called minimum tillage) sometimes need to plow to break up soil compacted by machinery traffic, for example, or to disrupt the buildup of weeds, insects, or diseases. However, moldboard plows bury crop residue, increasing soil erosion potential.

Using a modified sweep plow for those purposes would save crop residue to fight erosion. The residue blanket plays three key roles in managing water: It prevents crusts that limit infiltration, it slows evaporation, and it enables soil to take in more water and thus reduces erosion by surface runoff.

It's easier for water to seep into soil made porous by modified sweep tillage than to infiltrate denser conservation-tilled soil, Mielke notes. And sweep-tilled soil stores more water for crop growth. The water is trapped in subterranean reservoirs, a series of troughlike corrugations that the shanks create just below the tilled zone.

In typical field use, three sweep plows are aligned and pulled abreast. Modified sweeps require more than twice as much tractor drawbar power as sweep blades alone. It is possible to scale down the modified sweeps for small farms by using a single sweep, even one that is under 5 feet, if desired.

Mielke developed the sweep plow with assistance from soil scientist Alice Jones and agricultural engineer Leonard Bashford. Both are with the University of Nebraska, Lincoln.

Some refinements to the system need to be made. Mielke says, "Soil can't be too wet; if it is, it won't fracture."

Mielke envisions a tillage system that always keeps crop residue and organic matter on and near the surface, soil conditions that the first settlers encountered when they began farming the prairies.

"Those soils had excellent structure and aeration, and they teemed with microbial life," he says. "We should try to manage our soil systems to help them approach a more natural state."

Porous soil helps foster microbial activity that unlocks extra nutrients for crops. Soil pores must hold a proper balance of water and air if microbes are to make nutrients available for plant nourishment. Earlier research at Lincoln by ARS soil scientist John W. Doran showed that when about 60 percent of the soil pore spaces are filled with water, conditions favor the aerobic, or oxygen-loving, microbes that decompose organic matter and release nitrogen, which becomes available to the crop.

By contrast, when pore space filled with water exceeds 80 percent, anaerobic microbes thrive. They waste plant-available nitrogen, whether from organic matter or commercial fertilizer, converting it into gases that escape into the atmosphere. Tests indicate that soil porosity in the lower part of the sweep-tilled zone creates a water and oxygen status that is ideal for aerobic microbial life, Mielke says.

Lloyd N. Mielke is in USDA-ARS Soil and Water Conservation Research, East Campus, University of Nebraska, Lincoln, NE 68583. Phone (402) 472-1516. ♦

United States Department of Agriculture

Research Technology Licensing Opportunities

Agricultural Research Service

Protecting Chickens Against Marek's Disease

Vaccines have been used since 1970 to protect from Marek's disease the 4 billion chickens raised in the United States annually. Nevertheless, the poultry industry continues to experience losses from this virally transmitted disease, which is characterized by the development of tumorous lesions in infected birds. One reason for these losses is the recent appearance of more virulent strains of the virus.

A new vaccine has been developed which offers better protection against the virulent strains. It uses a specially selected nonpathogenic strain, classified as serotype 2, to combat the disease caused by its pathogenic, and deadly, cousins.

The new vaccine can be replicated rapidly. This makes for stronger protection in the chicken and a vaccine that is easier to produce in vitro. The vaccine is designed to be combined with a turkey herpes virus vaccine.

For technical information, contact Richard L. Witter, USDA-ARS Regional Poultry Research Laboratory, 3606 East Mount Hope Road, East Lansing, MI 48823. Phone (517) 337-6828. *Patent Application Serial No. 07/071,949, "Serotype 2 Marek's Disease Vaccine."*

For inquiries concerning rights for the commercial use of this invention should be addressed to

Office of Federal Patent Licensing
Center for the Utilization of Federal Technology
Room 13R, NTIS
Springfield, VA 22161; (703) 487-4738

Refer to Patent Application 7-071,949/TN

NASA Tech Brief
National Aeronautics and Space Administration
NASA's Jet Propulsion Laboratory, Pasadena, California

Screening for Alcohol-Producing Microbes

A dye reaction rapidly identifies alcohol-producing microbial colonies.

A method visually detects alcohol-producing micro-organisms, such as yeast and bacteria, and distinguishes them from other microbial colonies that do not produce alcohol. Hundreds of colonies on agar plates can be screened at a time by this nonlethal, alcohol-specific method.

The technique, still being perfected, uses a visual dye linked to the reaction of alcohol dehydrogenase to indicate the presence of alcohol. A change in the color of the dye surrounding a microbial colony readily distinguishes it from other colonies. The method, which should be of interest to the brewing industry, should also be useful for screening mixed microbial populations in environmental samples.

This work was done by Wayne W. Schubert of Caltech for **NASA's Jet Propulsion Laboratory**.

NPO-15842 /TN

FOR ADDITIONAL INFORMATION: *Contact: Director, Technology Transfer Division, P.O. Box 8757, BWI Airport, MD. 21240; (301) 621-0100 Ext. 241*

REFER TO THE NUMBER LISTED AT THE END OF THE ARTICLE

Computers

547 Data-Acquisition System for Rotor Vibrations — A new system trades hardware for software to reduce cost.

548 Digital-Difference Processing for Collision Avoidance — The difference in frequency between two signals is tracked digitally. (Licensing Opportunity)

549 Handling Flight-Research Data in Real Time — Researchers at widely separated locations will be able to participate in tests and analyze data immediately. (Licensing Opportunity)

550 Real-Time Processor for Synthetic-Aperture Radar — Images are formed aboard the airplane. (Licensing Opportunity)

551 Research in Optical Processing of Data — Potential advantages include high speed and low cost. (Licensing Opportunity)

552 Signal Generator Compensates for Phase Shift in Cable — A stabilized reference signal is delivered to a remote unit.

NASA Tech Brief
National Aeronautics and Space Administration
Lewis Research Center, Cleveland, Ohio

Data-Acquisition System for Rotor Vibrations

A new system trades hardware for software to reduce cost.

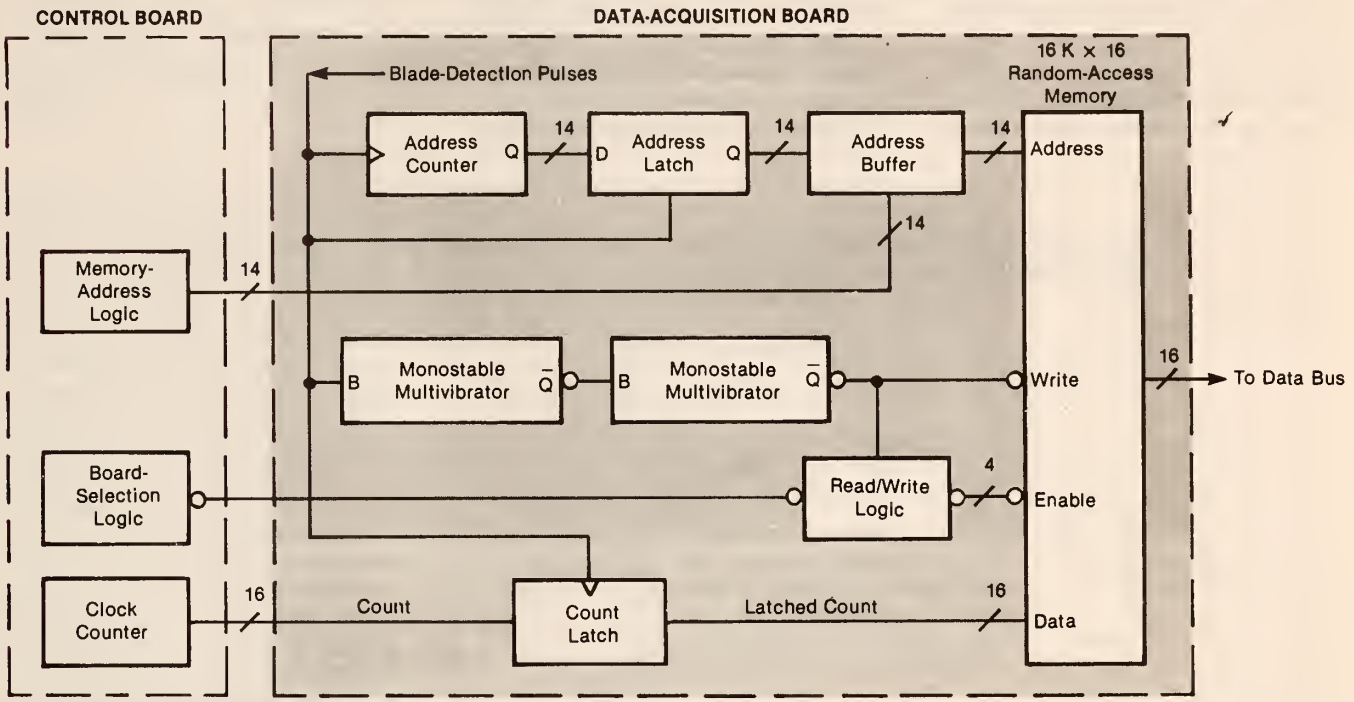

A Composite Train of Interspersed Blade-Detection Pulses is produced by gates at the four probe ports on a data-acquisition board. The pulses latch the count from a high-speed wraparound clock counter and initiate the writing of the count into the current address of memory. As a result, a time corresponding to each blade passage is stamped into memory.

An optical data-acquisition system measures the vibrations of rotor blades. The system records raw data — a set of blade-arrival times — in memory and processes the data after the run. This approach yields a simple and inexpensive system with the least possible hardware.

The system replaces a more complex system in which a set of fixed optical probes sensed blade passages, a microcomputer received and processed data from the probes, and a control computer sorted the data into usable form. The older system was costly and was difficult to maintain and repair. The new system requires fewer circuit boards. Because it is simpler, it is more reliable; and self-testing circuitry can be eliminated as well.

The new system, nevertheless, retains the important performance characteristics. Its maximum allowable deflection, deflection resolution, maximum (unaliased) frequency, and frequency resolution are equal to or better than those of the older system.

There are 16 probes equally spaced about the circumference of the chamber that contains the rotor. Each probe contains three high-resolution optical reflective sensors and associated electronics. The sensors are focused light-emitting diodes (LED's) and matched photodetectors in unitary packages. A visible light beam from each LED is focused at the blade-tip path.

As a blade passes by the probe at high speed, the event is detected, converted to a signal compatible with logic circuitry, and sent to one of four data-acquisition boards. The probes variously measure the start of a revolution and the positions of the leading edge of the blade tip, the tip midchord, and the tip trailing edge at four different locations.

Because four optical probes share a single memory (see figure), the address size of the memory on each board had to be increased from 4K to 16K to obtain the same number of data points per probe as in the original system. However, the total address sizes of the memories for all the probes remain unchanged.

One penalty for the simplicity of the new system is that the size of a memory word

must increase. The 8-bit memory-word size of the original system is not adequate when a high-speed wraparound clock counter is used to measure time. Although counter wraparound can be handled by software, the counter must not wrap around before the next blade arrives if it is to produce meaningful, unscrambled timing records. A 16-bit word size satisfies this racing limitation at clock speeds as high as 20 MHz for the worst case of a two-bladed rotor at 3,000 r/min.

Additional measures were taken to simplify the data-acquisition boards and to reduce the number of components. The interval of time incorporated into the equipment design to correct for missing or extraneous blade signals was eliminated and replaced by an equivalent interval generated by a controlling computer program. This offers the further advantage of easy modification of the interval as needed.

The master clock and wraparound clock counter are located on a separate control board, which also has control circuits for connection to an external computer. During the acquisition, storage, and retrieval phases of a data-collection run, the control circuits enable or disable control lines to the data-acquisition boards, as called upon by software.

This work was done by Stephen J. Posta and Gerald V. Brown of **Lewis Research Center.** *Further information may be found in NASA TM-88907 [N87-14730/NSP], "A Low-Cost Optical Data Acquisition System for Vibration Measurement." [A02]*

Copies may be purchased [prepayment required] from the National Technical Information Service, Springfield, Virginia 22161, Telephone No. (703) 487-4650. Rush orders may be placed for an extra fee by calling (800) 336-4700.
LEW-14557 /TN

FOR ADDITIONAL INFORMATION: *Contact: Director, Technology Transfer Division, P.O. Box 8757, BWI Airport, MD 21240; (301) 621-0100 Ext. 241*
REFER TO THE NUMBER LISTED AT THE END OF THIS ARTICLE

NASA Tech Brief
National Aeronautics and Space Administration
Lyndon B. Johnson Space Center, Houston, Texas

Licensing Opportunity

Digital-Difference Processing for Collision Avoidance

The difference in frequency between two signals is tracked digitally.

A digital system for automotive crash avoidance measures and displays the difference in frequency between two sinusoidal input signals of slightly different frequencies. The system was designed for use with Doppler radars. In a single-transmitter system like a law-enforcement highway speed detector, the two inputs are the transmitted and returned signals, which may differ in frequency by the Doppler shift caused by the target path. In a two-transmitter system, the inputs are the two return signals with two different Doppler shifts.

The system (see Figure 1) can be characterized as a digital mixer coupled to a frequency counter that measures the difference frequency in the mixer output. First, the sinusoidal inputs are amplified, tracking filtered, and converted by phase-lock loop to square waves. When a positive-going edge of the squared version of waveform B occurs while squared A is in the low state, the latch output is set high. When a positive-going edge of squared A occurs while squared B is low, the latch output is then set low (see Figure 2).

Thus, the latch output alternates between the high and low states as frequently as the occurrence of the positive-going edge of squared A alternates between the high and low states of squared B. The frequency of this alternation, averaged over a large number of cycles, is just the difference in frequency between signals A and B. By use of two more basic digital circuits shown in Figure 1, the digital-difference processor can detect if A > B or

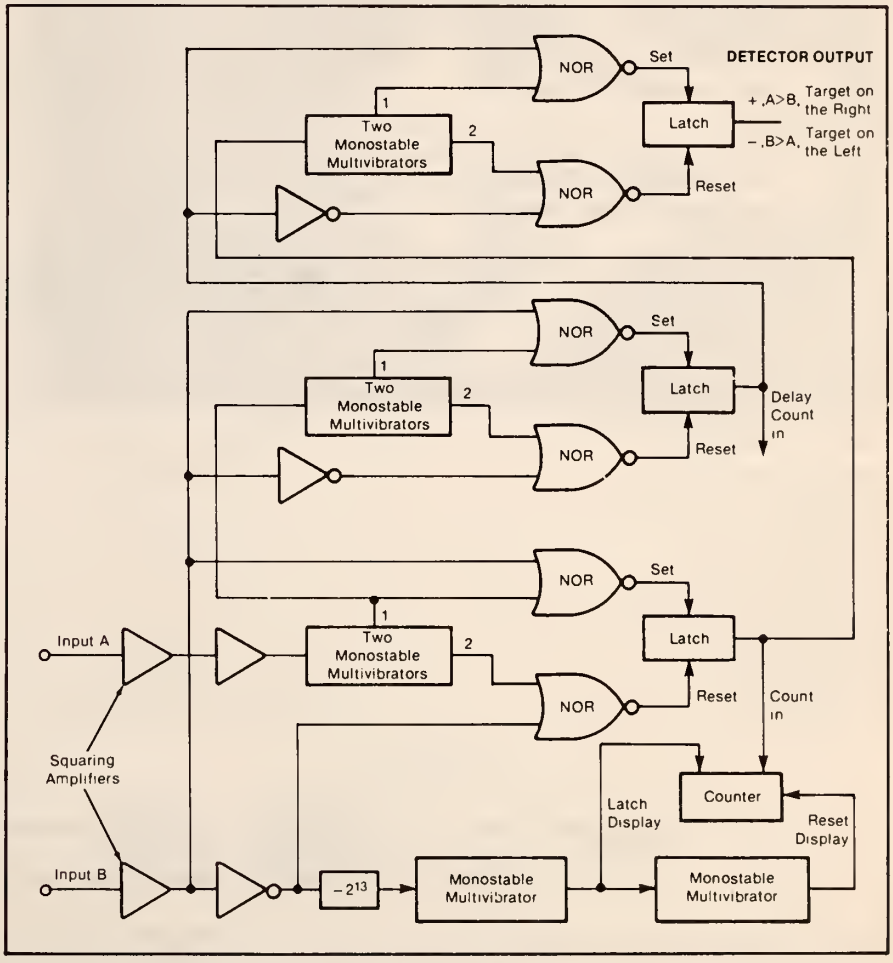

Figure 1. This **Digital Frequency-Difference Counter** measures and displays the difference in frequency between sinusoidal inputs 1 and 2, using signal 2 as a time-and-frequency reference.

A< B. This indicates target path, and a low Doppler difference indicates a target collision path.

The number of cycles in the latch output is counted during 2^{13} cycles of signal B, which serves as the frequency-and-time reference. The count thus equals 2^{13} times the ratio of the difference (or Doppler) frequency to the frequency of signal B. The count is displayed, and the counter is reset every 2^{13} cycles for repeated updating. By measuring digital difference for distance traveled, the same difference readout is obtained for all speeds.

Other uses for the digital-difference processor are for frequency discrimination in frequency demodulation, digital phase detection, frequency-shift-keying demodulation, and the like. The technique determines the target path mathematically, which makes its response faster than that of the tracking antenna. The technique therefore, can be used for tracking cars, missiles, bullets, baseballs, and other fast-moving objects.

This work was done by Paul Shores, Chris Lichtenberg, Herbert S. Kobayashi, and Allen R. Cunningham of **Johnson Space Center**.

This invention is owned by NASA, and a patent application has been filed. Inquiries concerning nonexclusive or exclusive license for its commercial development should be addressed to the Patent Counsel, Johnson Space Center
Refer to MSC-20865 /TN

Lyndon B. Johnson Space Center
Technology Utilization Officer: Dean C. Glenn
Mail Code EA4
Houston, TX 77058
(713) 483-3809
Patent Counsel: Edward K. Fein
Mail Code AL3
Houston, TX 77058
(713) 483-4871

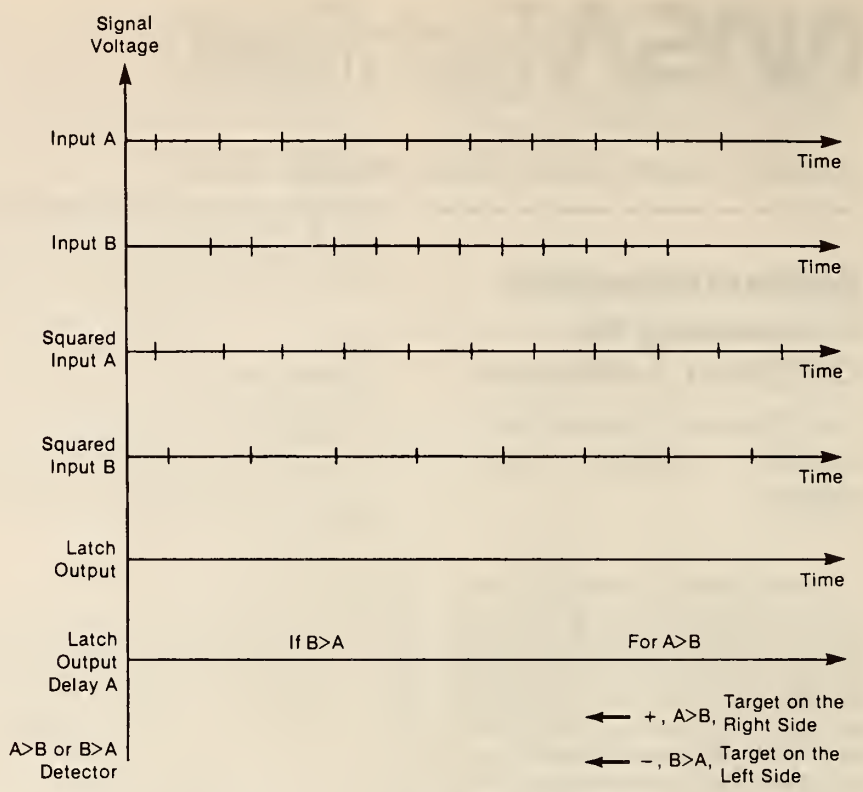

Figure 2. This **Timing Diagram** shows the relationships between the inputs and the key digital waveforms in the counter. The positive (negative) transitions of the latch output occur when the positive transitions of squared B occur during the upper (lower) states of squared

FOR ADDITIONAL INFORMATION: *Contact: Director, Technology Transfer Division, P.O. Box 8757, BWI Airport, MD 21240; (301) 621-0100 Ext. 241*
REFER TO THE NUMBER LISTED AT THE END OF THIS ARTICLE

NASA Tech Brief
National Aeronautics and Space Administration
Ames Research Center, Moffett Field, California

Licensing Opportunity

Handling Flight-Research Data in Real Time

Researchers at widely separated locations will be able to participate in tests and analyze data immediately.

Real-time data-handling facilities play a growing role at the NASA Western Aeronautical Test Range. The facilities perform the vital functions of data acquisition, communication (video, audio, and data), data processing, display, and tracking.

The amount of data acquired and telemetered to ground-based experimental support facilities has increased dramatically in recent years. If the facilities can handle the data in real time, the cost and time of flight research are greatly reduced, and productivity is greatly increased.

Although specific requirements vary widely among programs, certain basic data-handling needs are common:

- To communicate with the vehicle, pilot, and test team;
- To acquire, compute, and display data; and
- To know the exact location of the research vehicle at all times.

The continuing challenge for the designers and operators of ground support facilities is to perform these tasks in real time and to present the integrated results to the research team in real time. The paper presents several approaches to satisfaction of the requirements of representative types of aircraft research programs at the NASA Western Aeronautical Test Range of Ames Research Center.

Probably the most-important data-handling technique employed by the test range is the transmission of data in real time to sites across the North American Continent via satellite (see figure). Such links have been used on all Space Shuttle landings at Edwards Air Force Base in California. In addition, data acquired at Edwards on the Harrier aircraft have been sent by satellite and microwave land link to the Naval Air Test Center in Maryland. Data from flight tests of the X-29A aircraft are sent by a secure satellite link to the Grumman Aerospace Corp. in Calverton, New York, so that the research team there can participate in flight tests as they occur.

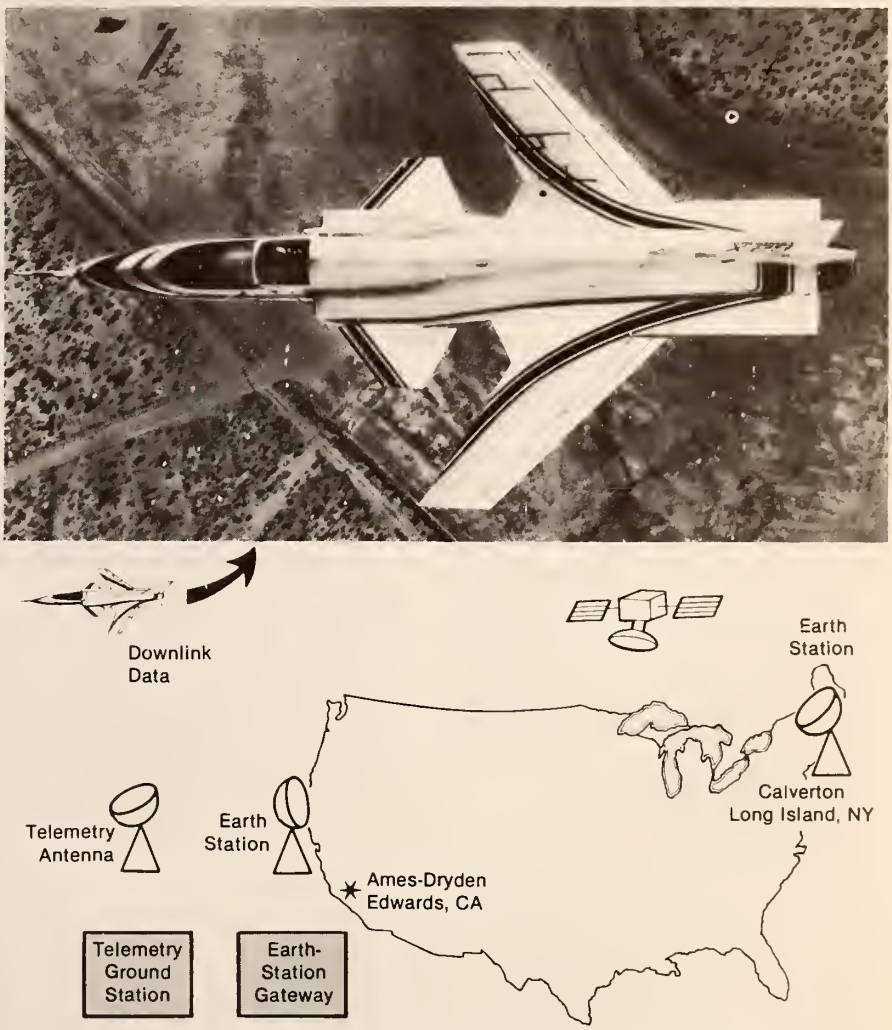

Data are Transmitted from a flight test of the X-29 airplane across the continent via satellite communication links.

This work was done by Archie L. Moore of **Ames Research Center**. *Further information may be found in NASA TM-86805 [N86-19330/NSP], "The Role of a Real-Time Flight Support Facility in Flight Research Programs." [A02]*

Copies may be purchased [prepayment required] from the National Technical In-

formation Service, Springfield, Virginia 22161, Telephone No. (703) 487-4650. Rush orders may be placed for an extra fee by calling (800) 336-4700.

Inquiries concerning rights for the commercial use of this invention should be addressed to the Patent Counsel. Ames Research Center
Refer to ARC-11746. /TN

Ames Research Ctr.
Technology Utilization Officer: Laurance Milov
Mail Code 223-3
Moffett Field, CA 94035
(415) 694-6471
Patent Counsel:
Darrell G Brekke
Mail Code 200-11
Moffett Field, CA 94035
(415) 694-5104

FOR ADDITIONAL INFORMATION: *Contact: Director, Technology Transfer Division, P.O. Box 8757, BWI Airport, MD 21240; (301) 621-0100 Ext. 241*

REFER TO THE NUMBER LISTED AT THE END OF THIS ARTICLE

NASA Tech Brief
National Aeronautics and Space Administration
NASA's Jet Propulsion Laboratory, Pasadena, California

Licensing Opportunity

Real-Time Processor for Synthetic-Aperture Radar

Images are formed aboard the airplane.

A data processor for a synthetic-aperture radar (SAR) operates aboard the airplane with the radar equipment to produce images of the scanned terrain in real time. Previously, SAR data were either recorded on magnetic tape or else transmitted to stations on the ground for subsequent processing into images. By providing an image immediately, the new processor enables the SAR operator to monitor the scanning activity — an advantage especially when targets are obscured by weather. The processed images can be recorded on tape or transmitted to ground stations as before, but the required capacities for the storage and transmission of data are lower because the volume of image data is much smaller than the volume of raw SAR data.

The SAR operates aboard a CV-990 airplane at a frequency of 1.225 GHz and at angles of incidence of 0° to 60°. The radar has one horizontally polarized (H) antenna and one vertically polarized (V) antenna. The radar is capable of simultaneously acquiring data for the HH, VV, HV, and VH polarization states, where the first and the second characters represent the transmitting and the receiving polarization, respectively. The airplane is flown at a nominal altitude of 6 to 12 km with a nominal speed of 200 to 250 m/s. The radar antennas are mounted on the baggage door pointing at 90° from the ground track. The radar chirp bandwidth is 19.8 MHz, and the radar pulse width is 4.9 μs. The peak transmitter power is 4 kW. The radar pulse-repetition frequency is proportional to the aircraft speed and is 750 Hz at 250 m/s.

Radar echo signals are received by the antennas, amplified, and heterodyned to video frequencies. The video signals are sent to an optical recorder and to analog-to-digital converters (ADC's). The ADC outputs are merged in a formatter with the radar header information, which is supplied by the radar-control computer and the inertial-navigation system. The merged digital data are then sent to the processor and to a digital tape recorder. The output of the processor is displayed on a scrolling display device and recorded on videotape.

In the processor (see figure) the input signal is received by the input data conditioner from the SAR data formatter. The received echo data are reduced in rate by the input data conditioner before being processed in both range and azimuth dimensions to generate images. The range correlator performs a frequency-domain fast-Fourier-transform algorithm, including a correction for range curvature. The output of the range correlator is sent to the corner-turn memory. Data from the range-correlator output flow along the range direction. The corner-turn memory rotates the flow of data to the azimuth direction.

The azimuth correlator also performs a fast-Fourier-transform algorithm. However, the azimuth correlation involves only azimuth compression, with correction for range curvature. The data from the azimuth correlator flow along the azimuth direction. The recorner-turn memory rotates the flow direction to the range axis for a line-by-line display along the flight track by the scrolling display device.

This work was done by Kuang Y. Liu of Caltech for **NASA's Jet Propulsion Laboratory**.

This invention is owned by NASA, and a patent application has been filed. Inquiries concerning nonexclusive or exclusive license for its commercial development should be addressed to the Patent Counsel, NASA Resident Office-JPL
Refer to NPO-17188. /TN

Jet Propulsion Lab.
NASA Resident Office
Technology Utilization Officer: Gordon S Chapman
Mail Stop 180-801
4800 Oak Grove Drive
Pasadena, CA 91109
(818) 354-4849

Patent Counsel Paul F McCaul
Mail Code 180-801
4800 Oak Grove Drive
Pasadena, CA 91109
(818) 354 2734
Technology Utilization Mgr for JPL Norman L Chalfin
Mail Stop 156-211
4800 Oak Grove Drive
Pasadena, CA 91109
(818) 354 2240

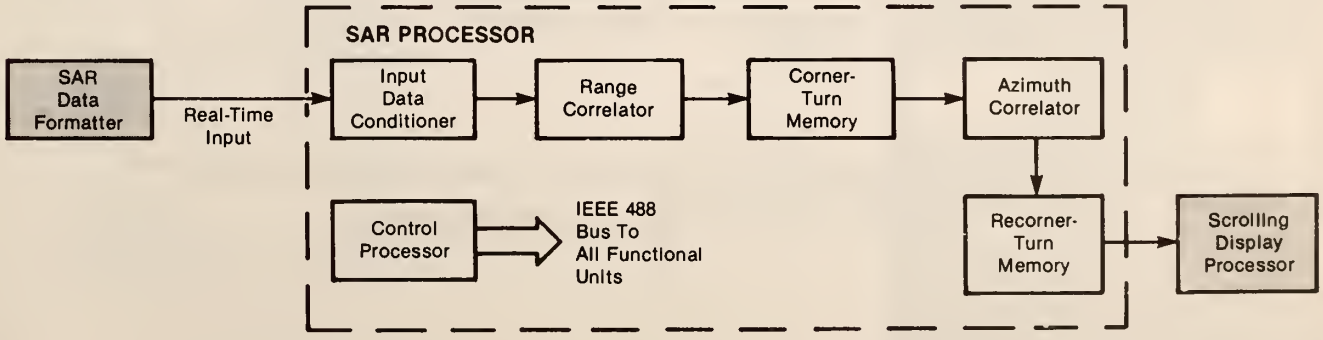

The **SAR Processor** makes images in real time from raw SAR data.

FOR ADDITIONAL INFORMATION: *Contact: Director, Technology Transfer Division, P.O. Box 8757, BWI Airport, MD 21240; (301) 621-0100 Ext. 241*
REFER TO THE NUMBER LISTED AT THE END OF THIS ARTICLE

NASA Tech Brief
National Aeronautics and Space Administration

Licensing Opportunity

Research in Optical Processing of Data

Potential advantages include high speed and low cost.

A report describes current research in the optical processing of data at NASA's Ames Research Center. The research is prompted by plans for automation systems for use on the proposed Space Station; in particular, an optical pattern-recognition system that can be developed into robotic-vision and spectral-analysis systems and an optical processor for control of the wave front of an adaptive-mirror experiment. If successfully developed, these optical processors will offer several advantages over electronic systems with similar capabilities, including an optimum match for optical input; low power consumption; and reduced cost, size, and weight.

The classifier type of pattern-recognition system performs three operations: extraction of features, reduction of dimensionality, and classification. A feature extractor must be able to function in the presence of such distortions as changes in scale, rotation, changes in focus, and blur. A feature extractor might organize a set of descriptors (e.g., color, curvature, elongation, geometric moments, length, width, and area) into a feature vector. The feature vector is useful because it transforms an image into a point in feature space. Typically, such a space has more than 50 dimensions, and it is preferable to reduce the dimensionality to less than 5. Classification can then be performed by comparison of the reduced feature vector with test data for identification of the object.

The report describes an advanced optical feature extractor that would perform the Fourier-Mellin transform to generate a feature vector that is invariant under changes of scale and position and that responds to rotation with a simple translation. The Fourier-Mellin feature vector facilitates the reduction of dimensionality by means of the Fourier transform and variation of the resolution of the detector array in the processor. Classification must still be performed electronically by symbolic and digital processors.

A proposed correlator type of pattern-recognition system would involve (a) synthetic discriminant functions that can be made invariant under distortions of scale, translation, rotation, and class and (b) matched spatial filters that insert the reference images corresponding to the discriminant functions, for correlation with the scene. The matched spatial filters are Fourier-transform images generated by computer and written to a magneto-optic spatial light modulator. The system would have to be "trained" by a human operator, who would develop a library of recognizable patterns.

The mirror/wave-front-control problem has elements in common with efforts to control other high-dimensional dynamic systems. The report discusses candidate digital and analog architectures for the optical execution of state-estimation algorithms that arise in such problems. The system chosen for demonstration includes a segmented, adaptive mirror and a wave-front sensor consisting of a point-diffraction interferometer. The interferogram is sensed by a video camera and processed to yield the state estimate and control signals.

This work was done by David Ennis of **Ames Research Center** *and David Jared of Sterling Software. To obtain a copy of the report, "Optical Processing and Space Station Automation,"*

Inquiries concerning rights for the commercial use of this invention should be addressed to the Patent Counsel, Ames Research Center Refer to ARC-11758 /TN

Ames Research Ctr.
Technology Utilization Officer: Laurance Milov
Mail Code 223-3
Moffett Field, CA 94035
(415) 694-6471
Patent Counsel:
Darrell G Brekke
Mail Code 200-11
Moffett Field, CA 94035
(415) 694-5104

FOR ADDITIONAL INFORMATION: *Contact: Director, Technology Transfer Division, P.O. Box 8757, BWI Airport, MD 21240; (301) 621-0100 Ext. 241*

REFER TO THE NUMBER LISTED AT THE END OF THIS ARTICLE

NASA Tech Brief
National Aeronautics and Space Administration
NASA's Jet Propulsion Laboratory, Pasadena, California

Signal Generator Compensates for Phase Shift in Cable

A stabilized reference signal is delivered to a remote unit.

A signal-generating subsystem delivers a stabilized 5/N-MHz (where N is an integer) pulse and a stabilized 20-MHz tone to a receiver at one end of a cable. Intended for use in a system that generates precise time and frequency signals, the signal-generating subsystem compensates for the phase shift in the cable.

The system is capable of transferring a hydrogen-maser atomic-clock reference over a 1,000-ft (305-m) cable with no significant loss of stability. The transmitter generates the 5/N-MHz signal and an auxiliary 20-MHz signal from a 5-MHz reference oscillator. The 20-MHz signal is passed through a voltage-controlled phase shifter, and the two signals are sent through the cable to the receiver where they are separated by filters and fed to a double balanced mixer. The mixer output — a 20-MHz carrier amplitude-modulated at 5/N-MHz — is sent back through the cable to the transmitter. Because the receiver input impedance at 5/N MHz is higher than the 50-Ω characteristic impedance of the cable, a portion of the 5/N-MHz signal is also reflected back through the cable to the transmitter.

In the transmitter, a hybrid transmission-line junction separates the returning from the outgoing 5/N-MHz signal. The returning 5/N-MHz-modulated 20-MHz signal, which contains the two-way cable delay, is sent back through the phase shifter and mixed with the original 20-MHz signal. The mixer output is passed through a 3-MHz low-pass filter to obtain the low-frequency component of the mixer output, which is a 5/N-MHz signal of amplitude proportional to the cosine of ϕ_1, the sum of the two-way cable phase delay and the two-way voltage-controlled phase delay at 20 MHz. This signal is mixed with the returned 5/N-MHz signal and low-pass filtered to obtain a dc signal proportional to $\cos\phi_1 \cos\delta$, where δ is a small phase error introduced into the returned 5/N-MHz signal by dispersion in the cable and by imperfections in the hybrid junction.

The $\cos\phi_1 \cos\delta$ signal is integrated by a feedback-loop filter to generate the control signal for the voltage-controlled phase shifter. This completes the feedback loop, which continually strives to make $\cos\phi_1 = 0$, regardless of the 5/N-MHz phase error. In this way, the system acts to maintain the total 20-MHz delay through the voltage-controlled phase shifter and the cable constant at $\pi/2 + 2n\pi$ radians (where n is an integer).

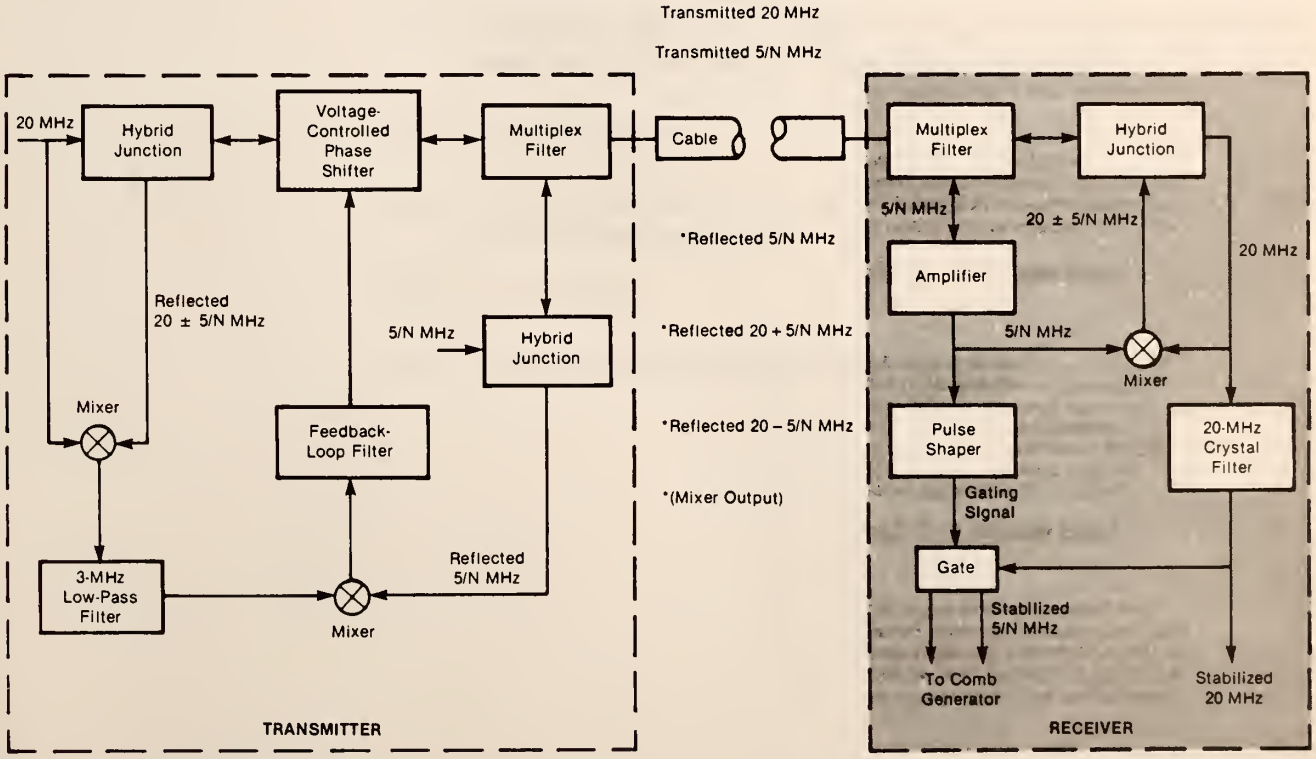

Signals at Two Different Frequencies are transmitted back and forth along a cable and mixed to measure the propagation delay in the cable. The delay-measuring circuitry is part of a feedback loop that constrains the overall delay at a stable value.

Thus, the 20-MHz signal arriving at the receiver is stabilized in phase. The 5/N-MHz signal arriving at the receiver is not stabilized, but it serves as a gate for individual cycles of the stabilized 20-MHz signal to obtain stabilized pulses at 5/N MHz. In the original application, the stabilized 5/N-MHz pulses drive a "comb" generator, which puts out microwave tones at all harmonics of the stabilized signal.

This work was done by E. H. Sigman of Caltech for **NASA's Jet Propulsion Laboratory**. *NPO-17001 /TN*

FOR ADDITIONAL INFORMATION: *Contact: Director, Technology Transfer Division, P.O. Box 8757, BWI Airport, MD 21240; (301) 621-0100 Ext. 241*

REFER TO THE NUMBER LISTED AT THE END OF THIS ARTICLE

Electrotechnology

553 Navy's VHSIC Program Proceeds on Course

554 Surface-Mount Technology at Fermilab

555 Coding Strategy for Critical Data — Repetition preserves the most critical data during severe attenuation.

556 Arc-Jet Power Sup[ply and Starting Circuit — Power efficiency is high, current is regulated, and starting is automatic. (Licensing Opportunity)

557 Diffractively Coupled, Refractively Guided Lasers — Semiconductor-laser arrays would be more reliable, more powerful, and easier to make. (Licensing Opportunity)

558 Improved Tracking of Square-Wave Subcarrier — The variance of the phase error is reduced.

559 Optical Rotary Joint for Data Transfer — A proposed joint would increase bandwidth and reduce errors.

560 Temperature-Controlling Circuit — Operational amplifiers control large current to a resistance heater. (Licensing Opportunity)

561 Wide-Band, Wide-Scan Antenna for Circular Polarization — Circular polarization is generated by linearly polarized elements.

Testing & Instrumentation

562 Difference-Equation/Flow-Graph Circuit Analysis — Solutions are reached quickly on small computers.

Other Items of Interest

597 Ultralow-Loss Infrared Optical Fibers Developed

Navy's VHSIC Program Proceeds on Course

As the development phase of DOD's Very High Speed Integrated Circuit (VHSIC) Program ramps down, it becomes increasingly critical to transition device fabrication techniques from the labor and time intensive laboratory environment to full-scale, high yield, high volume production capability. The high number of interconnects, the closeness of the connections, and the speed of signals require close design tolerances to avoid interaction between the conductors. Previously unheard of accuracy in lithographic pattern replication is essential to achieve design goals and economically viable production yields. Similarly, in many potential applications of VHSIC technology, the circuit design and system design are limited by state-of-the-art semiconductor packaging and interconnection technology.

The Navy Manufacturing Technology program, in coordination with the DOD VHSIC and Manufacturing Technology Advisory Group (MTAG) committees on integrated circuit technology, began addressing these issues in Fiscal Year 1984 with the initiation of two complementary photolithography projects. Sponsored by the Space and Naval Warfare Systems Command (SPAWAR), a team led by Westinghouse, Baltimore, MD, has established the manufacturing technology necessary for successfully depositing and selectively exposing multilayer photo-resist, and has demonstrated a dry etching process which accommodates VHSIC feature and topography requirements.

The multilayer resist lithography project (number X0409) was initiated to reduce the cost of VHSIC devices by increasing production yield through the reduction of problems caused by circuit leakage and out-of-dimensional tolerance or stress points caused by line narrowing across a step on the circuit topology. The problems occur because the practice of thinning the photoresist to achieve necessary line resolution causes permeability difficulties between layers, or excessive necking over the topological steps. These problems were resolved by the establishment of equipment and processes which deposit multiple layers of resist, each of which are sensitive to different wavelength energy sources.

The dry plasma etching project (number X0408) has resulted in a machine that can provide the line width control, selectivity, and stringer removal required for VHSIC chips with feature sizes of only 1.25 microns. Available wet etching and some batch plasma techniques were isotropic and incapable of providing the necessary line widths. The fully automated microprocessor controlled machine is the result of enhancing commercially available dry etching equipment and processes. The machine provides high throughput, single wafer reactive ion etching with reliable endpoint detection and etch characteristics that avoid radiation damage to the substrate. As a result of this project, enhanced dry etching is available for use in etching polysilicon gates and dielectric layers such as borophosphosilicate glass, silicon dioxide, and silicon nitride which are used as insulating layers in the multilevel metallization system.

Advancements in packaging and interconnection technology began to be realized by the Navy MT Program in Fiscal Year 1985 with the initiation of three additional VHSIC-related projects. The first of these (number A2001), sponsored by the Naval Air Systems Command and performed by Westinghouse, addresses the need for a ceramic substrate material that will meet the characteristics required for the high density, high signal speed packaging of VHSIC designs. Until now, printed wiring board technology utilized materials having dielectric constants of about six to nine. These high dielectric constants result in high drive requirements at VHSIC speeds. This leads to higher heat handling requirements, degraded performance, and the need for line driver devices either on or off the chip. As a result of this project, a ceramic substrate material with a relative dielectric constant (K) of four, less than half that of alumina ($A1_2O_3$), the traditional ceramic material for hybrid substrates and chip carriers, has now become available to maintain the propagation velocity of high speed digital signals in VHSIC circuits. Perhaps equally significant, this low K value advanced ceramic material has a thermal coefficient of expansion which matches that of the alumina chip carriers that may be soldered to circuitry printed on it.

The practical application of VHSIC technology also requires advances in multichip packaging in order to attain the desired performance levels, reduce the number of package contacts, and achieve other essential packaging requirements. The current state-of-the-art is essentially limited to chip and wire (aluminum or gold) joining of devices having sixty or less input/output pads (usually aluminum). VHSIC devices typically have far greater numbers of pads as well as a variety of metallizations. Project number X0501, sponsored by SPAWAR and being performed by Teledyne Microelectronics, Los Angles, CA is successfully addressing the VHSIC multichip packaging re-

quirements. Upon its completion in mid-1988, this project, together with a complementary Army-sponsored project, will have established a complete suite of advanced multichip packaging manufacturing technologies for VHSIC applications. Among these will be an interconnect substrate with finer lines, a controlled dielectric constant, and materials and processes suited to thermal, mechanical, and electrical connection to the hermetic package. Chip mounting will provide adequate compliance for thermal expansion accommodation, good heat transfer characteristics, and mounting height compensation for different chip thicknesses. Second level interconnection will accommodate solder chip pads, will ease problems of multilayer substrates, and will be more amenable to fine line definition. And lastly, a hermetic package will incorporate bump/grid input/output geometry in an alumina ceramic package suitable for use on alumina printed wiring boards.

The second VHSIC-related MT project initiated by SPAWAR in Fiscal Year 1985 (number X0502) is establishing the capability for fabricating chip-to-module and module-to-module (backplane) interconnects using new materials technology compatible with VHSIC devices.

This project is focused on improving materials, processes, and hardware associated with the module electrical interface and the chip package to support structure thermal interface. As exemplified by Figure 2, the result will be a 250 pin, surface mount backplane connector compatible with the module connector of MIL-STD-1389 and MIL-C-28754 to improve multilayer backplane circuit routing density, and a set of modular connectors containing MIL-C-28754 connector contacts plus RF and optical inserts. The project is scheduled for completion in March 1988.

The ultimate result of these and other VHSIC-related MT projects sponsored by the DOD is that the industrial capability to produce VHSIC devices that are affordable, reliable, and readily available to systems contractors for insertion into DOD weapon systems has become a reality.

For further information regarding the Navy's VHSIC-related MT program contact:
Commander, Naval Ocean Systems Center
Attn: Mr. Pat Reaves, Code 551
San Diego, CA 92152
Telephone: (619) 553-5381

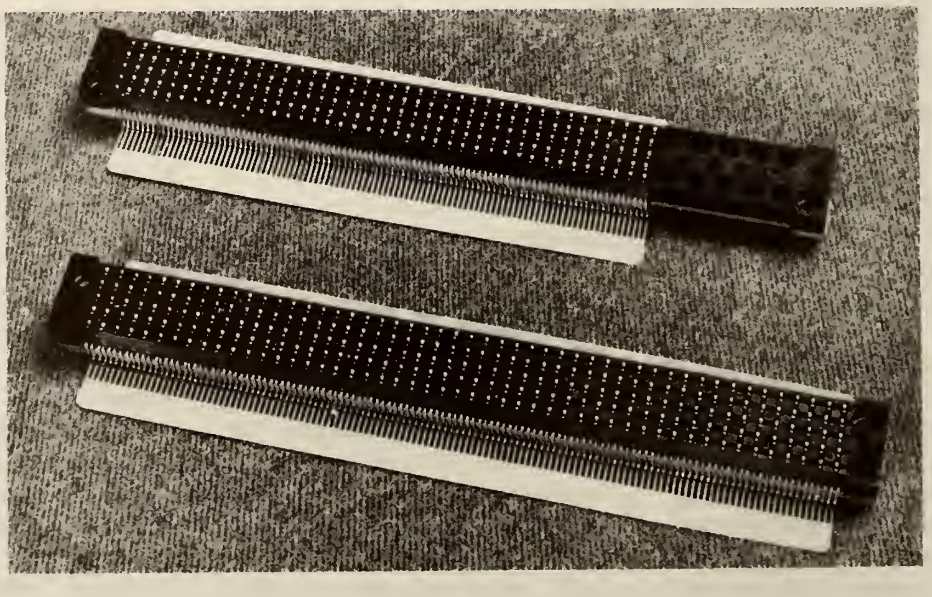

THIRD LEVEL CONNECTORS.

Technology Application

Fermi National Accelerator Laboratory

Surface-Mount Technology at Fermilab

Printed circuits with leaded components and hybrid circuits have traditionally been the backbone of electronic-circuit construction for high-energy physics. In recent years, semi-custom and custom integrated-circuit design have become popular. Surface-mount technology (SMT) now offers the electronics-design engineer another option for the fabrication of demanding circuits, and many industries are beginning to implement SMT designs to improve their products. To understand the advantages and problems associated with SMT, Fermilab engineers and scientists have been exploring SMT by using it in their electronics designs.

A surface-mount circuit is different from a conventional leaded component board because SMT components are attached to the substrate without the aid of holes or feed-through mechanical hardware. Generally, the components are miniaturized and commonly attached to both sides of the substrate. A hybrid circuit is a type of surface-mount circuit. The difference is that a hybrid is usually assembled on an alumina substrate and has screened and fired resistors. A surface-mount circuit is usually assembled on FR-4 substrate and uses chip resistors.

Both analog and digital surface-mount circuit boards, ranging in size from a tiny 0.8 sq in. to a large 210 sq in., have been designed and installed at Fermilab. The board types include: 1) several different detector preamplifier boards, 2) a flash analog-to-digital converter differential line receiver, 3) a front-end input latch and readout shift register board, and 4) multichannel ASD (amplifier-shaper-discriminator) boards for four different detectors in the Collider Detector at Fermilab.

Surface-mount circuits have found a niche in the electronics industry because of several advantages over other fabrication technologies. Compared to leaded printed-wire boards, surface-mount circuits are generally 40% to 60% smaller, have improved performance due to lower inductance and capacitance, and can be less expensive depending on choice of components.

In most cases, SMT does not compete with custom or semi-custom IC designs because extreme size reduction is often required with custom designs. The advantage of surface-mount over custom or semi-custom integrated circuits is primarily the lower cost for lower-quantity production runs and shorter turn-around time for construction of prototype and production quantities.

Contrary to common misconception, getting started in SMT is not expensive. Fermilab has found that for under $5000, and in 100 sq ft, an individual can assemble prototype surface-mount circuits as well as repair surface-mount and hybrid circuits.

As experiments and accelerators grow in complexity and size, the need for smaller, improved circuits will continue to drive future electronics designs. While custom integrated and hybrid circuits will play important roles, surface mount has taken a foothold at Fermilab and can be expected to assume added significance in the future.

FOR ADDITIONAL INFORMATION:

Office of Reseorch ond Technology Applicotions
Fermi Notionol Accelerator Laboratory
P.O. Box 500
MS 208
Batovio, IL 60510
(312) 840-3333

Refer to FAA-3283/TN

NASA Tech Brief
National Aeronautics and Space Administration
NASA's Jet Propulsion Laboratory, Pasadena, California

Coding Strategy for Critical Data

Repetition preserves the most critical data during severe attenuation.

Repetition coding can be used to protect a small but critical portion of a Reed-Solomon/convolutionally-encoded (RS/CE) data stream against loss during periods of signal attenuation due to bad weather. Each bit in the portion of the RS/CE data stream containing the critical data is repeated a number of times that depends on the degree of protection required. The noncritical majority of data is transmitted normally, without repetition.

The signal-to-noise ratios of some types of data channels, particularly those using radio links, vary with the transmission media fluctuations. Often the reliable reception of some portion of the data stream has a higher priority than does the reception of the remainder. When the available channel capacity is inadequate for reliable reception of all data under the worst transmission conditions, it is desirable to use an encoding strategy that reflects the relative importance of different types of data. The reception of the higher-priority (critical) data can then be assured even under poor transmission conditions, while exacting only a small penalty in the overall data rate under good conditions. The new repetitive coding scheme represents one such strategy. This scheme is superior to two other well-known low-rate codes (orthogonal and biorthogonal codes) at comparable rates and signal-to-noise ratios. Furthermore, only simple additional equipment is required to add repetition encoding to existing RS/CE equipment (see figure).

Without repetition, the RS/CE bit error rate deteriorates abruptly as the symbol signal-to-noise ratio decreases below a certain point. For example, the bit error rate rises from 10^{-5} to 10^{-2} as the bit signal-to-noise ratio drops from 2.3 to 1.9 dB; thus, a mere 0.4 dB can be the difference between successful data transmission and failure. In contrast, if the critical RS/CE data are transmitted five times in succession, the bit error rate for these data is less than 10^{-5} at a signal-to-noise ratio of -8.3 dB. If, for example, only 1 percent of the data is critical, then the overall loss in channel capacity due to the use of this repetitive scheme is only 0.18 dB.

This work was done by Laif Swanson and Joseph H. Yuen of Caltech for **NASA's Jet Propulsion Laboratory**.
NPO-16630 /TN

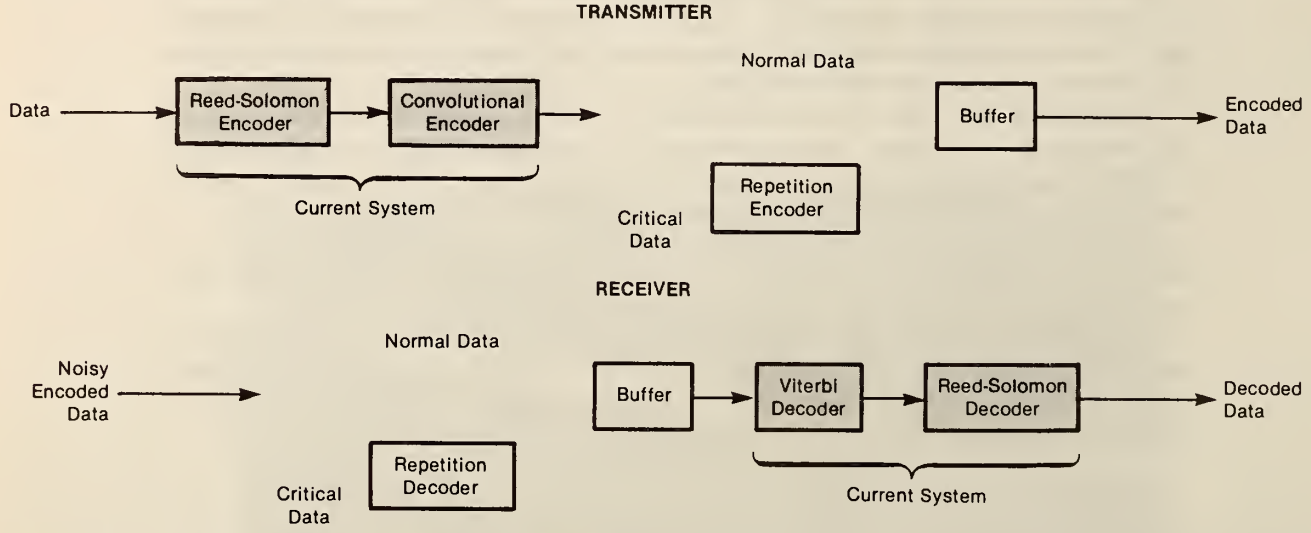

Repetition can be added to an existing system that uses Reed-Solomon and convolutional encoding by additional components shown in color.

FOR ADDITIONAL INFORMATION: *Contact: Director, Technology Transfer Division, P.O. Box 8757, BWI Airport, MD 21240; (301) 621-0100 Ext. 241*
REFER TO THE NUMBER LISTED AT THE END OF THIS ARTICLE

NASA Tech Brief
National Aeronautics and Space Administration
Lewis Research Center, Cleveland, Ohio

Licensing Opportunity

Arc-Jet Power Supply and Starting Circuit

Power efficiency is high, current is regulated, and starting is automatic.

An arc jet operates by heating a gas with an electric arc and expanding the heated gas through a nozzle to provide thrust. Typically, the arc-discharge voltage decreases with increasing current. This arc characteristic requires some form of current limiting to prevent the destruction of the thruster. Previously, power for arc jets in the laboratory was obtained from a high-voltage power supply with a ballast resistor in series with the thruster arc. The resistor wastes power, and the power supply does not act as a constant-current source.

Some means must be provided to initiate the arc discharge. At present, there are three basic methods for starting arc

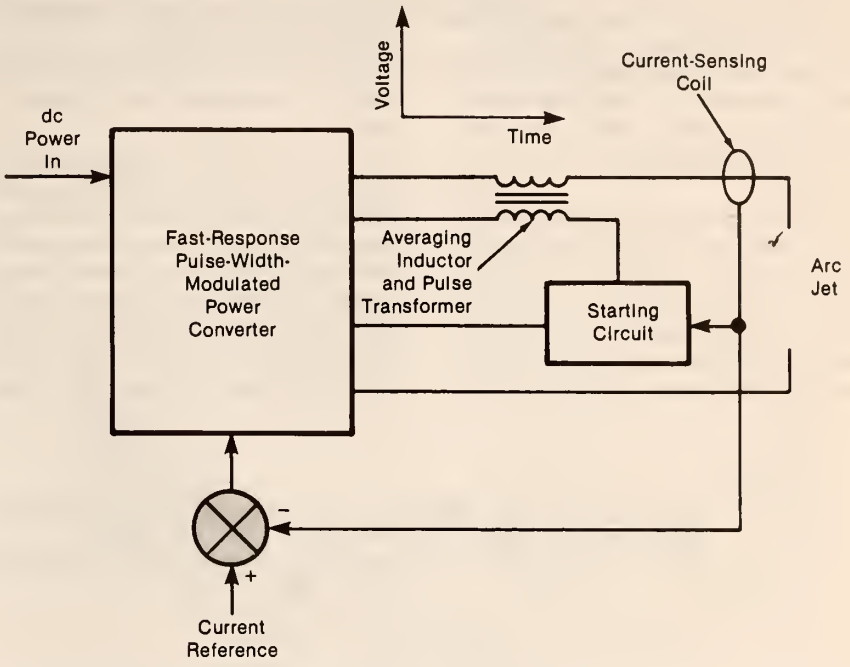

Figure 1. A **Feedback Control System** keeps the arc-jet current nearly constant, once the arc has been struck by the starting pulse.

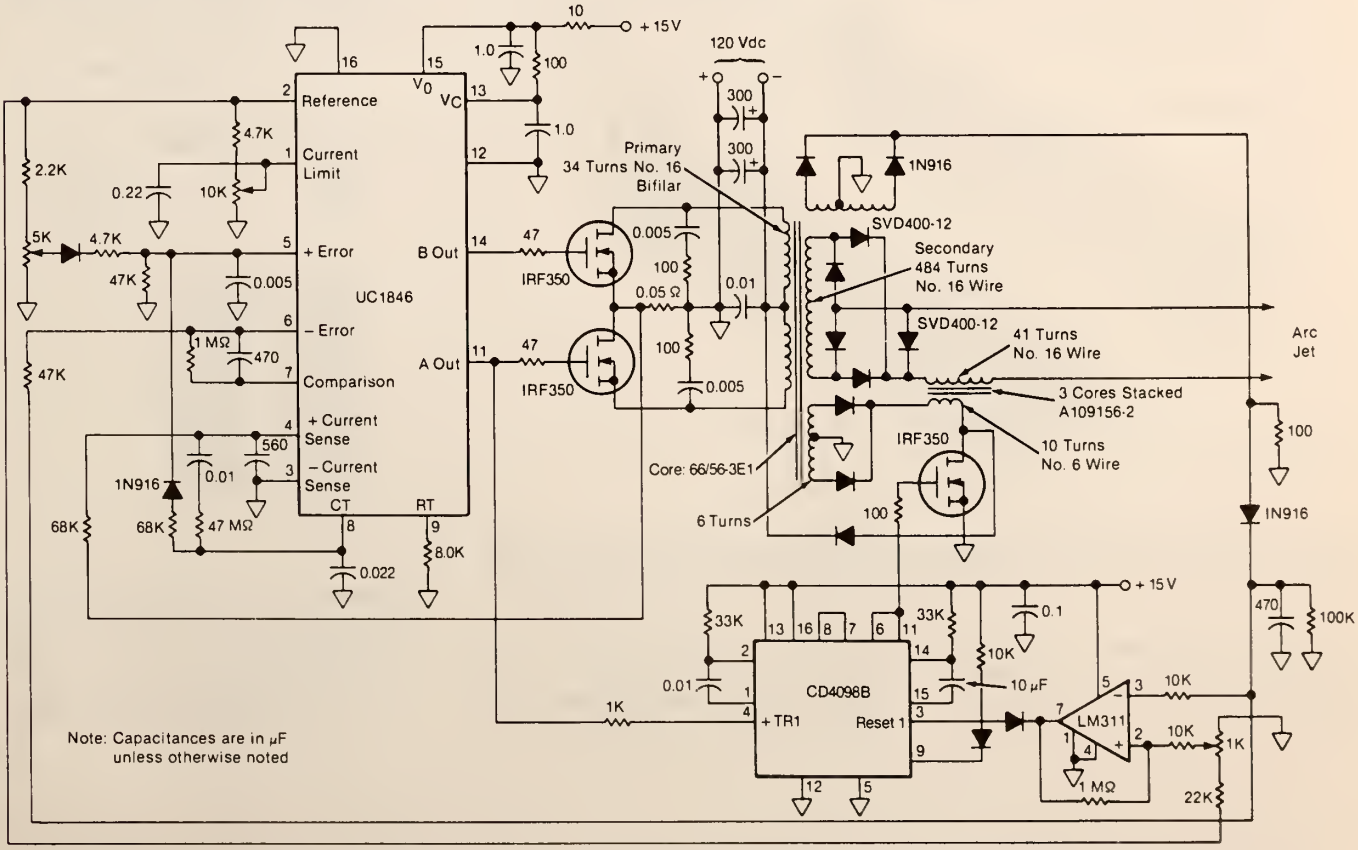

Figure 2. The **Circuit of Figure 1** is made of commercially available components. This design is capable of high power efficiency.

jets; each has advantages and disadvantages. In one mechanical method, the electrodes are momentarily brought together. In another method, the propellant-gas pressure or composition is adjusted until a Paschen discharge is established. In a third method, a high voltage (about 1 kV) is applied between the electrodes until the arc starts.

A new circuit for starting arc jets and controlling them in steady operation is capable of high power efficiency and can be constructed in a lightweight form. The design comprises a pulse-width-modulated power converter, which is configured in a closed control loop for fast current control.

A functional diagram of the circuit is shown in Figure 1. Figure 2 is a detailed schematic diagram. The arc-jet power supply is a current regulator with fast response. The series averaging inductor maintains nearly constant current during rapid voltage changes and thereby allows time for the fast-response regulator to adjust its pulse width to accommodate load-voltage changes.

An important feature of the circuit is that the output averaging inductor doubles as the high-voltage pulse transformer for ignition. This is significant because magnetic components are heavy and expensive. In addition, no external high-voltage power supplies or blocking diodes are needed to start the arc. Another advantage is that the limited-energy and limited-maximum-current features of the starting circuit minimize electrode erosion during initiation of the arc.

The starting circuit operates according to the same principle as that of an automobile ignition coil. Current flows through a low-voltage winding. When the current is interrupted by a transistor switch, the inductor magnetic field collapses, and a high-voltage pulse is produced. The pulse is initiated every 0.25 second until arc current is detected. Then the pulser is automatically turned off.

This work was done by Robert P. Gruber of **Lewis Research Center**. *Further information may be found in NASA TM-87340 [N86-25409/NSP], "Power Electronics for a 1-Kilowatt Arcjet Thruster."*

Copies may be purchased from the National Technical Information Service, Springfield, Virginia 22161, [A02]

This invention is owned by NASA, and a patent application has been filed. Inquiries concerning nonexclusive or exclusive license for its commercial development should be addressed to the Patent Counsel, Lewis Research Center

Refer to LEW-14374 /TN

Lewis Research Center
21000 Brookpark Road
Cleveland, OH 44135

Technology Utilization Officer: Daniel G. Soltis
Mail Stop 7-3
(216) 433-5567

Patent Counsel: Gene E. Shook
Mail Code 301-6
(216) 433-5753

FOR ADDITIONAL INFORMATION: *Contact: Director, Technology Transfer Division, P.O. Box 8757, BWI Airport, MD 21240; (301) 621-0100 Ext. 241*

REFER TO THE NUMBER LISTED AT THE END OF THIS ARTICLE

NASA Tech Brief
National Aeronautics and Space Administration
NASA's Jet Propulsion Laboratory, Pasadena, California

Licensing Opportunity

Diffractively Coupled, Refractively Guided Lasers

Semiconductor-laser arrays would be more reliable, more powerful, and easier to make.

A type of index-guided semiconductor-laser array now under development is expected to exhibit performance and amenity to manufacturing superior to those of gain-guided arrays. The improved design is intended, in part, to eliminate the undesired electromagnetic modes and mode shifts that sometimes occur in the gain-guided variety. Potential applications for such arrays include optical communications, ranging, printing, and recording.

Ordinarily, it is desired to make all the lasers in an array oscillate in or near the same phase. However, in gain-guided arrays, evanescent-wave coupling distributed along the laser cavity tends to make adjacent units operate in opposite phases. Even in gain-guided arrays designed for operation in phase, gain-saturation effects can alter the modal characteristics.

In the improved, index-guided array the lasers are uncoupled in their guided sections; instead, they are coupled by diffraction in the common section of the resonator. Upon reflection from the mirror (see Figure 1), a fraction of each laser field is fed to the adjacent laser, where it helps to establish the phase of the oscillation. Overall, the phase relationships among the lasers in the array are determined primarily by the length of the common resonator section.

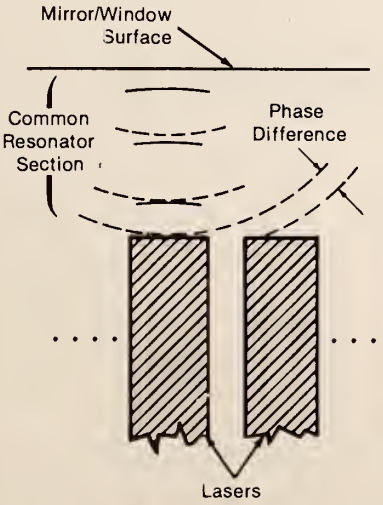

Figure 1. **Reflected From the Mirror/Window** at the end of the common resonator section of the laser, energy refracted from each laser enters the adjacent laser. This mutual coupling establishes the phase relationships among the lasers.

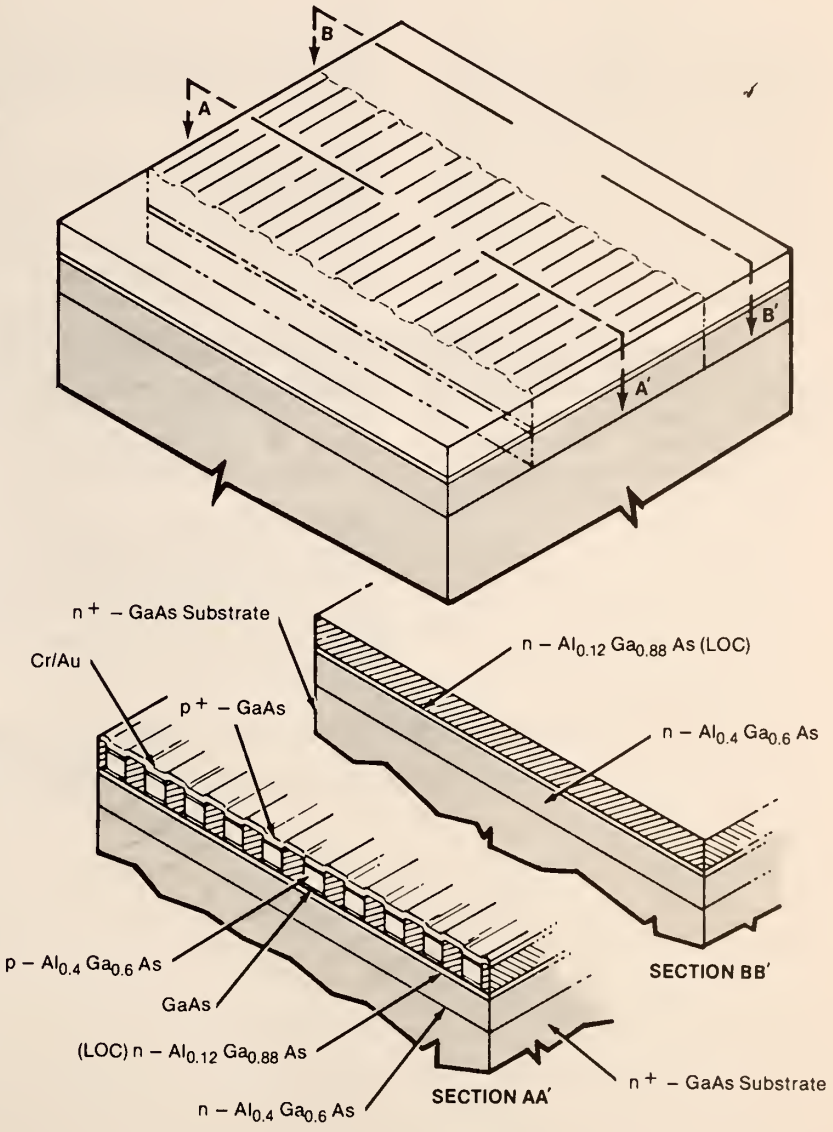

Figure 2. A **Monolithic Laser Array** could be made by standard epitaxial techniques. It could also be made in part with polymeric materials to mitigate some of the deleterious effects of all-epitaxial processing.

The array (see Figure 2) includes strip buried heterostructure lasers. The fabrication of the array could start with the growth of a large-optical-cavity (LOC) layer on a GaAs substrate by liquid-phase epitaxy. The individual lasers could be defined by selective etching down to the LOC layer. The spaces between the layers could be refilled, either by the deposition of polyimide or by epitaxial regrowth followed by metallization and cleaving.

Because most of the optical field is contained in the LOC layer, the dominant reflection is from the cleaved (end) mirrors, not from the etched interfaces of the active regions. The LOC-layer configuration helps to assure high output in each laser even in the absence of coupling. Each laser can be designed independently of the waveguide coupling with the other lasers because that coupling is relatively small.

Because the diffraction section of the laser is not pumped, it acts as a nonabsorbing mirror/window. This reduces the susceptibility of the mirror/window to damage, thereby increasing the power level at which the array can be operated without breakdown.

This work was done by Joseph Katz, Jim Cser, and William K. Marshall of Caltech for **NASA's Jet Propulsion Laboratory**.

Inquiries concerning rights for the commercial use of this invention should be addressed to the Patent Counsel, NASA Resident Office-JPL Refer to NPO-16927. /TN

Jet Propulsion Lab.
4800 Oak Grove Drive
Pasadena CA 91109

Technology Utilization Mgr.: Norman L. Chalfin
Mail Stop 156-211
(818) 354-2240

NASA Resident Technology Utilization Officer: Gordon S. Chapman
Mail Stop 180-801
(818) 354-4849

Patent Counsel: Paul F. McCaul
Mail Code 180-801
(818) 354-2734

FOR ADDITIONAL INFORMATION: *Contact: Director, Technology Transfer Division, P.O. Box 8757, BWI Airport, MD. 21240; (301) 621-0100 Ext. 241*
REFER TO THE NUMBER LISTED AT THE END OF THE ARTICLE

NASA Tech Brief
National Aeronautics and Space Administration

Improved Tracking of Square-Wave Subcarrier

The variance of the phase error is reduced.

A report discusses the application of a "windowing" concept to improve the ability of a telemetry receiver to track the phase of a square-wave phase-modulation subcarrier signal. The concept is based on setting the phase-tracking signal at zero outside narrow time "windows," thereby reducing the noise energy in the processed signal. The result is an increase in the signal-to-noise ratio in the tracking loop with a consequent increase in the accuracy of tracking and a reduction in the number of errors in the telemetric data.

In a telemetry system of the type considered, data are transmitted as binary modulation of the subcarrier. For correct reception of data, the receiver must track the carrier and subcarrier phases. In the conceptual receiver, the subcarrier-phase-tracking system is an all-digital Costas loop in which nominally the subcarrier-phase quadrature reference signal is zero except during the small fraction W/4 of each subcarrier cycle immediately preceding and following each zero crossing of the subcarrier.

Errors in the reception of data are treated as noise, and the phase-tracking performance is quantified in terms of the variance of the phase-tracking error. The report develops equations that describe the operation of the subcarrier-phase-tracking loop and are used to predict the performance. This analysis is based on the assumption of synchronization of the receiver with the received signals, ignoring such complications as quantization errors, nonzero data-signal rise time, and filtering distortions.

A linear treatment (valid for small phase-tracking errors and for W not too close to zero) shows that the variance of the phase-tracking error can be reduced to about $W\sigma_0^2$, where σ_0^2 is the value without "windowing." A computer simulation verifies this result and extends the prediction to regions of nonlinear response, yielding plots of variance of the phase-tracking error as a function of W, with the signal-to-noise ratio of the subcarrier-phase-tracking loop as a parameter. From these plots one can find the optimum W; in a typical case, the window can be made so narrow that the phase-error variance is reduced to $1.5\sigma_0^4$.

This work was done by William J. Hurd and Sergio Aguirre of Caltech for **NASA's Jet Propulsion Laboratory**. *To obtain a copy of the report, "A Method To Dramatically Improve Subcarrier Tracking," NPO-17135 /TN*

FOR ADDITIONAL INFORMATION: *Contact: Director, Technology Transfer Division, P.O. Box 8757, BWI Airport, MD 21240; (301) 621-0100 Ext. 241*

REFER TO THE NUMBER LISTED AT THE END OF THIS ARTICLE

NASA Tech Brief
National Aeronautics and Space Administration
Lyndon B. Johnson Space Center, Houston, Texas

Optical Rotary Joint for Data Transfer

A proposed joint would increase bandwidth and reduce errors.

A scheme for transferring digital data across a rotary joint would use light instead of electrical signals. The optical joint would offer greater bandwidth than that of conventional electrical sliprings and would probably operate at a considerably lower error rate. According to an estimate, a highly reliable, compact joint could be built for less than $1 per channel and could accommodate one or several channels, each with a 1-MHz bandwidth. The concept could be applied to the transfer of high-speed data to rotating antennas or across the joints of robots and manipulators in automated manufacturing.

The concept calls for a row of laser or light-emitting-diode transmitters on the outside member of a cylindrical joint and a series of corresponding photodiode receivers on the inner member (see figure). The receivers would be arranged as a stack of rings. A transmitter would continually beam light at its receiver ring as the latter rotates. Instead of facing each other across the gap, the transmitting and receiving diodes could be located away from the gap, connected to the transmission points and the receiving rings by optical fibers.

The joint could be made as long as necessary to accommodate the requisite number of transmitter/receiver pairs for each channel. For bidirectional data flow, a combination of transmitters and receivers would be mounted on both sides of the joint. There would be no mechanical contact between transmitters and receivers and, therefore, no wear.

In a variation of the concept (also shown in the figure), transmitters would be arrayed along a radius of a flat disk, and receiver rings would be arrayed along a pole surrounded by a conical mirror. The mirror would reflect light from the lasers — the only suitable transmitters in this case — into the receiving photodiodes.

This work was done by Fred J. Becker of McDonnell Douglas Corp. for **Johnson Space Center**. *MSC-21182 /TN*

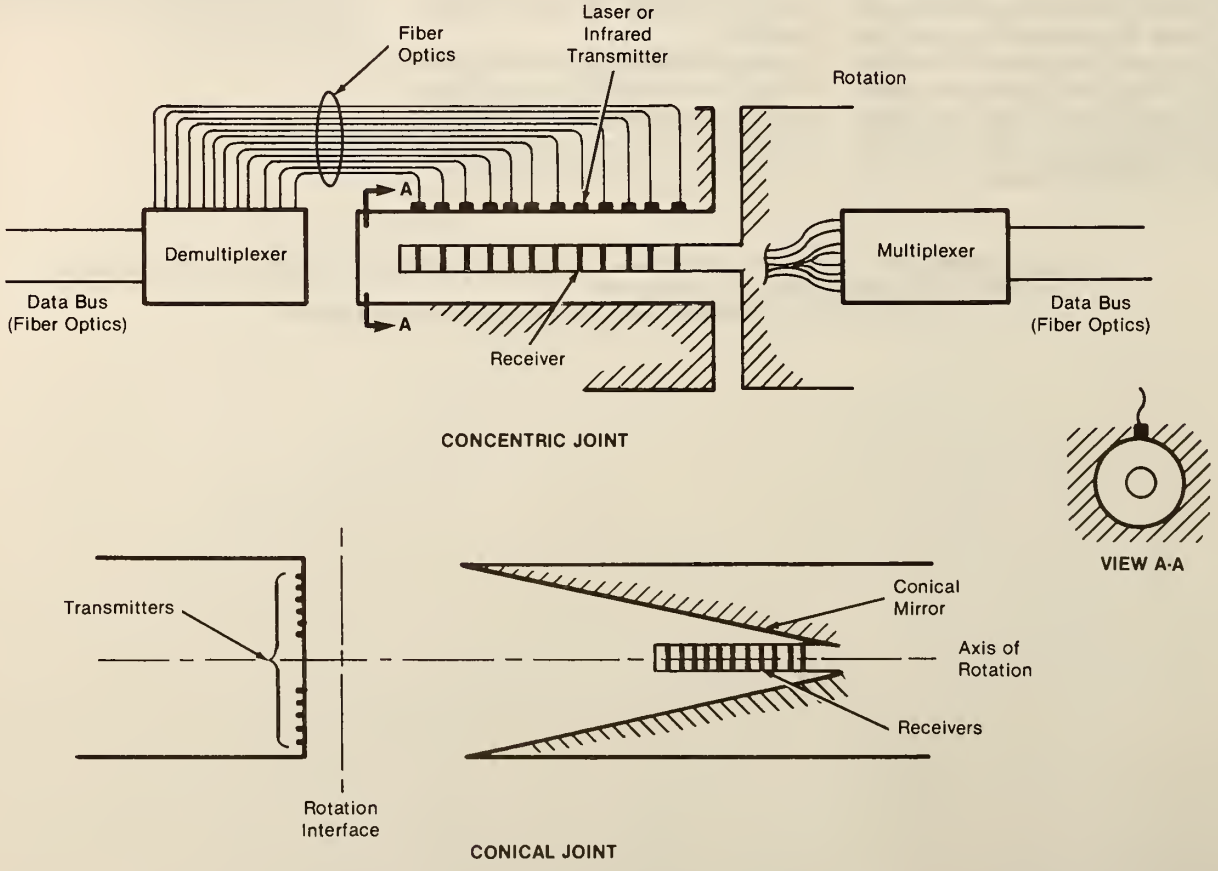

Light Pulses Would Be Transmitted across the gap of the rotary optical data joint. The conical form of the joint would be useful when one of the members must have a flat surface.

FOR ADDITIONAL INFORMATION: *Contact: Director, Technology Transfer Division, P.O. Box 8757, BWI Airport, MD 21240; (301) 621-0100 Ext. 241*

REFER TO THE NUMBER LISTED AT THE END OF THIS ARTICLE

NASA Tech Brief
National Aeronautics and Space Administration
Ames Research Center, Moffett, California

Licensing Opportunity

Temperature-Controlling Circuit

Operational amplifiers control large current to a resistance heater.

A simple circuit switches the current to an electrical heater on and off to maintain the temperature of a room at 25 ± 0.5 °C. The circuit is lightweight, compact, reliable, insensitive to electrical noise, and uses a single 5-Vdc power supply. The circuit can handle ac loads of 10 A. It is designed to operate outside the temperature-controlled environment over a range of −55 to +85 °C.

The temperature sensor is a thermistor, which provides a differential input (for reduced noise) to an operational amplifier connected as a differential amplifier with a small amount of gain (see figure). A 5-kilohm potentiometer is used to adjust the set point through a voltage divider; a value of 2.17 kilohms yields the 25 °C setting.

A second operational amplifier is connected as an inverting differential-input comparator. The hysteresis voltage of the output of operational amplifier 2 is determined by resistors R_1 and R_2. A value of 1.2 kilohms was chosen for R_1 to furnish the requisite input-level-setting voltage for the comparator. A value of 22 megohms was selected for positive-feedback resistor R_2 to provide a moderate amount of hysteresis for adequate immunity to noise while enabling rapid response to the slowly varying input. A reduction of R_2 would increase the hysteresis and therefore the delay in response to temperature changes, but would decrease the sensitivity to noise.

The output of operational amplifier 2 controls the electrical heater through a zero-crossing solid-state relay. A transistor/transistor-logic (TTL) gate adjusts the output to the proper level for the relay. A thermal switch is placed in series with the heater and the ac supply for safety in case of thermal runaway. A third operational amplifier monitors the output of the thermistor, providing a signal to a computer for data logging.

This work was done by Gerald Temple of **Ames Research Center**. *No further documentation is available.*

Inquiries concerning rights for the commercial use of this invention should be addressed to the Patent Counsel, Ames Research Center Refer to ARC-11707/TN

Ames Research Ctr.
Moffett Field, CA 94035

Technology Utilization Officer: Laurance Milov
Mail Code 223-3
(415) 694-6370

Patent Counsel: Darrell G Brekke
Mail Code 200-11
(415) 694-5104

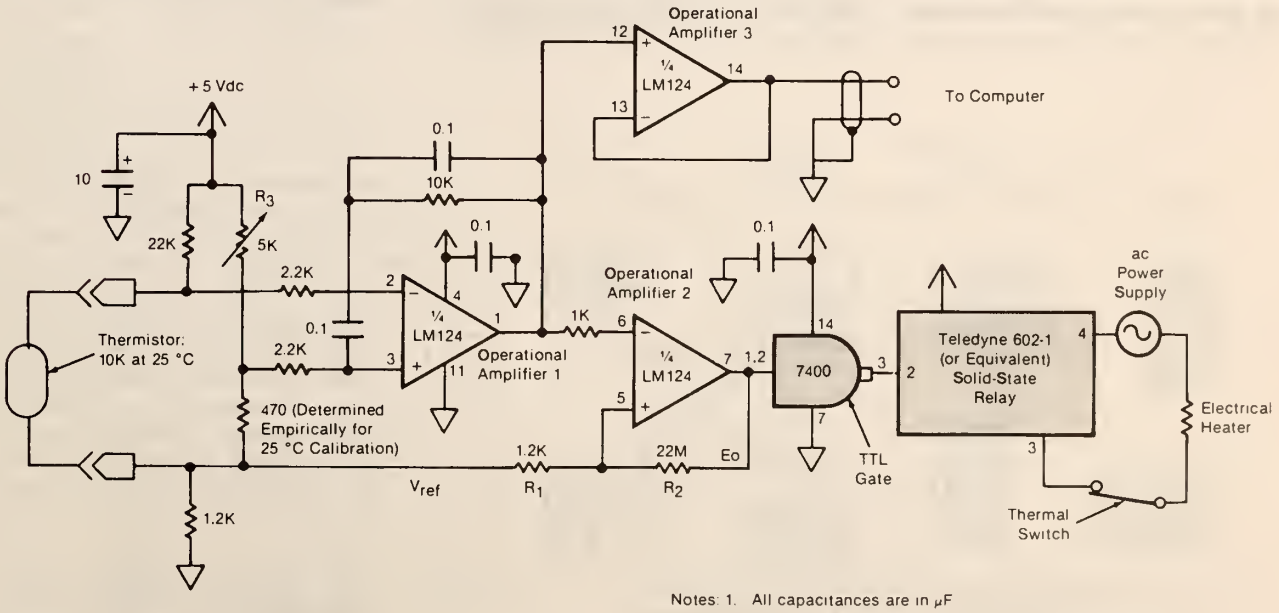

Notes:
1. All capacitances are in μF
2. The temperature set point increases or decreases with R_3, which is set at 2.17K for 25 °C.
3. The upper and lower tripping voltages of operational amplifier 2 are given by $V_{trip} = V_{ref} \pm E_0 R_1/(R_1 + R_2)$, where V_{ref} = the reference voltage and E_0 = the output voltage of the operational amplifier

A **Thermistor Provides the Input Signal** for a simple temperature controller. The output of the controller is applied to a solid-state relay, which in turn switches the current to a resistance heater.

FOR ADDITIONAL INFORMATION: *Contact: Director, Technology Transfer Division, P.O. Box 8757, BWI Airport, MD 21240; (301) 621-0100 Ext. 241*

REFER TO THE NUMBER LISTED AT THE END OF THIS ARTICLE

NASA Tech Brief
National Aeronautics and Space Administration
NASA's Jet Propulsion Laboratory, Pasadena, California

Wide-Band, Wide-Scan Antenna for Circular Polarization

Circular polarization is generated by linearly polarized elements.

Circularly polarized radio waves are generated by an array of linearly polarized elements composed of subarrays of four balanced elements. Within each subarray, the angular orientations and phases of the elements are 0°, 90°, 180°, and 270°, respectively. The axial-ratio bandwidth of such an array is greater than that of conventional circularly polarized antennas, and the main beam can be scanned to relatively wide angles without seriously degrading the circular polarization. A microstrip antenna based on this concept weighs less, has a less complex feed system, and has lower loss than does a conventional antenna for circular polarization.

In the microstrip version shown in the figure, the orthogonal sets of patches generate orthogonal electromagnetic fields, while the different phases of the feeds provide the 90° phase difference needed for circular polarization. At beam angles other than broadside (that is, other than perpendicular to the plane of the array) in the x-z and y-z planes, the spatial phase delays among elements do not degrade the circular polarization because the phases change by the same amount for both of the component linearly polarized waves. To an observer far away, the radiation appears to emanate from two circularly polarized sources.

In the broadside direction, the copolarized components from different radiating elements reinforce each other, while the cross-polarized radiation impurities cancel each other. This is a particular advantage in microstrip arrays having thick substrates, which generate undesired higher-order modes. The cancellation of the cross-polarized components results in large axial-ratio bandwidth.

In principle, the undesired fields do not cancel in beam directions outside the principal planes. In practice, however, the beam-narrowing and averaging effects in large arrays do suppress the radiation of spatial field impurities, with the result that the polarization is nearly circular over a wide range of beam directions in all planes. Another advantage of the spatial arrangement of elements is that the mutual coupling of this type of array is less than that of a conventional array: the orthogonality allows very little coupling between immediate neighboring elements.

Arrays of 2×2, 4×4, and 2×8 elements have been tested sucessfully. Although the development efforts have thus far concentrated on microstrip versions, the concept should be applicable to arrays of rod dipole or other radiating elements. Antennas of this general type should prove useful in communications and phased-array radar.

This work was done by John Huang of Caltech for **NASA's Jet Propulsion Laboratory**. *NPO-16831 /TN*

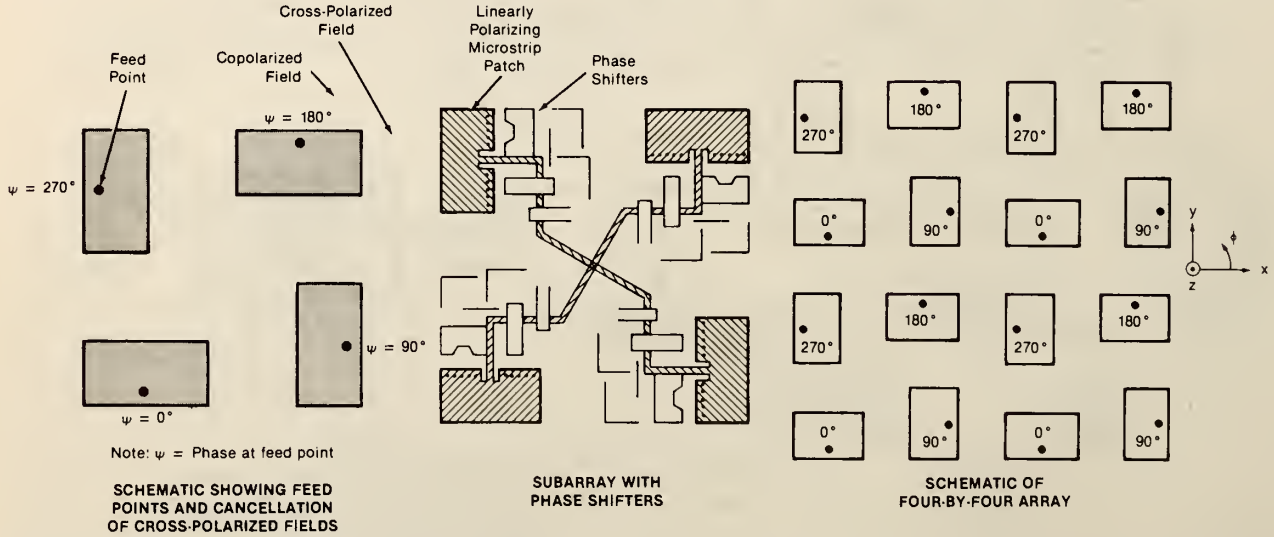

The **Basic Two-by-Two Subarray** of antenna elements can be made of microstrip patches. The patches are arranged in an orthogonal pattern. The patches are fed through different phase shifters so that the signals at their feed points have the same orthogonal relationship in phase.

FOR ADDITIONAL INFORMATION: *Contact: Director, Technology Transfer Division, P.O. Box 8757, BWI Airport, MD 21240; (301) 621-0100 Ext. 241*
REFER TO THE NUMBER LISTED AT THE END OF THIS ARTICLE

NASA Tech Brief
National Aeronautics and Space Administration
Marshall Space Flight Center, Alabama

Difference-Equation/Flow-Graph Circuit Analysis

Solutions are reached quickly on small computers.

A numerical technique enables rapid, approximate analyses of electronic circuits that contain linear and nonlinear elements. The technique can be practiced in a variety of computer languages on large and small computers; for circuits that are simple enough, programmable hand calculators can be used. Although some combinations of circuit elements can make the numerical solutions diverge, the technique enables the quick identification of divergence and the correction of circuit models to make the solutions converge.

A circuit to be analyzed by the technique can optionally be depicted by a signal-flow graph. The voltages at the circuit nodes and the currents between the nodes are represented in terms of the standard equations of nodal analysis. Using the flow graph of the schematic circuit diagram, one propagates a voltage signal forward mathematically from a first node to a second node via the equation for the current between them. Because the voltage at the second node affects the voltage at the first node, the voltage signal is also propagated backward by the iteration of nodal equations, using the forward-propagated voltage at the second node in the subsequent iteration for the voltage at the first node.

Finite-timestep difference equations are used to approximate the differential equations for transient voltages and currents in the presence of inductance or capacitance. Such nonlinear circuit elements as switches and diodes can be represented by time-, current-, or voltage-dependent resistances or changes of circuit configuration.

The technique can be illustrated by reference to the "boost" charging circuit of the figure. The signal is mathematically propagated from voltage source $e_S(t)$ rightward to resistor R. To avoid mathematical divergences caused by the treatment of

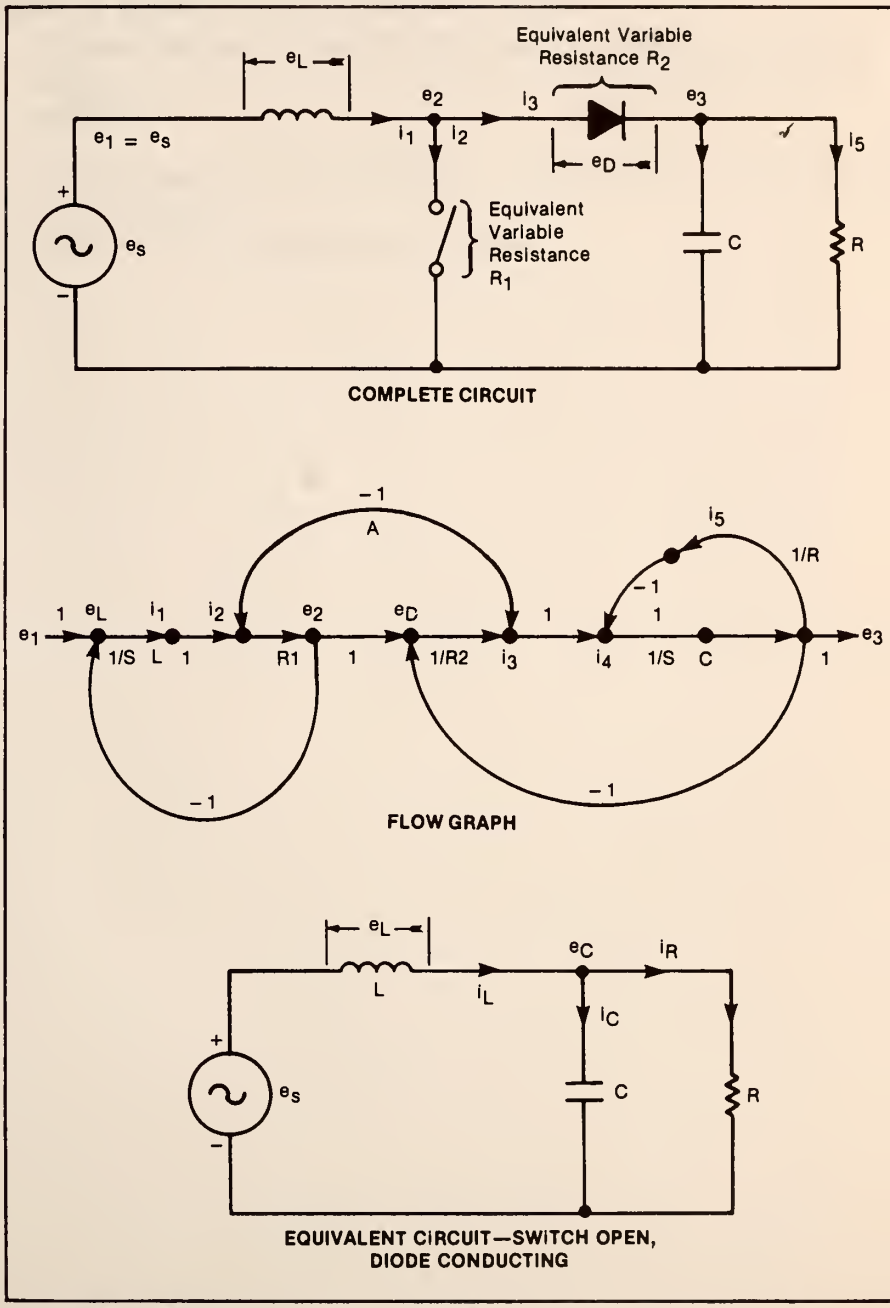

This **"Boost" Charging Circuit** resonantly charges capacitor C from the energy stored in inductor L during the preceding charging cycle. The voltage across C and R can exceed e_S.

the diode and switch as time-varying resistances, the circuit is mathematically reconfigured and new equations written for each of the four distinct combinations of diode and switch states. For example, when the switch is open and the diode is conducting, the algorithm and equations for the voltages and currents are the following, where t = time, and Δt = the increment of time:

- $e_L(t) = e_S(t) - e_C(t - \Delta t)$,
- $i_L(t) = i_L(t - \Delta t) + e_L \Delta t/L$,
- $i_C(t) = i_L(t) - i_R(t - \Delta t)$,
- $e_C(t) = e_C(t - \Delta t) + i_C(t)\Delta t/C$, and
- $i_R(t) = e_C(t)/R$
- Increment time by Δt and return to step 1.

(Note that R_1 and R_2 are nonlinear resistors and can cause loop A not to converge.)

This work was done by I. M. McVey of Rockwell International Corp. for **Marshall Space Flight Center**.

MFS-29245 /TN

FOR ADDITIONAL INFORMATION: *Contact: Director, Technology Transfer Division, P.O. Box 8757, BWI Airport, MD 21240; (301) 621-0100 Ext. 241*

REFER TO THE NUMBER LISTED AT THE END OF THIS ARTICLE

Energy

563 Horizontal Ground-Coil Heat Exchangers

564 Energy and Economic Efficiency Alternatives for Electric Lighting in Commercial Buildings

565 Systems Analysis of Advanced Coal-Based Power Plants — Fuel-cell technologies are evaluated and compared with advanced non-fuel-cell alternatives.

566 Testing Parabolic-Dish Concentrators — Experience at a solar-energy test site is described.

567 Motor Current Signature Analysis Process

Department of Energy

Technology Application

Oak Ridge National Laboratory

HORIZONTAL GROUND-COIL HEAT EXCHANGERS

Key words: Heat pump; ground-coupled heat pump; ground-source heat pump; ground coil

Ground-coupled heat pump (GCHP) systems have long been recognized for their potential for energy conservation and for reduction of electric power consumption during peak load periods. The ground-coil design is crucial to the success of the system. However, because existing design methods are very conservative, ground coils are longer and GCHP systems are more expensive than necessary.

As part of the U.S. Department of Energy/ORNL Building Equipment Research Program, improved computer models for horizontal ground-coil heat exchangers were developed. These models included more parameters and more realistic ground conditions than the existing design models; they were validated with testing in the field (Fig. 1). Three ground-coil models were formed: (1) a model with a radially symmetrical temperature profile and soil-freezing effect around the coil, (2) a model with a three-dimensional ground-temperature distribution caused by heat transfer between the ground surface and the ambient air, and (3) a model having both three-dimensional ground-temperature profiles and thermal interference effects for simulating two-coil arrangements (Fig. 2).

The models developed in this study provide realistic ground-coil designs. They can be run on

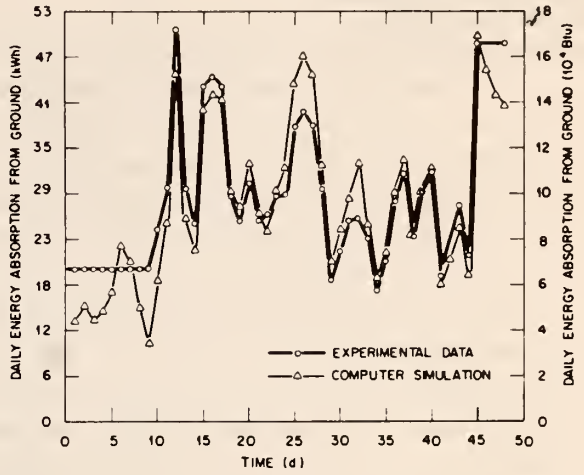

Fig. 1. Comparison between calculated and field experimental results for ground-coil daily energy absorption over 48 d.

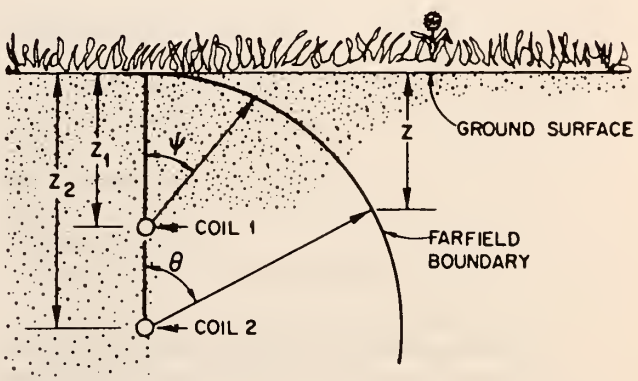

Fig. 2. Schematic diagram of a two-coil arrangement; z = depth from the surface. The angular directions ψ and θ are used to determine the farfield boundary, which marks the distance at which conditions will not be affected by the generation of the ground coils.

IBM-compatible personal computers and are readily adapted for mainframe application. They may be used to design ground-coil heat exchangers for GCHPs or to check designs created by other methods.

Additional information:

National Technical Information Service
U.S. Department of Commerce
5285 Port Royal Road
Springfield, VA 22161

V. C. Mei, *Horizontal Ground-Coil Heat Exchanger: Theoretical and Experimental Analysis,* ORNL/CON-193, Oak Ridge National Laboratory (December 1986).

V. C. Mei, "Theoretical Heat Pump Ground Coil Analysis with Variable Ground Farfield Boundary Conditions," *AIChE J.* **32**, 1211-15 (July 1986).

V. C. Mei, "Heat Pump Ground Coil Analysis with Thermal Interference," *86-WA/SOL-6, ASME Winter Annual Meeting, Anaheim, Calif., December 7-12, 1986;* accepted for publication in the *ASME J. of Solar Energy Engineering.*

Department of Energy

Technology Application

Oak Ridge National Laboratory

ENERGY AND ECONOMIC EFFICIENCY ALTERNATIVES FOR ELECTRIC LIGHTING IN COMMERCIAL BUILDINGS

Key words: Energy conservation; electric lighting; commercial buildings

Lighting is a major source of energy consumption in the commercial sector. Lighting also interacts with space-conditioning loads by decreasing and increasing heating and cooling requirements across seasons. A number of energy-efficient alternatives to traditional commercial lighting technologies are available. These can be grouped generally into renewable lighting (day lighting), task/ambient light combinations, and efficient equipment changes.

The report, *Energy and Economic Efficiency Alternatives for Electric Lighting in Commercial Buildings*, details the results of an investigation to determine the potential energy savings and economic efficiency gains from energy-conserving lighting alternatives in commercial applications. The study's objective was to estimate energy savings from alternative technologies and to estimate their economic efficiency under alternative assumptions. The DOE 2.1A computer program was used to model energy use in commercial buildings. The use of this program permitted examining the effects of different lighting technologies and correcting for changes in space-conditioning requirements while holding illumination levels constant.

All of the lighting concepts analyzed reduced lighting energy use and costs in varying degrees. In addition to the reduced lighting energy use, there was a consequent reduction in cooling energy use and capacity, which reduced total energy use and peak demand. From the standpoint of energy efficiency (not considering costs), the day lighting options scored highest; the task/ambient light combinations scored in the middle; and minor changes, such as fixtures, diffusers, and ballasts, made the smallest impact. From the standpoint of the cost of equipment, the ranking was almost exactly reversed: changes in fixtures, diffusers, and ballasts ranked highest, and day lighting options ranked the lowest. Minor fixture changes can be made at no cost, so they represent pure savings. The least cost-effective strategies had payback periods in excess of 15 years.

Additional information:

For a copy of the report contact:

Office of Technology Applications
Information Service
Martin Marietta Energy Systems, Inc.
P.O. Box X
Oak Ridge, TN 37831
Telephone: (615) 574-4192; FTS 624-4192

C. L. Robbins et al., *Energy and Economic Efficiency Alternatives for Electric Lighting in Commercial Buildings,* ORNL/Sub/84-90458/1, Oak Ridge National Laboratory (March 1987).

For more information about the research contact:

Solar Energy Research Institute
1617 Cole Boulevard
Golden, CO 80401

NASA Tech Brief
National Aeronautics and Space Administration

Systems Analysis of Advanced Coal-Based Power Plants

Fuel-cell technologies are evaluated and compared with advanced non-fuel-cell alternatives.

A report presents an appraisal of integrated coal-gasification/fuel-cell power plants. The report is based on a study that compared fuel-cell technologies with each other and with coal-based alternatives and recommended the most promising ones for research and development.

The study evaluated the capital cost, cost of electricity, fuel consumption, and conformance with environmental standards. It analyzed the sensitivity of the cost of electricity to changes in fuel cost, to economic assumptions, and to the level of technology.

The following seven of a total of ten types of plants were evaluated:

1. Molten-carbonate fuel cell;
2. Molten-carbonate fuel cell with hot gas cleanup;
3. Internal-reforming, molten-carbonate fuel cell with fluidized bed and hot gas cleanup (Internal reforming converts the higher fraction of methane produced by gasifiers in these plants.);
4. A version of type 3 that recirculates fuel-cell anode exhaust gas to the gasifier and eliminates the need for a separate oxygen feed to the gasifier. (This plant does not use a steam cycle.);
5. Pressurized solid-oxide fuel cell with hot gas cleanup;
6. Phosphoric acid fuel cell; and
7. A version of type 5 with a catalytic gasifier.

The three remaining types of plants, which are alternatives to fuel cells, were considered:

8. Integrated coal gasification, combined cycle, with a 2,200 °F (1,200 °C) turbine;
9. A version of the foregoing with a 2,600 °F (1,400 °C) turbine; and
10. Pulverized-coal-fired combustion with flue-gas desulfurization.

In the analyses, the plant capacity was assumed to be 675 megawatts. The levelized cost of electricity was projected for both 30-year and 10-year plant economic lives, based on a capacity factor of 65 percent.

The projected efficiencies of plants of type 3, 4, and 5 are significantly higher than the efficiencies of the other plants. Type 5 will consume 31 percent less coal than will type 8, for example.

The only fuel-cell plant that has the potential for competing with the low capital costs of the plants (8, 9, and 10), which do not use fuel cells, is type 5. The capital costs of types 2 and 6 are almost 50 percent higher than the equivalent costs for the other plants.

The report recommends further evaluation of integrated coal-gasification/fuel-cell, integrated coal-gasification/combined-cycle, and pulverized-coal-fired plants. The report concludes with appendixes detailing plant-performance models, subsystem-performance parameters, performance goals, cost bases, plant-cost data sheets, and plant sensitivity to fuel-cell performance.

This work was done by Joseph F. Ferrall, Charles N. Jennings, and Alfred W. Pappano of Caltech for **NASA's Jet Propulsion Laboratory**.

"Systems Analysis of Advanced Technology Coal-Based Power Plants," NPO-16842 /TN

FOR ADDITIONAL INFORMATION: *Contact: Director, Technology Transfer Division, P.O. Box 8757, BWI Airport, MD 21240; (301) 621-0100 Ext. 241*

REFER TO THE NUMBER LISTED AT THE END OF THIS ARTICLE

NASA Tech Brief
National Aeronautics and Space Administration

Testing Parabolic-Dish Concentrators

Experience at a solar-energy test site is described.

A report describes test equipment and tests at the Parabolic Dish Test Site at Edwards Air Force Base in California. The site was established in 1978 for testing point-focusing solar concentrators operating at temperatures above 600 °F (315 °C). It was used for six years to evaluate parabolic-dish concentrators, receivers, power-conversion units, and solar/fossil-fuel hybrid units. The report describes the evolution of the test program at the site, lists the experiments conducted there in chronological order, and summarizes the experimental data.

The site was used to check the performances of newly designed subsystems and components, to conduct tests to analyze the effect of independent variables on performance, and to develop rapid optical testing techniques of parabolic-dish concentrators.

The concentrators at the site included the following:

- A precursor concentrator simulating a portion of a parabolic concentrator, used to measure mirror performance and evaluate alignment techniques;
- An electricity-generating-concentrator power module with a two-axis Sun tracker developed by the industry;
- Two test-bed concentrators, 11 m in diameter; and
- A low cost concentrator designed for mass production.

Prior to the tests performed at the site, trackers and concentrators were mechanically checked. The mirror segments were aligned, and solar-tracking errors, mirror-surface reflectances, and moonlight focal-point locations were measured. Radiation fluxes were mapped in the focal zones, and thermal performances of receivers were measured by cold-water calorimeters. Systems were proof tested and leak tested. Performances of power conversion modules were measured.

This work was done by M. Kudret Selcuk of Caltech for **NASA's Jet Propulsion Laboratory**. *Further information may be found in DOE/JPL-1060-84 [N85-28447/NSP], "Parabolic Dish Test Site: History and Operating Experience."*

Copies may be purchased [prepayment required] from the National Technical Information Service, Springfield, Virginia 22161, Telephone No. (703) 487-4650. [A10] NPO-16848 /TN

FOR ADDITIONAL INFORMATION: *Contact: Director, Technology Transfer Division, P.O. Box 8757, BWI Airport, MD 21240; (301) 621-0100 Ext. 241*

REFER TO THE NUMBER LISTED AT THE END OF THIS ARTICLE

Department of Energy

Technology Application

Oak Ridge National Laboratory

MOTOR CURRENT SIGNATURE ANALYSIS PROCESS

Key words: Signature analysis; condition monitoring; motor-operated valves; electrical appliances

A new signature analysis technique developed at ORNL may find widespread application as a means for cost-effective condition monitoring of many types of electric-motor-driven mechanical equipment. Condition monitoring is a technique for anticipating breakdowns in machinery by monitoring and trending equipment condition rather than by performance, much the way a physician monitors blood pressure and pulse rate rather than the speed at which the patient runs or climbs stairs.

ORNL researchers have been studying methods to improve the operational readiness of motor-operated valves (MOVs), a type of valve found in large numbers in nuclear plant safety systems. The researchers have discovered that the electric power leads supplying the motor carry useful diagnostic information related to the valve and operator. The motor current signature analysis (MCSA) method was thus developed to provide a noninvasive means of extracting this valuable information from motor power leads.

The motor current signature was found to contain many types of information useful for condition monitoring. The most striking was the unique frequency spectrum obtained by processing the motor current signature and passing it through a frequency analyzer. This electronic device uses a mathematical operation called the fast Fourier transform to convert the signal from the time to the frequency domain.

The motor current frequency spectrum was found to contain peaks associated with all the periodic load variations encountered by the motor in driving the mechanical equipment. In that regard, the motor itself acts as a transducer, sensing mechanical load variations and converting them into electrical impulses, which are then transmitted down the electric power cable. When quantified and trended with time, this measurement has proven to be a valuable diagnostic tool for determining the operational readiness of MOVs.

The spectra obtained from MCSA are similar in many respects to those obtained from conventional machinery vibration analysis, where accelerometers directly mounted on the housing of the mechanical equipment are used to obtain the spectra. Advantages of MCSA include the use of noninvasive clamp-on current probes as sensors. These sensors can be located anywhere along the power line to the motor, including remote motor control centers. One sensor can detect all mechanical loads, while accelerometers can only sense in one plane.

MCSA can also evaluate fans, centrifugal pumps, and compressors. Figure 1 depicts a schematic of its application to a centrifugal pump. MCSA may also find use as a production-line

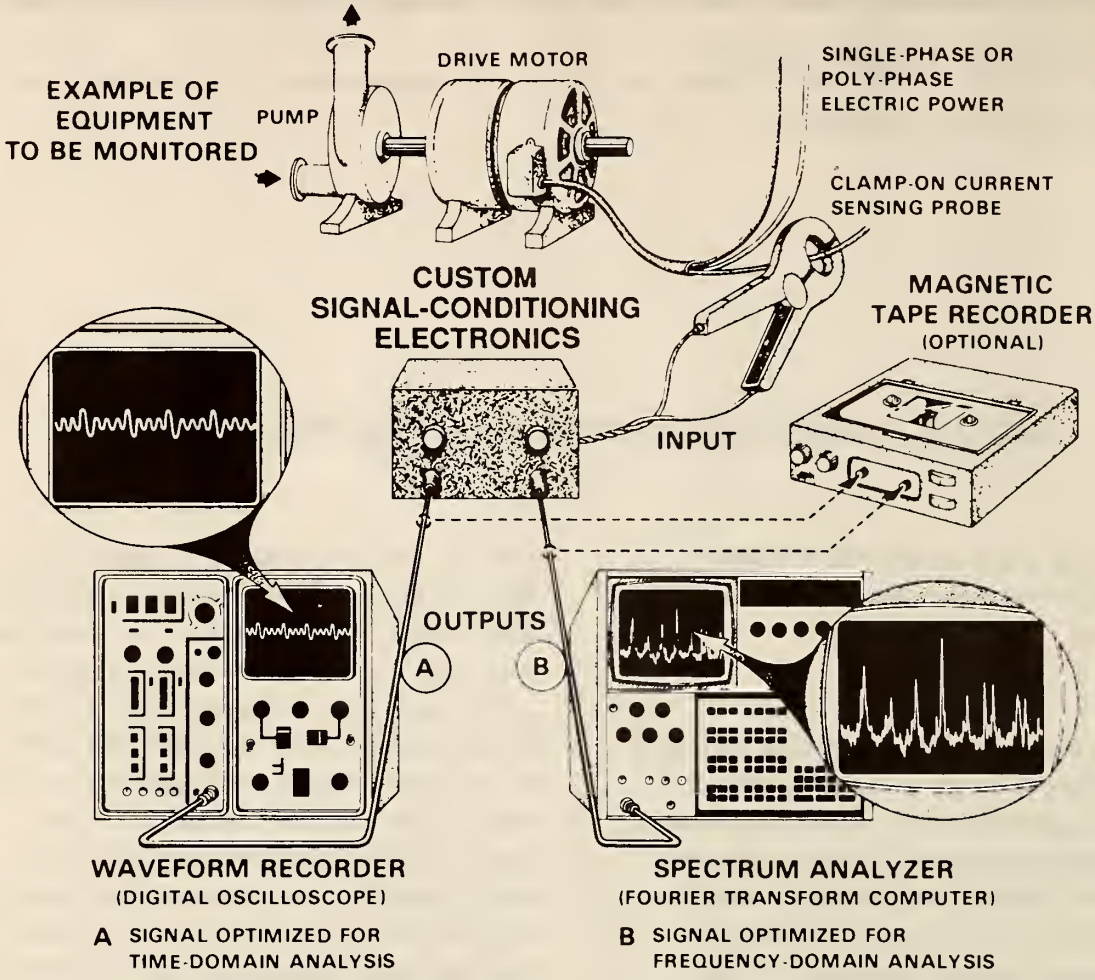

Fig. 1. Schematic of MCSA applied to a centrifugal pump. The output signals obtained in A and B are analyzed and trended with time to determine load changes within the pump and motor that correspond to degradation and service wear and thus provide evidence of incipient failure.

testing tool for motor-driven appliances (e.g., washing machines, heat pumps) and as a method for on-line monitoring of motor-driven production equipment (e.g., rolling mills and shipboard equipment).

Additional information:

Office of Technology Applications
Information Service
Martin Marietta Energy Systems, Inc.
P.O. Box X
Oak Ridge, TN 37831
Telephone: (615) 574-4192; FTS 624-4192

D. M. Eissenberg, "Application of Diagnostics to Determine Motor Operated Valve Operational Readiness," pp. 389-402 in *Fourteenth Water Reactor Safety Information Meeting Held at National Bureau of Standards, Gaithersburg, Maryland, October 27-31, 1986,* comp. A. J. Weiss, Brookhaven National Laboratory, February 1987.

Engineering

568 Acoustical Measurement of Mine-Shaft Length — The length is calculated from the measured resonant frequency. (Licensing Opportunity)

569 Adaptive-Wall Wind Tunnel — Side vents are controlled automatically to compensate for interference by walls. (Licensing Opportunity)

570 Analysis of Flow Across Cylinders — Despite its importance in engineering, the flow/cylinder interaction is understood poorly.

571 Minimum-Time Control Robotic Manipulators — Current Theories are examined critically.

572 Heat Exchanger for Rotating Modular Structures — Heat is transferred efficiently across plates without interstitial fillers. (Licensing Opportunity)

573 Television-and-Laser Range-Measuring System — Triangulation enables the measurement of distances from 1 to 200 ft (0.3 to 60 m). (Licensing Opportunity)

574 Simplified Analysis of Shock Waves — Semiempirical expressions and conventional analyses agree within about 3 percent.

Software

575 Calculating Flows in Multiple-Blade-Element Cascades — Blade shapes and spacings can be varied.

576 Computer Analysis of High-Speed Roller Bearings — Performance of highly stressed bearings are predicted.

577 Computer Program Predicts Turbine-Stage Performance — Complicated three-dimensional and dissipative effects are taken into account.

578 Strain-Energy-Release Rates in Delamination — Failures of composite laminates are analyzed under a variety of loads.

579 Software for Tomographic Reconstruction from Neutron Radiographs

580 REAL-OPS: Real-Time Expert System Control

Testing & Instrumentation

581 Calibrating Nonremovable Pressure Transducers — Units are calibrated en masse in a large pressure chamber. (Licensing Opportunity)

582 Laminar-Boundary-Layer Crossflow Sensor — Crossflow vorticity is detected with nonintrusive electronic sensor elements. (Licensing Opportunity)

Other Items of Interest

607 Super Grip

629 New Acoustic Treatment for Aircraft Sidewalls — Cabin noise is reduced with minimal addition of weight.

631 Unducted-Fan Engine — Counterrotating propellers are directly connected to turbines. (Licensing Opportunity)

632 Aerodynamic-Analysis Programs fr Microcomputers — Lifts, drags, and moments can be calculated for subsonic and supersonic speeds.

NASA Tech Brief

National Aeronautics and Space Administration

Langley Research Center, Hampton, Virginia

Licensing Opportunity

Acoustical Measurement of Mine-Shaft Length

The length is calculated from the measured resonant frequency.

An acoustical system (see figure) has been proposed to measure the depth of a "blind" shaft, such as a mined-out coal seam produced by boring machines, so that the amount of material removed can be determined. Direct optical measurements such as pulsed lasers do not work for shafts that are not straight. An acoustic wave, however, will be guided by the shaft and will provide an estimate of the shaft length, from which the volume can be estimated. This system can also be used for the measurement of any large cylindrical acoustic waveguide, such as a tunnel. The system is based on the generation of standing waves in the shaft, which acts as a waveguide for low-frequency sound waves. The frequency of resonance depends on the velocity of sound in the shaft, the harmonic number selected for measurement, and the length of the shaft.

An acoustic generator, such as a piston mounted on a shaker source, is directed at the accessible end of the mine shaft and set in motion at a specific frequency. A microphone at the source detects the sound from the shaft after the source has stopped. The frequency of the source is electronically adjusted to bring the device to the center of the mechanical resonance. This can be accomplished through a computer-controlled frequency source combined with an acoustic-amplitude detector or with a frequency-modulated source detecting the 180-degree phase shift that occurs at resonance. The frequency is recorded, and the computer-controlled device advances to the next harmonic, performs a measurement, and calculates the frequency difference between resonances, from which the shaft length is determined.

The basic simplified equation for an open pipe is $F_m = mV/2L$ and for a closed pipe is $F_m = mV/4L$, where m denotes the harmonic number, F_m the resonant frequency, V the speed of sound, and L the length. If the frequency of the fundamental, F_1, is measured, then $L = V/4F_1$ for the closed shaft. If the difference in frequency between harmonics is measured, then $L = V/4(F_m - F_{m-1})$. Thus, the measured frequency difference determines the same information as does the fundamental resonance. With this system, either the fundamental or the frequency difference can be used to measure the length of the mine shaft.

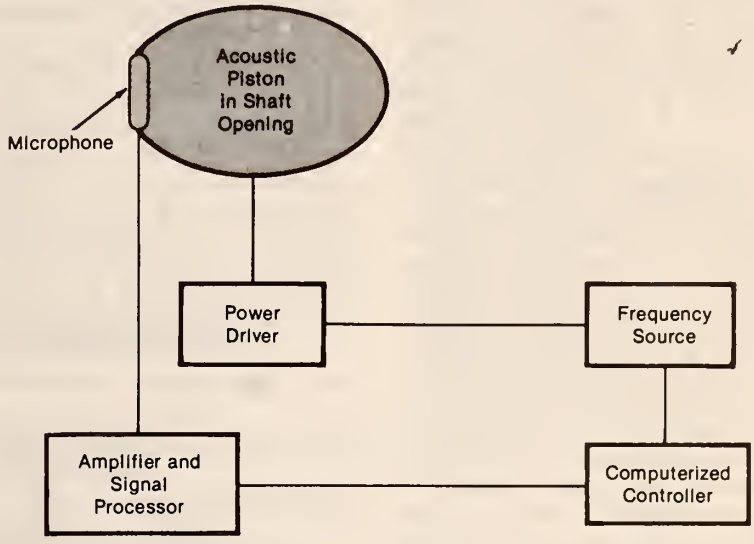

The **Acoustic-Generator System** determines the resonant-frequency difference to measure the shaft length.

This work was done by Joseph S. Heyman of **Langley Research Center**. *No further documentation is available.*

This invention is owned by NASA, and a patent application has been filed. Inquiries concerning nonexclusive or exclusive license for its commercial development should be addressed to the Patent Counsel, Langley Research Center Refer to LAR-13519 /TN

Langley Research Ctr.
Hampton, VA 23665
Technology Utilization Officer: John Samos
Mail Stop 139A
(804) 865-3281
Patent Counsel:
George F. Helfrich
Mail Code 279
(804) 865-3725

FOR ADDITIONAL INFORMATION: *Contact: Director, Technology Transfer Division, P.O. Box 8757, BWI Airport, MD. 21240; (301) 621-0100 Ext. 241*

REFER TO THE NUMBER LISTED AT THE END OF THE ARTICLE

NASA Tech Brief
National Aeronautics and Space Administration
Ames Research Center, Moffett Field, California

Licensing Opportunity

Adaptive-Wall Wind Tunnel

Side vents are controlled automatically to compensate for interference by walls.

An improved test station for the 2- by 2-Foot Adaptive-Wall Wind Tunnel at Ames Research Center is equipped for automatic sensing and correction of the effects of the walls on the airflow in the vicinity of the test model. The new facility is well suited for advanced research and development; for example, tests of airfoils in separated flows and flows with strong shock waves, tests of circulation-control rotors or other exotic airfoils, and detailed airfoil tests to develop computer codes for viscous flows.

Wall-interference-assessment algorithms (see figure) have been written to compute the flow velocities of the free air at designated control points and to compare them with measured velocities. Differences between the measured and computed velocities reflect interference by the walls and are used as control signals to set new wall conditions. The iteration of measurements, calculations, and adjustments continues until the wall-interference velocities are sufficiently small.

The wall conditions are adjusted by blowing air in or sucking air out at various locations on the top and bottom walls. To facilitate the control of inflow and outflow, each adaptive-wall assembly contains 32 cross-stream plenums of various widths. The smallest compartments are placed over the model for fine control. Partial-vacuum and compressed-air lines are connected to the plenums through slide valves that are positioned by computer-controlled stepping motors to provide the required amount of injection or withdrawal or to block the flow.

The side walls of the test section consist of schlieren-quality glass mounted in hinged frames. The window frames can be swung open to give access to the tunnel for installation of the model. A hole in each window is used to mount the model. The windows provide optical access for a fast-scan laser velocimeter and for a holographic interferometer to be installed subsequently.

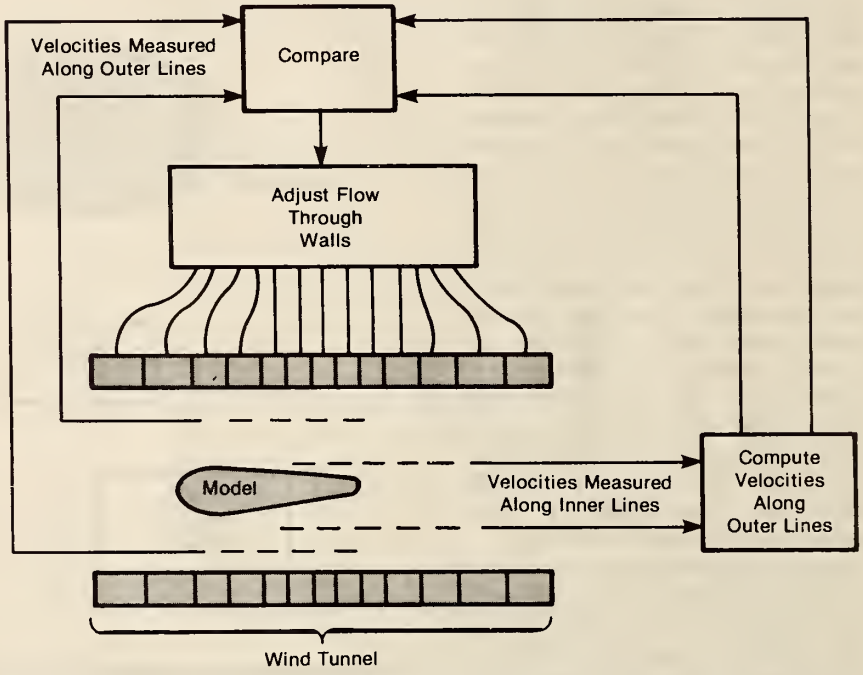

Velocities Measured Along Lines Near the Model are used to calculate the velocities that would be observed along lines farther from the model if the model were in free air. These calculated values are compared with velocities measured along the farther lines.

The laser velocimeter system measures the velocities for the wall-interference-assessment algorithm. A 5-W argon laser and its associated optics on an external table generate a matrix of four beams with two colors. A transmitting scanner driven by computer-controlled motors aims the laser beams to position the measurement volume at each measurement point along the center line of the tunnel. For automatic alignment, the beam-steering mirrors are driven by motors in response to control inputs from light sensors. The light scattered from the measurement volume strikes a retroreflector, which returns it along the path of incidence to the optical table for color separation and processing.

This work was done by Daniel G. Morgan and George Lee of **Ames Research Center**.

Inquiries concerning rights for the commercial use of this invention should be addressed to the Patent Counsel, Ames Research Center Refer to ARC-11717/TN

Ames Research Ctr.
Moffett Field, CA 94035

Technology Utilization Officer: Laurance Milov
Mail Code 223-3
(415) 694-6370

Patent Counsel: Darrell G. Brekke
Mail Code 200-11
(415) 694-5104

FOR ADDITIONAL INFORMATION: *Contact: Director, Technology Transfer Division, P.O. Box 8757, BWI Airport, MD. 21240; (301) 621-0100 Ext. 241*
REFER TO THE NUMBER LISTED AT THE END OF THE ARTICLE

NASA Tech Brief
National Aeronautics and Space Administration

Analysis of Flow Across Cylinders

Despite its importance in engineering, the flow/cylinder interaction is understood poorly.

A report reviews various experimental, theoretical, and numerical methods of analysis of the interactions between a fluid and one or more cylinders across which it flows. This is a topic of extreme importance in engineering: tubes subject to crossflow are found in heat exchangers, chimneys, aircraft, offshore platforms, and marine towing cables, for example. The flows cause these structures to vibrate, and the vibrations alter the flow fields, so that the flows and the vibrations are strongly coupled. An understanding of flow/cylinder interactions is necessary for the prediction of vibration-induced failures and for design to avoid such failures.

The review begins with a discussion of the mechanisms that induce vibrations in nests of cylinders. The best understood mechanisms are vortexes, fluctuations of pressure caused by turbulence, and fluidelastic or aeroelastic instabilities, which are fully-coupled cooperative motions of the fluid and all the tubes in a structure. Other less-well-understood mechanisms include aeroacoustic noise, oscillating mean free-stream velocity, and jet switching. In connection with these mechanisms, there is a discussion of equations derived through physical arguments or mathematical modeling, with empirically determined coefficients; recent developments in the semianalytical/seminumerical modeling of vibrations due to multiple mechanisms; and accumulated experimental data that serve as guides for the design of banks of tubes.

A major portion of the review is devoted to methods for the numerical analysis of flow/cylinder interactions. Numerical analysis is essential because the nonlinearities inherent in such interactions preclude closed-form solutions of the equations of motion. A typical approach would involve the numerical solution of the Navier-Stokes equations with an appropriate model for turbulence. This solution would include the pressure distribution and skin friction on the surface of the structure, from which one could solve iteratively the equations for vibration. The vibration-inducing mechanisms could be obtained as part of the numerical solution.

The discussion of numerical analysis covers the following topics:

- Interactions between solid objects and laminar flows;
- Interactions between solid objects and turbulent flows;
- Mathematical models of turbulence;
- Vibrations in structures with small, large, or permanent deformations; and
- Flow through a nest of cylinders.

The author concludes that despite its importance in engineering and despite recent progress in numerical modeling, the understanding of the flow/cylinder interaction is still quite limited, and designs of banks of tubes still depend mostly on experiments or on equations with experimentally determined coefficients. A yet-to-be-developed numerical method powerful enough for the simulation of general flow/cylinder interactions will probably involve improved models for turbulence, finite-element and finite-difference computational techniques, nonlinear structural-analysis techniques, and existing analytical methods applicable to laminar and turbulent flow/solid interactions.

This work was done by Sang-Wook Kim of **Marshall Space Flight Center**. *Further information may be found in NASA CR-178996 [N87-18781/NSP], "A Critical Evaluation of Various Methods for the Analysis of Flow-Solid Interaction in a Nest of Thin Cylinders Subjected to Cross Flows."*

Copies may be purchased from the National Technical Information Service, Springfield, Virginia 22161, [A05]

MFS-27180 /TN

FOR ADDITIONAL INFORMATION: *Contact: Director, Technology Transfer Division, P.O. Box 8757, BWI Airport, MD. 21240; (301) 621-0100 Ext. 241*

REFER TO THE NUMBER LISTED AT THE END OF THE ARTICLE

NASA Tech Brief
National Aeronautics and Space Administration

Minimum-Time Control for Robotic Manipulators

Current theories are examined critically.

A report surveys the state of the art in the theory of minimum-time control of robotic manipulators. It discusses some of the promising developments, pointing out, however, that the optimal-control problem in its full generality remains unsolved. It compares the various solution methods, indicating their merits and flaws.

The discussion begins with a brief overview of the field. Because analytic solutions are not possible except for the simplest of robot configurations, many approaches based on iterative/gradient-type algorithms have been proposed. Each is based mainly on one of the following ideas:

1. Analyze the two-point boundary-value problem derived from the maximum principle.
2. Assume some parametric form of the solution and optimize the parameters.
3. Iteratively modify the performance index so that the solutions of the easier optimization problem converge to the optimal one.

To date, none of these algorithms has exhibited consistent convergence over a wide class of robots. This situation has given rise to suboptimal solution methods based on linearization of the nonlinear dynamic equation.

The report discusses some qualitative aspects of the minimum-time control problem. It begins by applying the variation principle to obtain the equation of motion in generalized-momentum form. After stating the control objective in terms of time optimality, it presents derivations of four theorems, including simpler derivations of two key results that have appeared recently in the literature.

Next, the report reviews the variety of computational approaches that have been applied to the optimal-control problem. The author notes that the source of difficulty has been the possible existence of singular arcs and that the singular-perturbation approach offers promise as a remedy.

This is followed by a review of suboptimal algorithms. Special mention is accorded to the double-integrator algorithm based on the exact linearizing transform. The advantages of this scheme are the following:

1. It computes efficiently the exact linearizing torque.
2. The travel time is computable a priori and can be used to size the actuators.
3. The scheme is robust against sampling delay in control and against modeling errors.

This work was done by John T. Wen of Caltech for **NASA's Jet Propulsion Laboratory**. *To obtain a copy of the report, "On Minimum Time Control for Robotic Manipulators," NPO-17070 /TN*

FOR ADDITIONAL INFORMATION: *Contact: Director, Technology Transfer Division, P.O. Box 8757, BWI Airport, MD. 21240; (301) 621-0100 Ext. 241*
REFER TO THE NUMBER LISTED AT THE END OF THE ARTICLE

NASA Tech Brief
National Aeronautics and Space Administration
Marshall Space Flight Center, Alabama

Licensing Opportunity

Heat Exchanger for Rotating Modular Structures

Heat is transferred efficiently across plates without interstitial fillers.

A heat exchanger transfers heat from one structure to another while accommodating rotary motion of the structures. Developed for modular space stations, the heat exchanger can be adapted to the transfer of fluids and heat across the joints of machine tools and robot arms and to the flow of coolant through portable electronic equipment.

In the heat exchanger (see Figure 1), the hot fluid from one structure flows through the middle one of the three heat-exchanger panels. The cold fluid from the second structure flows through the two outer panels. Fins inside the panels promote the transfer of heat between the circulating fluid and the panel surfaces. Thus, heat flows from the center panel to the outer panels and is carried off by the cold fluid.

Ordinarily, contacting surfaces must be very flat for efficient heat transfer between panels. Even when they are carefully manufactured for flatness, mechanical fasteners warp the surfaces when the panels are assembled, and the contact area may then be considerably smaller that of the surface areas. Often, interstitial materials such as grease or foil have to be used to increase thermal conductance.

The new heat exchanger avoids these problems because the inner surfaces of the outer panels are flexible and act as diaphragms. When the fluid in an outer panel is pressurized even slightly, the pressure forces its working surface to conform to the mating surface of the middle panel. Any additional pressure in the outer panels merely increases the contact pressure, driving the contact thermal resistance down and increasing the rate of heat transfer across the interface. The heat-transfer rate can therefore be adjusted by changing the pressure of the fluid in the outer panels.

The cold fluid can be a two-phase medium that condenses in the outer panels. An increasing heat load causes the pressure in the outer panels to rise and thereby increase the contact conductance and the heat-transfer rate.

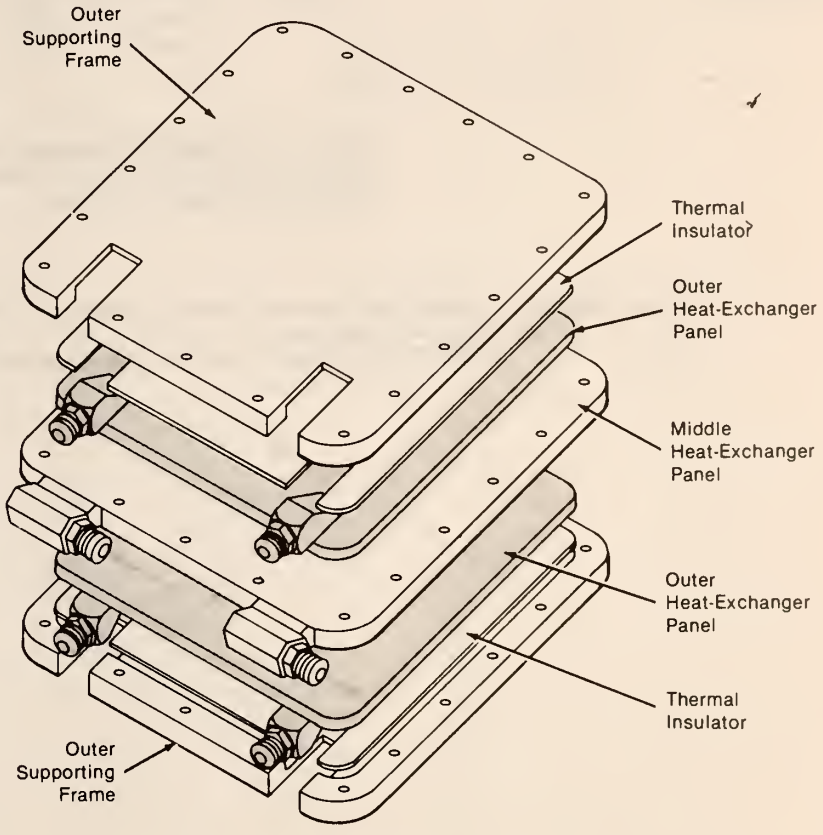

Figure 1. **Flat-Panel Heat Exchanger** passes heat from the fluid in its middle panel to the fluid in its outer panels. The diaphragmlike outer panels swell to conform to the surfaces of the middle panel, ensuring thermal contact.

A rotating joint carries fluid to and from either the outer panels or the middle panel. The joint is an in-line axial-flow unit that can rotate freely (see Figure 2). The internal flow passages are concentric to the center of rotation, so that the same housing can accommodate both the supply and return flows.

Because the heat-exchanger panels can be disconnected from each other without disconnecting any fluid lines, the two connecting structures can be thermally coupled or decoupled without the loss of fluid. Before disconnection, it is necessary only to depressurize the outer panels to prevent the diaphragms from bursting. Once the panels are reconnected, they can be repressurized when heat transfer is needed.

This work was done by William E. Clark of Applied Technology Association for **Marshall Space Flight Center**.

In accordance with Public Law 96-517, the contractor has elected to retain title to this invention. Inquiries concerning rights for its commercial use should be address-

ed to

William E. Clark
Applied Technology Association
401 Hyder St., N.E.
Palm Bay, FL 32907

Refer to MFS-26037, /TN

George C. Marshall Space Flight Center
Marshall Space Flight Center, AL 35812
Technology Utilization Officer: Ismail Akbay
Code AT01
(205) 544-2223
Patent Counsel: Leon D. Wofford, Jr.
Mail Code CC01
(205) 544-0024

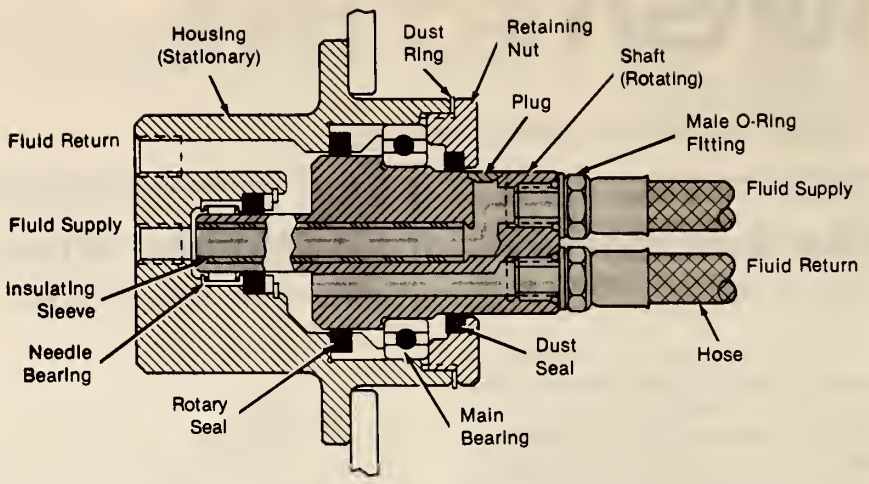

Figure 2. The **Rotary Fluid Coupling** provides a connection for both supply fluid and return fluid. The flexible hoses that carry fluid to and from the coupling accommodate the tilt of one structure with respect to the other.

FOR ADDITIONAL INFORMATION: *Contact: Director, Technology Transfer Division, P.O. Box 8757, BWI Airport, MD. 21240; (301) 621-0100 Ext. 241*

REFER TO THE NUMBER LISTED AT THE END OF THE ARTICLE

NASA Tech Brief
National Aeronautics and Space Administration
Lyndon B. Johnson Space Center, Houston, Texas

Licensing Opportunity

Television-and-Laser Range-Measuring System

Triangulation enables the measurement of distances from 1 to 200 ft (0.3 to 60 m).

A triangulation system measures the angle between two lines of sight to a point on an object, thereby determining the distance to the object. Unlike older triangulation-type ranging devices, this system is amenable to automation.

The system (see figure) is mounted on an optical platform. A charge-coupled-device (CCD) camera views the object along two lines of sight emanating from the opposite ends of a stereo arm. The lines of sight are oriented by two rotatable mirrors, the angular positions of which are controlled by stepping motors. A light beam from a helium/neon laser is directed by mirrors and a beam splitter along the line of sight in optical channel 1. Thus, the reflection of the laser light from the object, as seen in channel 1, appears at the center of the CCD image at any range. The laser reflection is also seen through channel 2, but initially it may not be at the center.

The optical platform is rotated to bring the object into the view of the CCD in both channels. A 633-nm narrow-band-pass filter placed over the central portion of the CCD allows only the laser light to figure prominently near the center. The rotatable mirrors are adjusted alternately until the lines of sight intersect, as indicated by the convergence of both laser spots at the center of the CCD. The stepping-motor sequence is automatically controlled to vary the convergence angle, $\theta_1 + \theta_2$, in increments of 0.001°, and so that θ_1 does not differ from θ_2 by more than 0.001°.

The camera is focused automatically. A servocontrol loop samples the video signal from the picture elements in the central region and activates a camera-focusing stepping motor to maximize the signal peak at the center.

Since the automatic control system continues to aim the platform and mirrors to maintain convergence, the system provides a continuous reading of the half convergence angle, $\theta = \theta_1 = \theta_2$. Then the distance, R, between the object and the optical center of the stereo arm is given by $R = (d/2)\csc\theta$, where d is the length of the stereo arm as shown on the figure. The approach or recession speed, V, of the object can also be calculated in terms of θ_1, the

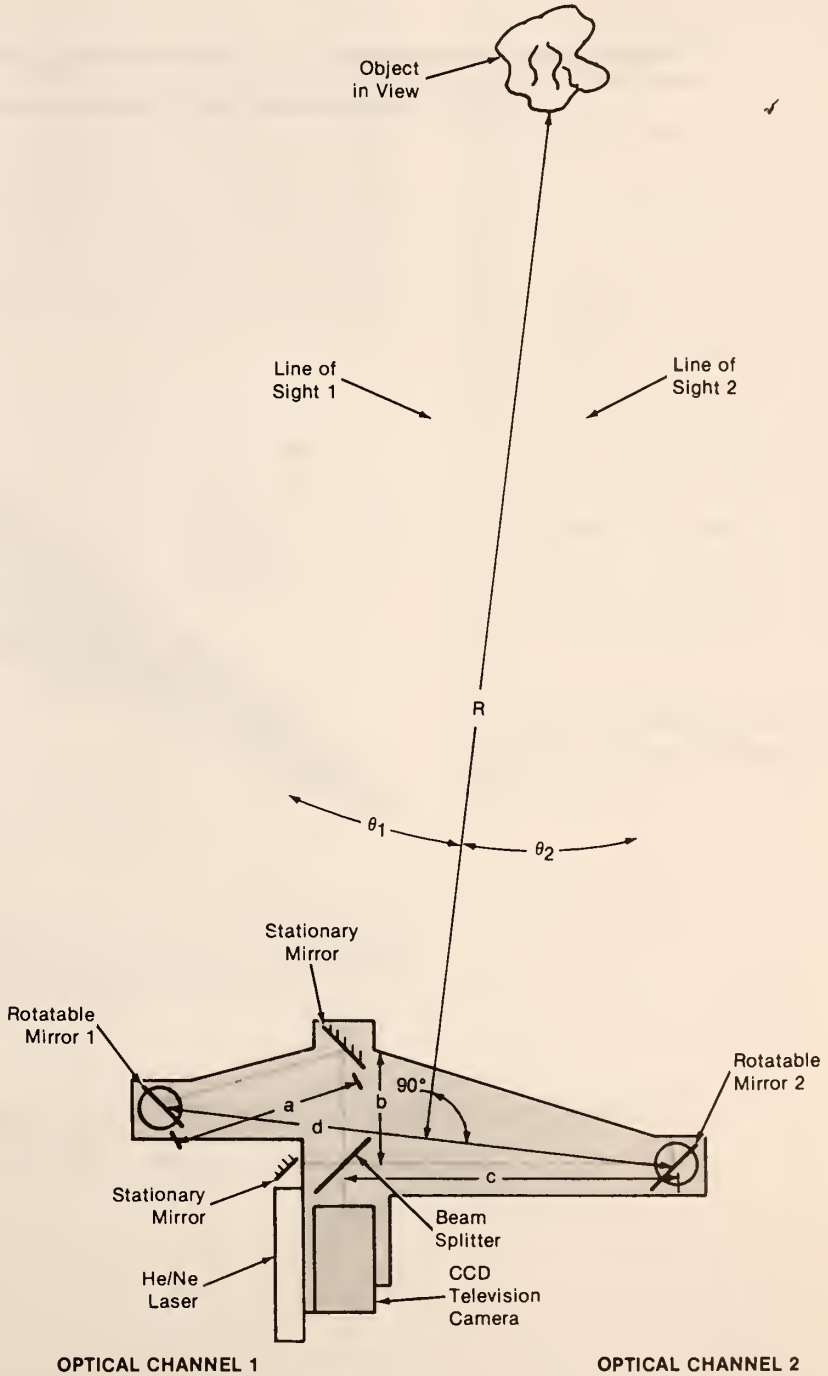

The **Triangulation System** includes automatically aimed rotatable mirrors and a laser beam to define one of the lines of sight. The system adjusts itself automatically to bring the two lines of sight into convergence at a common point on the object.

rate of change of θ, using $V = -(d/2)\,\theta \cot\theta \csc\theta$.

This work was done by J. Kevin Russell of Lockheed Engineering and Management Services Co. Inc., for **Johnson Space Center**.

This invention is owned by NASA, and a patent application has been filed. Inquiries concerning nonexclusive or exclusive license for its commercial development should be addressed to the Patent Counsel, Johnson Space Center
Refer to MSC-20867/TN

Lyndon B. Johnson Space Center
Houston, TX 77058
Technology Utilization Officer: Dean C. Glenn
Mail Code EA4
(713) 483-3809
Patent Counsel: Edward K. Fein
Mail Code AL3
(713) 483-4871

FOR ADDITIONAL INFORMATION: *Contact: Director, Technology Transfer Division, P.O. Box 8757, BWI Airport, MD. 21240; (301) 621-0100 Ext. 241*
REFER TO THE NUMBER LISTED AT THE END OF THE ARTICLE

NASA Tech Brief
National Aeronautics and Space Administration
Lyndon B. Johnson Space Center, Houston, Texas

Simplified Analysis of Shock Waves

Semiempirical expressions and conventional analyses agree within about 3 percent.

A set of semiempirical formulas enables the direct calculation of supersonic and hypersonic shock-wave parameters without the use of iterative procedures. Formulas are provided for calculating shock deflection angle (see figure) and the downstream static pressure and enthalpy over the mach number range of 2 to 25. A relationship describing the thermodynamic behavior of partially dissociated air has also been developed.

Conventionally, such shock-wave parameters are determined by using iterative procedures to find a simultaneous solution of the continuity, momentum, and energy equations, the thermodynamic equation of state, and a shock-wave angle equation. The new formulas are derived from semiempirical data based on observations and experience and from comparisons with analytical data using conventional analysis techniques. Over a wide variety of flight conditions, results from the new equations agree with those from conventional analyses within about 3 percent. The new results also compare favorably with actual pressure data from a Space Shuttle orbiter flight.

The first of the new formulas gives the shock deflection angle as a function of the freestream mach number and the tangent of the angle of attack. The second formula gives the downstream static pressure as a function of the aforementioned quantities and of the freestream static pressure. The third formula gives the downstream static enthalpy as a function of the previously calculated shock deflection angle and the freestream airspeed. Finally, a set of four equations gives the relationships among the downstream temperature, kinetic specific heat, and dissociation level, as functions of the previously calculated downstream static enthalpy and pressure. The equations will be useful to the aircraft industry and in wind-tunnel and plasma-arc testing.

This work was done by Wilmer E. Neuenschwander of Rockwell International Corp. for **Johnson Space Center**.
MSC-20738 /TN

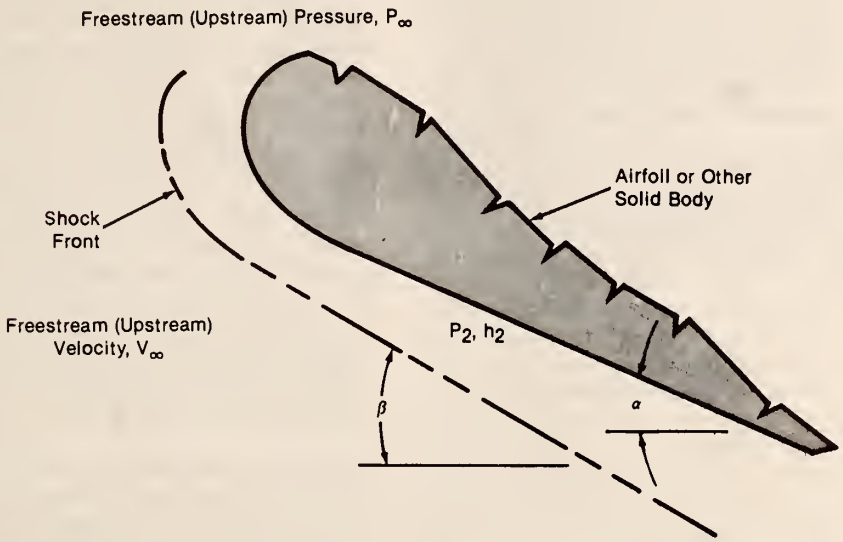

The **Shock-Wave Parameters,** including the downstream pressure (P_2), downstream enthalpy (h_2), and the shock deflection angle (β), are approximated closely by semiempirical equations in terms of the upstream quantities and the angle of attack (α).

FOR ADDITIONAL INFORMATION: *Contact: Director, Technology Transfer Division, P.O. Box 8757, BWI Airport, MD. 21240; (301) 621-0100 Ext. 241*
REFER TO THE NUMBER LISTED AT THE END OF THE ARTICLE

Calculating Flows in Multiple-Blade-Element Cascades

Blade shapes and spacings can be varied.

A computer code has been written to analyze flows on blade-to-blade surfaces of turbomachinery. The code can analyze rows that contain blades of several different shapes and/or spacings. This capability makes the code useful for calculating flows in centrifugal machinery with splitter blades or in mistuned blade rows, where the blade spacing varies.

The number of varying blade shapes that can be used in a blade-row design is not limited by the code. However, the amount of computer storage available does impose a practical limit on any problem. The code described here is dimensioned to handle from one to four bodies in cascade. After redimensioning, this same code can be used to calculate a flow problem with as many as 15 bodies.

The code solves approximate governing equations for blade-to-blade, steady-state flow problem in turbomachinery. The effects of compressibility, radius change, blade-row rotation, and variable streamsheet thickness are included. The working fluid is assumed to be inviscid, irrotational, and a perfect gas. The code can also handle flows of incompressible fluids. Overall, the code produces good results for subsonic flow, but the accuracy decreases for high subsonic and supersonic flows.

The multiple-body-panel code is written primarily in FORTRAN IV and uses double-precision arithmetic. Storage for the four-body version of the code is approximately 650,000 words when run in double precision. A typical running time for the code on the central processing unit (CPU) of the IBM 370/3033 computer at NASA Lewis Research Center is 25 s. A slightly different version of the code, which runs on the CRAY IS computer at NASA Lewis Research Center, requires less than 5 s of CPU time per run.

This program was written by Eric F. McFarland of **Lewis Research Center**. *LEW-14359 /TN*

FOR ADDITIONAL INFORMATION *CONTACT:*

COSMIC®
112 Barrow Hall
University of Georgia
Athens, GA 30602
(404) 542-3265

Computer Analysis of High-Speed Roller Bearings

Performances of highly stressed bearings are predicted.

The engine performance that will satisfy the anticipated efficiency, speed, and specific-thrust requirements for aircraft in the coming decade places increased demands on the performances of engine components. Engines will be required to operate at high temperatures and speeds while maintaining low overall mass and high structural integrity. Bearings, in particular, emerge as critical elements of system design for the new engines.

The high-speed cylindrical roller-bearing analysis program (CYBEAN) was developed to compute the behavior of cylindrical rolling-element bearings at high speeds and with misaligned shafts. With CYBEAN, an accurate assessment of geometry-induced roller preload is possible for a variety of outer-ring and housing configurations and loading conditions. CYBEAN enables detailed examination of bearing performance and permits exploration of the causes and consequences of bearing skew. CYBEAN provides a general capability for the assessment of designs of bearings that support the main shafts of engines.

CYBEAN is structured as a software tool for the analysis of bearings, involving the coordinated execution of modules that perform specific analytic tasks. The bulk of the calculations performed by CYBEAN consist of the repetitive computation of displacements and forces resulting from solid/solid and solid/fluid interactions. These interactions are permitted to occur in a thermally varying environment and are viewed as part of a system in quasi-static thermodynamic equilibrium.

The system is defined by geometric and material descriptions of the bearing complement and the rheology of the lubricant used. The system is considered to be driven by external forcing functions that consist of a constant vector set representing definitions of shaft rotation, speed, and applied radial force. Additional system stimulation is accepted from heat generated within the boundaries of the defined system volume.

Once the configuration and the material properties are defined, specific interaction mechanisms are used to determine the set of field equations for the equilibrium of forces. Solid/solid interactions are used to calculate contact stresses, contact sizes, and associated elastic forces. Solid/fluid interactions are used to determine raceway/rolling element tractions, flange/rolling element tractions, roller drags, and cage-related frictions. The completion of the detailed interaction mechanisms enables the generation of the equations of the equilibrium of quasi-dynamic forces. A Newton-Raphson iterative procedure is used to solve the equations. A Lundberg-Palmgren method is employed to compute the fatigue life of the bearing. Thermal effects on the system can be computed in either a steady or transient mode.

The input to CYBEAN consists of the bearing configuration, material properties, and imposed operating conditions. The output includes evaluated lubricant data, geometric and fit information, cage forces, speeds, maximum contact stresses, lubricant-film thicknesses, roller tilt and skew angles, and the temperature distribution for the complete nodal network.

The CYBEAN program is written in FORTRAN IV for batch execution and has been implemented on a UNIVAC 1100 computer operating under EXEC 8 with a segmented-memory requirement of approximately 91K of 36-bit words. CYBEAN has also been implemented on a CRAY series computer operating under COS. CYBEAN was developed in 1978. The UNIVAC version was last updated in 1981, and the CRAY version was released in 1986.

This program was written by H. Coe of **Lewis Research Center**.
LEW-14512 /TN

FOR ADDITIONAL INFORMATION *CONTACT:*

COSMIC®
112 Barrow Hall
University of Georgia
Athens, GA 30602
(404) 542-3265

Computer Program Predicts Turbine-Stage Performance

Complicated three-dimensional and dissipative effects are taken into account.

The MTSBL computer program for predicting the performances of turbine stages accounts for the effects of complex passage configurations. MTSBL is an updated version of the flow-analysis programs MERIDL and TSONIC coupled to the boundary-layer program BLAYER.

The method uses a quasi-three-dimensional, inviscid, stream-function flow analysis iteratively coupled to calculated losses so that changes in losses result in changes in the flow distribution. In this manner the effects of both the configuration on the flow distribution and the flow distribution on losses are taken into account in the prediction of the performance of a stage.

Boundary-layer analyses account for losses due to friction. Empirical loss models are used to account for incidence, secondary flow, disk windage, and clearance losses. Each boundary-layer analysis is performed using BLAYER. The results of the boundary-layer analyses are used to determine profile and end-wall friction losses. These losses, plus additional losses calculated from empirical models, are used to calculate the efficiencies of stators, rotors, and stages. The analysis has been applied to both axial and radial turbines.

This program has evolved over time, and a number of references should be consulted to determine the method used for the solutions. Also included is a reference that shows the specific application of the analysis to the design of a radial turbine and would be helpful in the analysis of a radial or mixed-flow machine.

The input required to analyze a blade row by use of MTSBL is only slightly more than is required to do the hub-to-shroud flow analysis for a blade row using the program MERIDL. A control block of information using a namelist input is entered prior to the data for MERIDL. The significance of all of the variables that can appear in the control block is described in the beginning of the program listing.

The program is written in FORTRAN IV for use on an IBM 3033 computer.

This program was written by Robert J. Boyle, Jeffrey E. Haas, and Theodore Katsanis of **Lewis Research Center.**
LEW-14218 /TN

FOR ADDITIONAL INFORMATION
CONTACT:

COSMIC®
112 Barrow Hall
University of Georgia
Athens, GA 30602
(404) 542-3265

Strain-Energy-Release Rates in Delamination

Failures of composite laminates are analyzed under a variety of loads.

The Q3DG computer program was developed to perform a quasi-three-dimensional stress analysis of composite laminates that may contain delaminations. Delamination may result from low-velocity impacts, eccentricities in load paths that induce out-of-plane loads, or discontinuities in the structure that create out-of-plane stresses. Q3DG calculates the strain-energy-release rates for long, rectangular composite laminates containing delaminations and subjected to any combination of mechanical, thermal, and hygroscopic loading.

Q3DG uses a quasi-three-dimensional analysis in conjunction with concepts of linear fracture mechanics and fininte-element methods. Total strain-energy-release rates can be calculated by the use of the classical theory of laminated plates. Finite-element analysis is used to separate the total strain-energy-release rates into the three components associated with the three modes of fracture (opening mode, sliding mode, and tearing mode). Special eight-noded parabolic isoparametric elements are used to model the laminates. A rectangular-mesh and data-file-generator capability is included with the package. The input to Q3DG includes data on the geomerty, material, and loading of the composite object. The output includes nodal forces, nodal stresses, nodal displacements, stiffness matrix, and strain-energy-release rates for each fracture mode (including percentages and cross-terms).

The Q3DG program is written in FORTRAN V for batch execution and has been implemented on a CDC Cyber 170-series computer with a central-memory requirement of approximately 343K of 60-bit words. The mesh and data-file generator can be run interactively. This program was developed 1985.

This program was written by I. S. Raju of Analytical Services and Materials, Inc., for **Langley Research Center**.

LAR-13698 /TN

FOR ADDITIONAL INFORMATION *CONTACT:*

COSMIC®
112 Barrow Hall
University of Georgia
Athens, GA 30602
(404) 542-3265

TECHNOLOGY PROFILES

Bringing Argonne Research and Development to Industry

03-03-0188

Software for Tomographic Reconstruction from Neutron Radiographs
Noninvasive, nondestructive examination

Software developed at Argonne National Laboratory enables a user to reconstruct cross-section images (including internal configuration details) of any object that can be neutron-radiographed. The end product is a set of computer-constructed color graphics. This means that there is a noninvasive, nondestructive alternative to the usual destructive examination of the object. The tomographic technique could eliminate the need for some time-consuming and destructive post-test or post-failure examinations. Further, where destructive examination is required, the tomographic technique can enhance the interpretation of destructive examination results.

Future applications might cover objects that might be X-rayed normally, but are not amenable to a tomographic X-ray reconstruction because of size, shape, or location. The only limits on the use of this technique might be the limits of resolution. Although no tests have been made to determine the ultimate limits of resolution with the digitized radiographs that are available, the ability to resolve wire 0.040 inches in diameter and tubing 0.230 inches in diameter with a wall thickness of 0.015 inches provides a benchmark of the present-day resolution capability of the technique. Also it is possible to distinguish between materials of similar densities, such as steel and uranium dioxide.

Additional Information

Key Words: tomography, neutron radiographs, nondestructive examination

Patent Status: Not patented.

Potential Applications/Spinoffs: Noninvasive study of the internal detail of objects that can be neutron-radiographed and for which the resolution achieved is adequate.

For More Information: Contact the Technology Transfer Center, 9700 S. Cass Ave., Argonne, IL 60439 (312/972-7694).

REAL-OPS: REAL-TIME EXPERT SYSTEM CONTROL

Key words: Expert system; software; real-time control; multitasking; asynchronous control; OPS5

REAL-OPS is real-time expert systems software for engineering applications. This product extends and enhances Carnegie-Mellon's OPS5 expert system language for real-time, multitasking, asynchronous control problems in which complexity demands expert-system technology but where time and data-access constraints preclude use of the technology as it is traditionally applied. This system's most radical improvement over the standard version of OPS5 is the capability for asynchronous data entry from the real world via the IEEE-488 instrument bus.

REAL-OPS was developed for real-time control applications where rapid response of expert-systems applications software features (e.g., rules and pattern matching) are required. It can also be used for coordinating multiple software programs via an expert system or for interactively developing an OPS5 expert system.

With the recent introduction of high-speed microprocessors, other applications are also possible. For example, REAL-OPS can be used to control dedicated, on-board systems executing at thousands of rules per second (e.g., autonomous vehicles).

REAL-OPS is unique. It is the first product for a real-time control system to address both the issues of complexity and rapid response in a coherent, integrated fashion. REAL-OPS is not only fast, it also is compact. A complete control system having, for example, 2000 rules, 5000 data elements, graphics display, user-written I/O, and control algorithms will easily fit into a desktop computer having a 1-MB memory.

REAL-OPS is designed for rapid prototyping in that it provides the user with incremental compilation and interactive programming with immediate error recovery.

Additional information:

Office of Technology Applications
Information Service
Martin Marietta Energy Systems, Inc.
P.O. Box X
Oak Ridge, TN 37831
Telephone: (615) 574-4192; FTS 624-4192

W. B. Dress, "AI Goes Forth," *Telematics and Informatics* 3(3), 191-7 (1986).

W. B. Dress, "A Real-Time Expert Systems Language for Engineering Applications," pp. 290-93 in *IEEE Proceedings of the Eighteenth Southeastern Symposium on System Theory, April 7-8, 1986, Knoxville, Tenn.*, IEEE Computer Society, Washington, D.C., 1986.

W. B. Dress, "Communicating Asynchronous External Data to Expert Systems," pp. 294-96 in *IEEE Proceedings of the Eighteenth Southeastern Symposium on System Theory, April 7-8, 1986, Knoxville, Tenn.*, IEEE Computer Society, Washington, D.C., 1986.

NASA Tech Brief
National Aeronautics and Space Administration

Licensing Opportunity

Calibrating Nonremovable Pressure Transducers

Units are calibrated en masse in a large pressure chamber.

A report describes a supplementary calibration procedure for pressure transducers. The method was developed for transducers that cannot be removed without damage — in particular, for transducers hard-mounted in a helicopter rotor blade for aerodynamic and acoustic measurements. The entire blade and its 188 pressure transducers are enclosed in a chamber in which their responses to known pressures and temperatures are measured.

The standard calibration procedure for pressure transducers is to place them individually in a small vacuum chamber and measure their responses. The new calibration supplements this initial calibration for units that cannot be recalibrated individually. In fact, it identified 15 units in the helicopter blade that had changed beyond acceptable limits.

The calibration was carried out in an environmental chamber 23 ft (7 m) long — 3 ft (0.9 m) longer than the rotor blade. A ribbon cable carried sensor signals through the seal around the chamber door. Leakage through the seal was compensated by pumping air out of the chamber at the rate at which air leaked in. A pressure range of 400 to 760 torr (53 to 101 kPa) could be achieved in the chamber with this arrangement.

The chamber was pumped down in 50-torr (6.7-kPa) increments. At each pressure step, readings of the transducer outputs were recorded manually by dialing through a rotary switch connected to the units through the ribbon cable. The numerical results were used as input for a computer analysis of errors.

This work was done by Michael E. Watts of **Ames Research Center**. *Further information may be found in NASA TM-88312 [N87-12830/NSP], "Supplementary Calibration Test of the Tip-Aerodynamics- and Acoustics-Test Pressure Transducers."*

Copies may be purchased [prepayment required] from the National Technical Information Service, Springfield, Virginia 22161, [A03]

Inquiries concerning rights for the commercial use of this invention should be addressed to the Patent Counsel, Ames Research Center
Refer to ARC-11792. /TN

Ames Research Ctr.
Moffett Field, CA 94035
Technology Utilization Officer: Laurance Milov
Mail Code 223-3
(415) 694-6370
Patent Counsel:
Darrell G. Brekke
Mail Code 200-11
(415) 694-5104

FOR ADDITIONAL INFORMATION: *Contact: Director, Technology Transfer Division, P.O. Box 8757, BWI Airport, MD. 21240; (301) 621-0100 Ext. 241*
REFER TO THE NUMBER LISTED AT THE END OF THE ARTICLE

NASA Tech Brief
National Aeronautics and Space Administration
Langley Research Center, Hampton, Virginia

Licensing Opportunity

Laminar-Boundary-Layer Crossflow Sensor

Crossflow vorticity is detected with nonintrusive electronic sensor elements.

The accurate determination of both the location and the cause of the boundary-layer transition from a laminar to a turbulent flow is important in basic research, for the validation of theory, and in developmental testing for validation of design. The laminar-boundary-layer crossflow sensor provides a means for remotely detecting the presence of crossflow vorticity in a laminar boundary layer.

A boundary-layer flow on a three-dimensional surface (such as a wing with a sweep or nonaxisymmetric fuselage) is formed with one velocity component in the direction of and one normal to the external flow. The resultant velocity profile is inflected in a fashion that creates vorticity in the boundary layer. If this boundary layer is laminar, the vortexes that form in the streamwise direction can grow in strength, eventually causing transition to turbulence. Large variations in local heat transfer and skin friction exist in the lateral direction normal to the vortex cores. Crossflow vorticity, therefore, may be detected using a method for sensing these variations of heat transfer or skin friction.

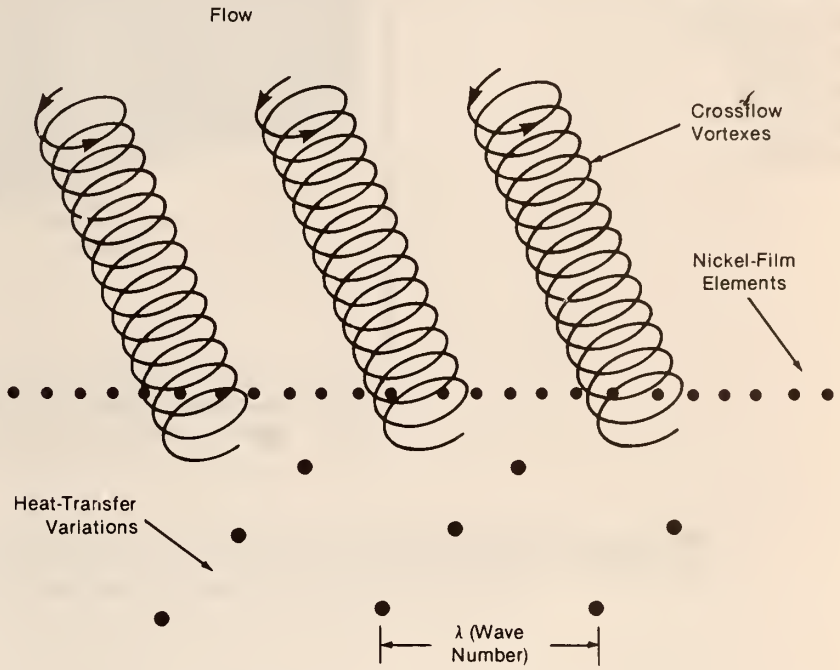

Figure 1. The individual **Crossflow Sensor** elements respond to the variation in heat transfer caused by laminar-crossflow vortexes.

The present technique provides a means of detecting the crossflow vorticity, using thin, surface-mounted arrays of hot-film sensing elements. One crossflow sensor (Figure 1) consists of several electronically heated elements exposed to the airflow. Since each element responds to the heat transfer in the boundary layer, the signal characteristics of an array of elements will display the spanwise variations in heat transfer resulting from the crossflow vorticity.

The array of elements consists of a series of thin-film nickel sensors with a polymer backing dissected to create a predetermined sensor geometry and electrical resistance. These are placed in an appropriate matrix on a thin polymer sheet and bonded with an adhesive. The resulting sensor thickness is small enough not to cause a boundary-layer transition to turbulence for most flight applications of interest. Silver-plated copper wires are soldered to the edge of the sensing grid and routed to terminal strips for the attachment of external lead wires. Each film element in the array is operated as a constant-temperature anemometer. At the time of measurement, the films are heated and the data taken.

The sensors may be installed in a staggered fashion or fabricated into one continuous multielement strip of sensors, providing for the streamwise measurement of crossflow vorticity (Figure 2). The device senses the crossflow continuously, allowing variable free-stream conditions during a single flight or wind-tunnel run. The hot-film anemometer signals respond in distinct ways to different boundary-layer phenomena. Since each phenomenon has a distinctive signal characteristic, the crossflow sensor can detect and measure the surface temperature, skin friction, transition, and relative vorticity amplitude, as well as resolve the characteristics of vorticity wavelength (vortex core spacing) in the crossflow pat-

tern.

This work was done by Bruce J. Holmes, Harlan K. Holmes, Thomas C. Moore, and Gregory S. Manuel of **Langley Research Center** *and Debra L. Carraway of Old Dominion University.*

This invention is owned by NASA, and a patent application has been filed. Inquiries concerning nonexclusive or exclusive license for its commercial development should be addressed to the Patent Counsel, Langley Research Center Refer to LAR-13436./TN

Langley Research Ctr.
Hampton, VA 23665
Technology Utilization Officer: John Samos
Mail Stop 139A
(804) 865-3281
Patent Counsel: George F. Helfrich
Mail Code 279
(804) 865-3725

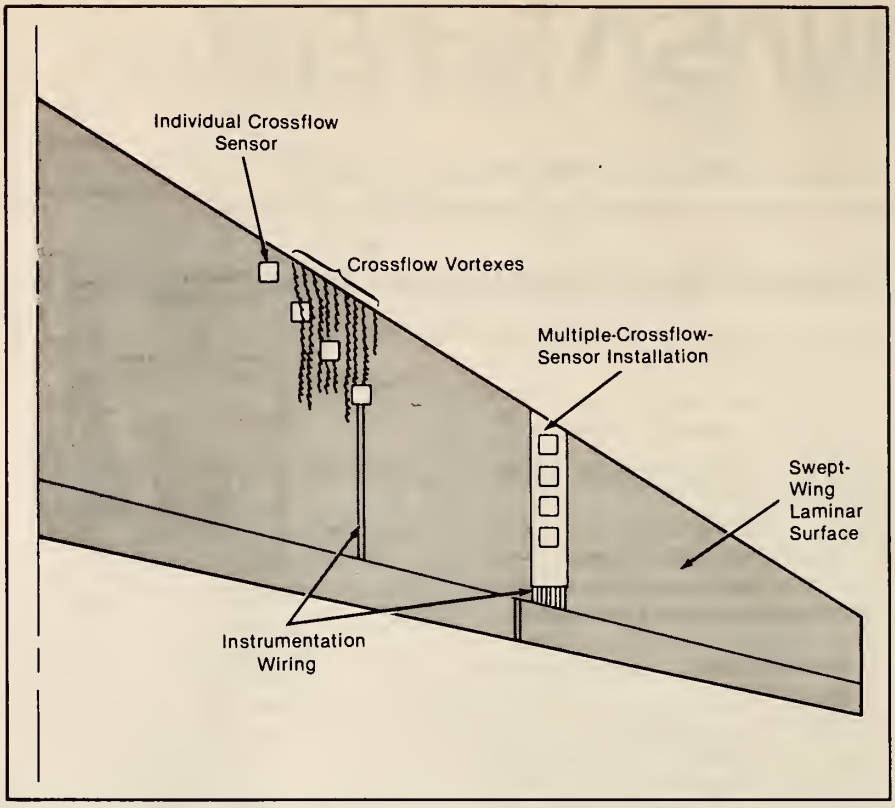

Figure 2. **Crossflow Sensors** can be installed in a variety of patterns, including staggered or combined into a continuous longitudinal strip.

FOR ADDITIONAL INFORMATION: *Contact: Director, Technology Transfer Division, P.O. Box 8757, BWI Airport, MD. 21240; (301) 621-0100 Ext. 241*

REFER TO THE NUMBER LISTED AT THE END OF THE ARTICLE

Environmental Science & Technology

583 Vibrating Mesh Screen Conveyor Solves Solid Waste Disposal Needs

584 Manual for Preventing Spills of Hazardous Substances at Fixed Facilities

Vibrating Mesh Screen Conveyor Solves Solid Waste Disposal Needs

Disposal of municipal solid waste is a growing problem. As the costs of land and environmental controls have increased, landfill disposal of waste has become more expensive. There has been a growing interest in the production of fuel from municipal solid waste. This new vibrating mesh screen conveyor mechanism removes grit and fines from coarse shred refuse-derived fuel. It combines the characteristics of a conveyor with that of a screen for separation of fines from fuel. The resulting fuel has about half the heating value of coal and can be substituted for or cofired with conventional fuels.

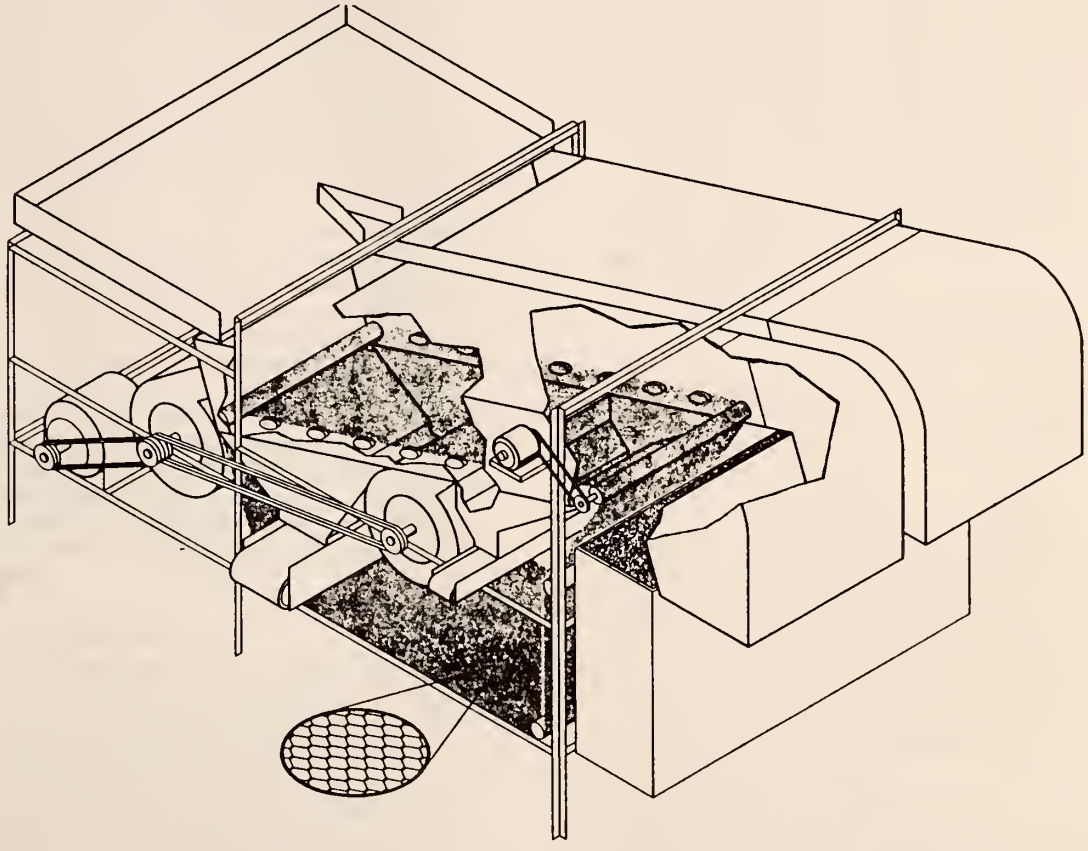

Figure 8. Vibrating mesh screen conveyor

FOR ADDITIONAL INFORMATION:

Dr. Jane M. Welch, Manager, ORTA, Idaho National Engineering Laboratory, P.O. Box 1625, Idaho Falls, ID 83415; (208) 526-8318. Refer to DOE/INEL-028/TN.

United States
Environmental Protection
Agency

Hazardous Waste Engineering
Research Laboratory
Cincinnati OH 45268

Research and Development

EPA

Project Summary

Manual for Preventing Spills of Hazardous Substances at Fixed Facilities

The purpose of this project was to prepare a manual that provides guidance on preventing spills of hazardous substances in fixed facilities that produce substances from raw or starter materials, store the substances, or transfer the substances to and from transportation terminals. The emphasis is on smaller-sized chemical manufacturing facilities.

The manual consists of seven sections and an Appendix: 1. Introduction; 2. Manual of Practice; 3. Hazardous Substances and Their Characteristics; 4. Fixed Facilities; 5. Facility Spill Prevention Practices; 6. Preventive Engineering Practices; and 7. Bibliography. The appendix contains descriptions of fixed facility chemical processing equipment components, from which a checklist of equipment items interacting with hazardous substances can be derived for use in preparing a Spill Prevention Plan.

Introduction

The purpose of this project was to prepare a manual that provides guidance on preventing spills of hazardous substances from fixed facilities that produce hazardous substances from raw or starter materials as products, byproducts or waste products; store hazardous substances; or transport hazardous substances. The audience to be addressed includes managerial and supervisory personnel as well as "hands on" personnel associated with smaller-sized chemical manufacturing facilities. The hazardous substances in question number almost 700, excluding oil, and are those designated pursuant to Section 101 (14) of the Comprehensive Environmental Response, Compensation and Liability Act of 1980, otherwise known as CERCLA or Superfund (Public Law 96-510).

The earlier Clean Water Act (Public Law 92-500) in Section 311, required that the President issue regulations "establishing procedures, methods and equipment . . to prevent discharges of oil and hazardous substances from vessels and from onshore and offshore facilities . . ." Under a 1973 executive order, the U.S. Environmental Protection Agency (EPA) was to promulgate regulations for preventing nontransportation-related spills.

In 1973, EPA issued oil pollution prevention regulations (40 CFR Part 112) that require certain fixed facilities to have on file a spill prevention, control and countermeasures plan (SPCC plan). These regulations have been largely accepted by industry and have proven to be effective in preventing oil spills.

In the case of hazardous substances, no similar federal regulations exist at this time. In its own interest, a large segment of the industry producing, storing, and handling hazardous substances has instituted internal spill prevention plans. However, many of the smaller affected facilities may not have generated spill prevention plans for various reasons. This manual is designed to assist them in preparing such plans.

Source material for this manual was derived from government, industry and commercial publications. Related oil spill prevention literature included: the Guide for Inspectors; a report on Prevention Practices at Small Petroleum Facilities; state contingency plans, such as the Oil Spill Contingency Plan of the State of California; and the extensive Oil Spill Prevention Control and Countermeasure Plan Review. Publications dealing with hazardous substances included cost analyses for hazardous substance pollution prevention, Best Management Practices (BMP) documents, an industrial spill prevention plan, and a treatise on Safety

and Accident Prevention in Chemical Operations.

Facility Spill Prevention Practices

In general, spill prevention practices (SPPs) are independent of the exact nature of the facility, its processes and products. While most SPPs are based on common sense and experience and provide few new revelations, it is useful to have this compilation of procedures when preparing a spill prevention master plan.

SPPs have been drawn from government and industry reports and publications. Some, listed here, overlap into related areas such as response to a spill, maintenance, and training. If the facility already has plans and procedures in these areas, they can be adapted to the present purpose. A short discussion for each SPP listed below is given in the manual.

- SPILL PREVENTION ORGANIZATION
- RISK IDENTIFICATION AND ASSESSMENT
- MATERIALS COMPATIBILITY
- REPORTING AND RECORDKEEPING
- GOOD HOUSEKEEPING
- PREVENTIVE MAINTENANCE
- INSPECTION SYSTEMS
- SECURITY
- EMPLOYEE TRAINING

Preventive Engineering Practices

Preventive engineering practices (PEPs) may be thought of as SPPs that are oriented toward equipment rather than procedures. They are specific to groups of toxic and hazardous substances and to the potential sources of spill, that is: storage areas, loading/unloading areas; inplant transfer, process and materials-handling areas; drainage from plant site and secondary containment structures; and waste storage, treatment and disposal facilities.

PEPs are divided into pre-release and post-release groups, both designed to confine release within the facility boundaries. The difference between the two is that pre-release PEPs are of a general precautionary nature, whereas post-release PEPs are activated as spill control devices by a release. Typical pre-release PEPs include monitoring and alarm systems, non-destructive testing, labeling all storage, process and flow equipment, and proper storage procedures. Typical post-release PEPs include secondary containment of liquids and solids by dikes and berms, flow diversion, vapor control, and dust control.

The manual discusses the following subsections (grouped by equipment categories, emphasizing components found in chemical manufacturing facilities).

- Bulk Storage
  - Tank Construction
  - Tank Support
  - Tank Placement
  - Tank Monitoring
  - Material Storage
  - Alarms
  - Fire Protection Systems
  - Secondary Containment
- Loading and Unloading Areas
  - Tank Truck Loading/Unloading
  - Railroad Tank Car Loading/Unloading
  - Marine Loading/Unloading
- In-Plant Process and Transfer
  - Process Materials/Equipment
  - Instrumentation
  - Piping
  - Valving
  - Venting
  - Color Coding/Labeling
- Drainage Control
  - Facility Diking
  - Road Drainage
  - Plant Drainage
  - Drainage Valving
  - Secondary Containment
- Waste Storage, Treatment and/or Disposal.

Walter Unterberg, Robert W. Melvold, Kathleen S. Roos, and Patricia A. Scofield are with Combustion Engineering, Environmental Monitoring Services, Inc., Newbury Park, CA 91320

***Leo T. McCarthy** (deceased) was the EPA Project Officer (see below for present contact)*

The complete report, entitled "Manual for Preventing Spills of Hazardous Substances at Fixed Facilities," (Order No. PB 87-232 815/AS, Cost $18.95, subject to change) will be available only from

National Technical Information Service
5285 Port Royal Road
Springfield, VA 22161
Telephone 703-487-4650

***John S. Farlow** can be contacted at*
Releases Control Branch
Hazardous Waste Engineering Research Laboratory—Cincinnati
U.S. Environmental Protection Agency
Edison, NJ 08837

Manufacturing, Machinery, & Tools

585 High Disposition Welding Process

586 Transpiration Cooled Combustor Liner

587 Flexible Protective Shield for Newly Welded Joints — A simple device promotes defect-free welds in oxidation-prone metals. (Licensing Opportunity)

588 Computer-Graphical Simulation of Robotic Welding — Limitations on equipment can be investigated in advance to prevent expensive mistakes.

589 Micromachining of Silicon — Diffusion and preferential etching make new structures possible.

590 Portable Horizontal-Drilling and Positioning Device — This portable device drills horizontal holes in irregularly shaped objects.

591 Rotation Control in a Cylindrical Acoustic Levitator — A second driver introduces net circulation around the levitated sample. (Licensing Opportunity)

Testing & Instrumentation

592 Checking Fits with Digital Image Processing — Computer-aided video inspection of mechanical and electrical connectors if feasible. (Licensing Opportunity)

593 Optical-Fiber Temperature Sensor — Temperature could me measured in rotating machinery without speed-limiting mechanical sliprings. (Licensing Opportunity)

594 Real-Time X-Ray Inspection — An x-ray imaging instrument is adapted to continuous scanning. (Licensing Opportunity)

Other Items of Interest

567 Motor Current Signature Analysis Process

571 Minimum-Time Control Robotic Manipulators — Current Theories are examined critically.

579 Software for Tomographic Reconstruction from Neutron Radiographs

US Army Fact Sheet

High Deposition Welding Process

Since welding is one of the largest cost elements in tracked combat vehicle fabrication, a project was undertaken to find refinements to the gas metal arc welding (GMAW) process currently in use. Six different processes were evaluated based on technical dependability, applicability to current M1 production, and potential speed and cost benefits. The test plan for the six processes considered included weldability testing, horizontal/vertical position welding, mechanized and semiautomatic welding and ballistic testing of the H-plates. Of the six processes evaluated, two processes have been implemented. These are: (1) Submerged Arc with Powder Metal Additions and (2) High Current Density GMAW. It is projected that these two will result in savings totalling $27.4 million in the 1988-93 period.

FOR ADDITIONAL INFORMATION:

To discuss this effort further, contact Mr. Frank Beiwel, US Army Industrial Base, Engineering Activity, ATTN: AMXIB-PG, Rock Island, IL 61299-7260; (309) 782-5235.

US Army Fact Sheet

Transpiration Cooled Combustor Liner

Combustion lines for gas turbine engines operate at temperatures approaching the upper limits for common superalloys. As cycle temperatures increase, more complex cooling schemes need to be employed. Transpirationally cooled combustion liners meet this need by using laminates made of porous sheet materials (Lamilloys). Until this project, the manufacturing processes to make such liners were not cost effective. This effort developed some low cost techniques to make larger sheets of finished Lamilloy. In addition, many processes have become automated and generic, a more oxidation resistant alloy was developed and basic pattern generation procedures were refined to improve reliability, dimension control and machined surface quality. The processes developed were scaled up and used to make a fold back Lamilloy combustor liner for the Allison Advanced Technology Demonstrator Engine (ATDE)/GMA500. This technology will be implemented in new and modified turbine engines.

FOR ADDITIONAL INFORMATION:

To discuss this effort further, contact Mr. Frank Beiwel, US Army Industrial Base, Engineering Activity, ATTN: AMXIB-PG, Rock Island, IL, 61299-7260; (309) 782-5235.

NASA Tech Brief
National Aeronautics and Space Administration
Marshall Space Flight Center, Alabama

Licensing Opportunity

Flexible Protective Shield for Newly Welded Joints

A simple device promotes defect-free welds in oxidation-prone metals.

A flexible trailing shield for a welding torch protects hot metals from oxygen of the surrounding air until the weld bead has cooled. The shield bends to follow the contours of the weld joint and protects such metals as titanium, which oxidizes easily when it is hot.

The trailer flexes to fit the contours of the welded surfaces. It can follow a curved or straight joint on a curved or flat surface; for example, a straight joint on a curved surface like a pipe (see Figure 1). The flexible trailer makes it unnecessary to build a special trailer to match the joint, as has been done with the rigid trailers of the past.

A thin stainless-steel bellows forms the body of the trailer (see Figure 2). It is packed with steel wool, which distributes argon over the newly welded bead. The trailer also blows a jet of argon slightly forward of the torch to shield the hot metal before it is welded. A copper-tube manifold extends like a spine along the length of the trailer, supplying argon to the steel-wool distributor.

This work was done by Gerald E. Dyer of Rockwell International Corp. for **Marshall Space Flight Center**. *For further information, Circle 69 on the TSP Request Card.*

Inquiries concerning rights for the commercial use of this invention should be addressed to the Patent Counsel, Marshall Space Flight Center Refer to MFS-29260 /TN

George C. Marshall Space Flight Center
Technology Utilization Officer: Ismail Akbay
Code AT01
Marshall Space Flight Center,
AL 35812
(205) 544-2223
Patent Counsel:
Leon D Wofford, Jr
Mail Code CC01
Marshall Space Flight Center,
AL 35812
(205) 544-0024

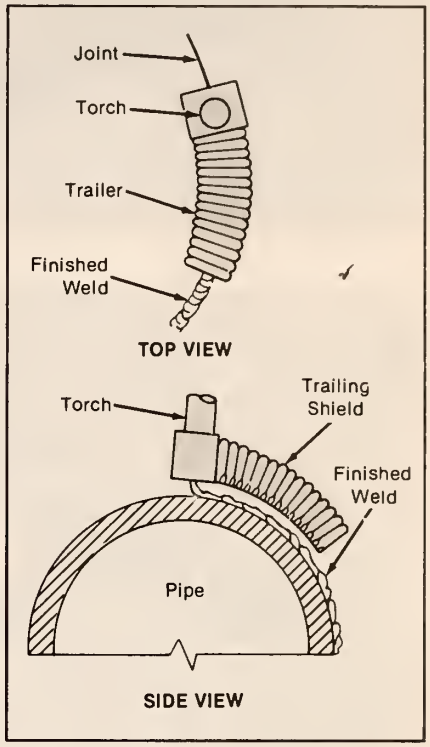

Figure 1. The **Welding Torch Pulls a Trailing Shield** behind it to provide a protective shield of argon gas over the hot weld bead. A guide at the front of the torch holder feeds welding wire to the joint.

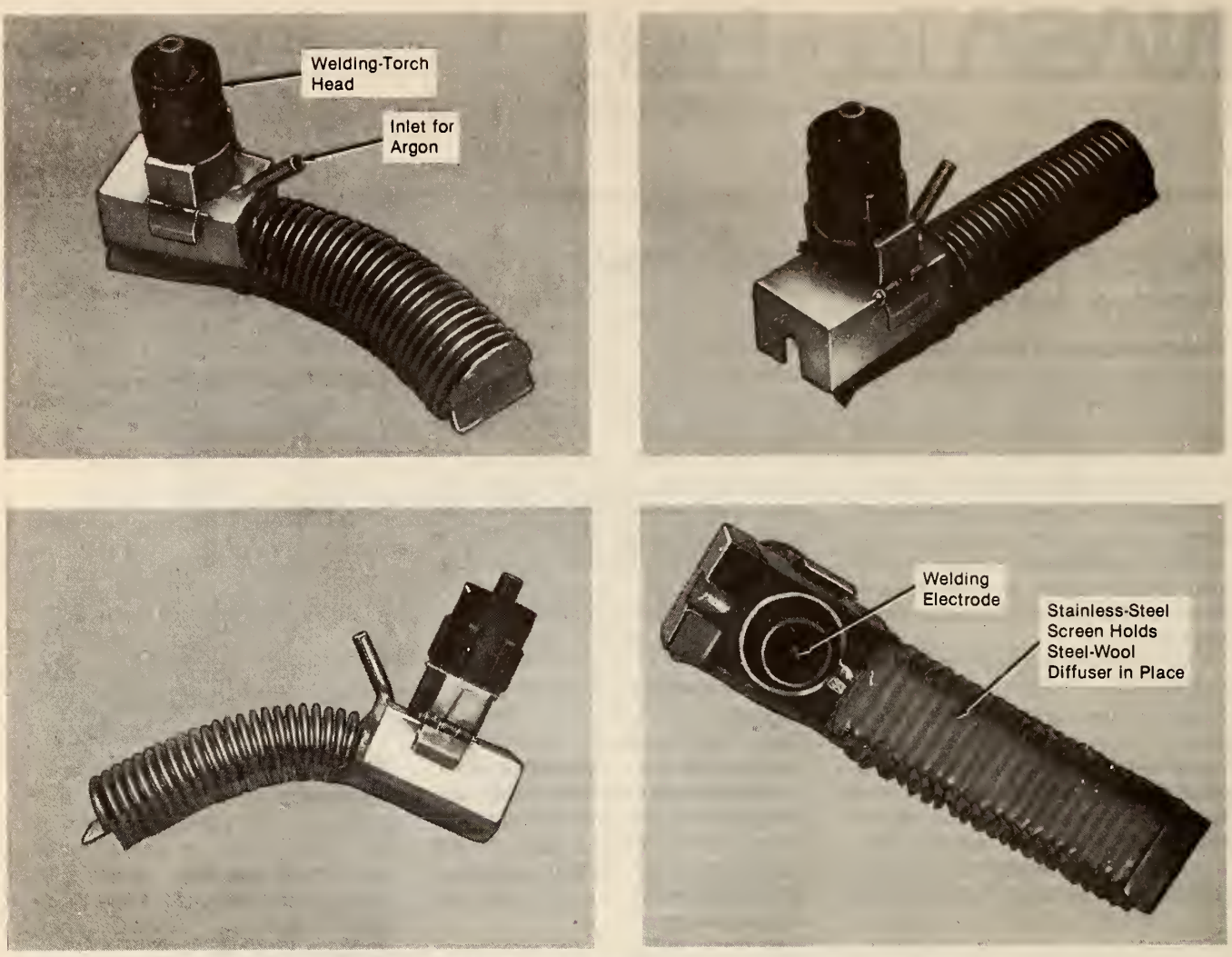

Figure 2. The **Shield Can Be Bent** or straightened to fit closely against the weld joint.

FOR ADDITIONAL INFORMATION: *Contact: Director, Technology Transfer Division, P.O. Box 8757, BWI Airport, MD 21240; (301) 621-0100 Ext. 241*

REFER TO THE NUMBER LISTED AT THE END OF THIS ARTICLE

NASA Tech Brief
National Aeronautics and Space Administration
Marshall Space Flight Center, Alabama

Computer-Graphical Simulation of Robotic Welding

Limitations on equipment can be investigated in advance to prevent expensive mistakes.

The computer program ROBOSIM, developed by NASA to simulate the operations of robots, has been applied to the preliminary design of a robotic arc-welding operation. When the simulation program is run alone or with a robotic program supplied by the user, the output of the computer is a picture of the welding operation that can indicate such potential problems as collisions between the robot and other objects, the inability of the welding head to reach some weld locations, and the impossibility of maintaining the correct orientation or velocity of the welding head or the workpiece during some operations. By performing the simulation before a welding operation, the user can also prevent damage to an expensive workpiece or injury to workers.

The simulated robotic welder has six degrees of freedom and operates on a workpiece mounted on a two-degrees-of-freedom positioner (see figure). The control algorithms of the robot and positioner have to satisfy the special requirements of arc welding, the most important of which are the following:

- The workpiece should be held in an orientation (called the "downhand position") in which gravitation holds the molten metal in the weld pool and aids the fusion process; in practice, this often means making the workpiece surface at the weld joint as horizontal as possible.
- The speed of the torch relative to the workpiece should be held constant to heat the weld at a constant rate.
- The torch has to track the weld joint accurately despite thermal distortions and other dimensional inaccuracies in the workpiece and equipment.

A transformation algorithm based on the geometric relationships among the robot joints, torch, workpiece, and positioner helps to satisfy the first two requirements. This algorithm enables the robot and positioner to be "taught" by manually positioning and orienting the torch relative to the workpiece at successive, closely spaced points along the weld path. During "teaching," it is not necessary to maintain the downhand position.

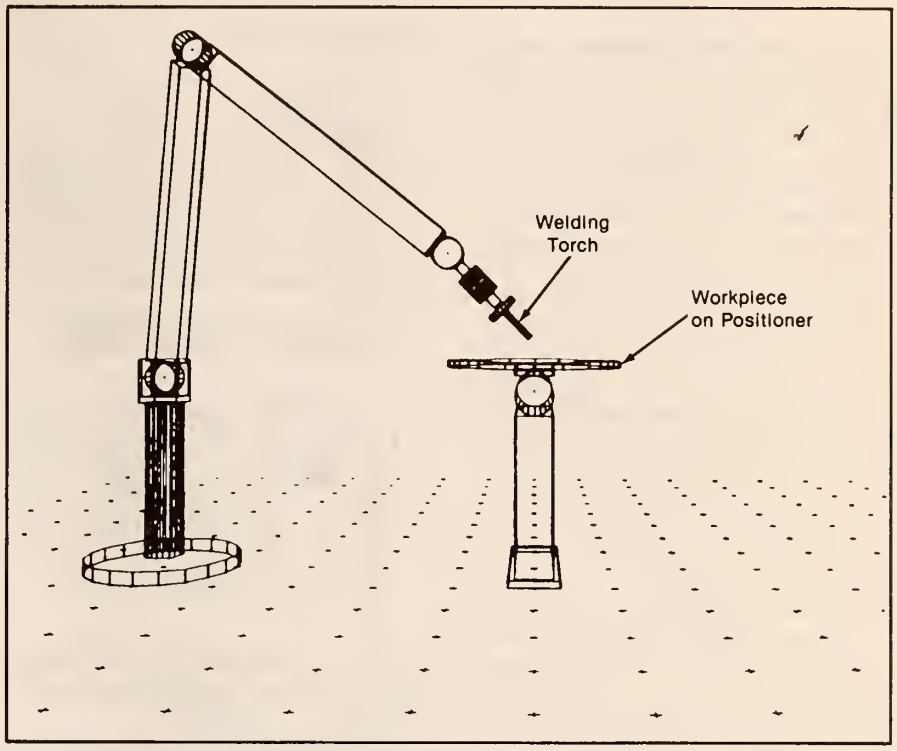

A **Computer Makes a Drawing** of a robotic welder and a workpiece on a positioning table. Such a numerical simulation can be used to perform rapid, safe experiments in computer-aided design or manufacturing.

The algorithm reorients the torch and the workpiece with respect to the horizontal and vertical axes of the workspace to maintain both the desired weld path and the downhand position. It computes the kinematic transformation matrix for the robot joints, the velocity of the torch, and the velocities of the positioner axes to ensure (or attempt to ensure) that the weld is performed in the downhand position and that the weld travel speed is constant. Because the downhand position may not be achievable in all programmed welds, the simulation can be valuable in quickly identifying and correcting the weld design, without the cost of a failed weld, or the loss of time in a practice run without welding current.

This work was done by Ken Fernandez and George Cook of the Society of Manufacturing Engineers for **Marshall Space Flight Center**. *MFS-28199 /TN*

FOR ADDITIONAL INFORMATION: *Contact: Director, Technology Transfer Division, P.O. Box 8757, BWI Airport, MD. 21240; (301) 621-0100 Ext. 241*
REFER TO THE NUMBER LISTED AT THE END OF THE ARTICLE

NASA Tech Brief
National Aeronautics and Space Administration
Lewis Research Center, Cleveland, Ohio

Micromachining of Silicon

Diffusion and preferential etching make new structures possible.

The etching rates of alloys and heavily-doped semiconductor materials can be significantly higher than that of a lightly doped semiconductor if the proper etching system is used. This selectivity can be used to etch regions of a semiconductor preferentially while not etching other unmasked regions. When this selective etching is used with laser-induced-diffusion techniques, it will be possible to make structures that cannot be made at present. Thus, it will be possible to produce well-defined structures in and through a wafer while not damaging existing structures on the wafer. Since these structures are patterned on the front surface of the wafer by the use of conventional microelectronic techniques, it will be possible to make these structures well aligned to such existing front-surface patterns or structures as integrated circuits.

The figure illustrates an example of the type of process described. The top left part shows an aluminum pattern deposited on the front surface of a silicon wafer. The top right part shows infrared radiation from a high-power CO_2 laser incident on the silicon wafer from the back side. Because silicon is transparent to infrared radiation while Al/Si absorbs the radiation, only the Al/Si regions will be heated. The Al/Si will diffuse through the silicon wafer by laser-induced temperature-gradient zone melting with no lateral diffusion, as shown at the bottom left. The removal of the Al/Si regions by a selective etchant will result in a micromachined structure in the silicon wafer, as shown at the bottom right.

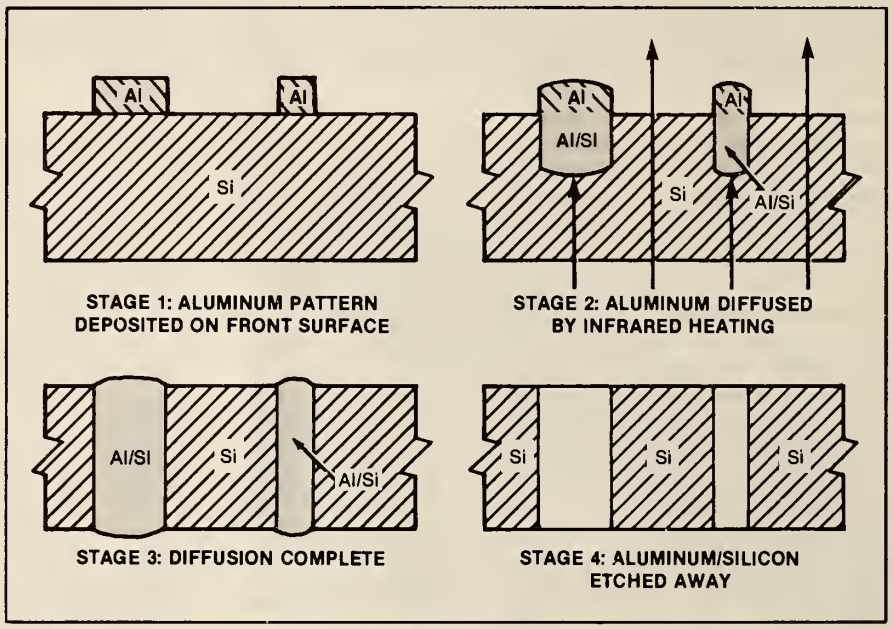

Aluminum Is Diffused into a silicon wafer by selective infrared heating. The resulting aluminum/silicon plugs are then preferentially etched away, leaving small holes in the silicon.

The method would be a significant improvement on the present micromachining techniques used to fabricate structures for sensors and isolation of devices. This technique will make it possible to manufacture smaller devices and structures than those produced by the currently available methods.

This work was done by John E. Dickman of **Lewis Research Center**. *No further documentation is available.* *LEW-14481 /TN*

FOR ADDITIONAL INFORMATION: *Contact: Director, Technology Transfer Division, P.O. Box 8757, BWI Airport, MD. 21240; (301) 621-0100 Ext. 241*
REFER TO THE NUMBER LISTED AT THE END OF THE ARTICLE

NASA Tech Brief
National Aeronautics and Space Administration
Goddard Space Flight Center, Greenbelt, Maryland

Portable Horizontal-Drilling and Positioning Device

This portable device drills horizontal holes in irregularly shaped objects.

A portable horizontal-drilling and positioning device (see figure), constructed mainly of off-the-shelf components, accurately drills horizontal small holes in irregularly shaped objects. With this device, holes can be precisely placed and drilled in objects that cannot conveniently be moved to a shop area.

This device was designed specifically to drill accurately, ream, and pin a series of holes in some irregularly shaped hardware in a semiclean room without using any lubricants. Because the fragility and the irregularity of shape of the hardware precluded the use of standard fixtures or guides, previous methods of locating and drilling holes relied on free-hand drilling or on specially designed fixtures. The use of handheld drills gave inconsistent results, poor hole shape, poor depth control, and angularity.

These difficulties were overcome with the new device (see figure), which provides three axes of movement while maintaining horizontal drilling. A 48 in. (122 cm) length of dual linear ball bearings provides friction-free travel in the x-direction (horizontal), and a dovetailed vertical column, at least 26 in. (66 cm) high, of anodized aluminum secured to the linear bearing base provides the required travel in the y-direction (vertical). A standard, commercially-available, variable-speed, sensitive drill press with a sensitive hand feed is secured to a standard x-y positioning table that provides the fine, graduated movements required for positioning the drill press.

Once the part to be drilled is aligned with the horizontal axis, any number of horizontal holes can be drilled. The use of the linear ball bearings provides a quick, accurate means of establishing a reference plane. A locking device secures the drill assembly prior to drilling, a quill coupled to a depth dial indicator provides accurate depth (2-axis) control, and the self-contained, variable-speed drill head enables the drilling of a variety of materials.

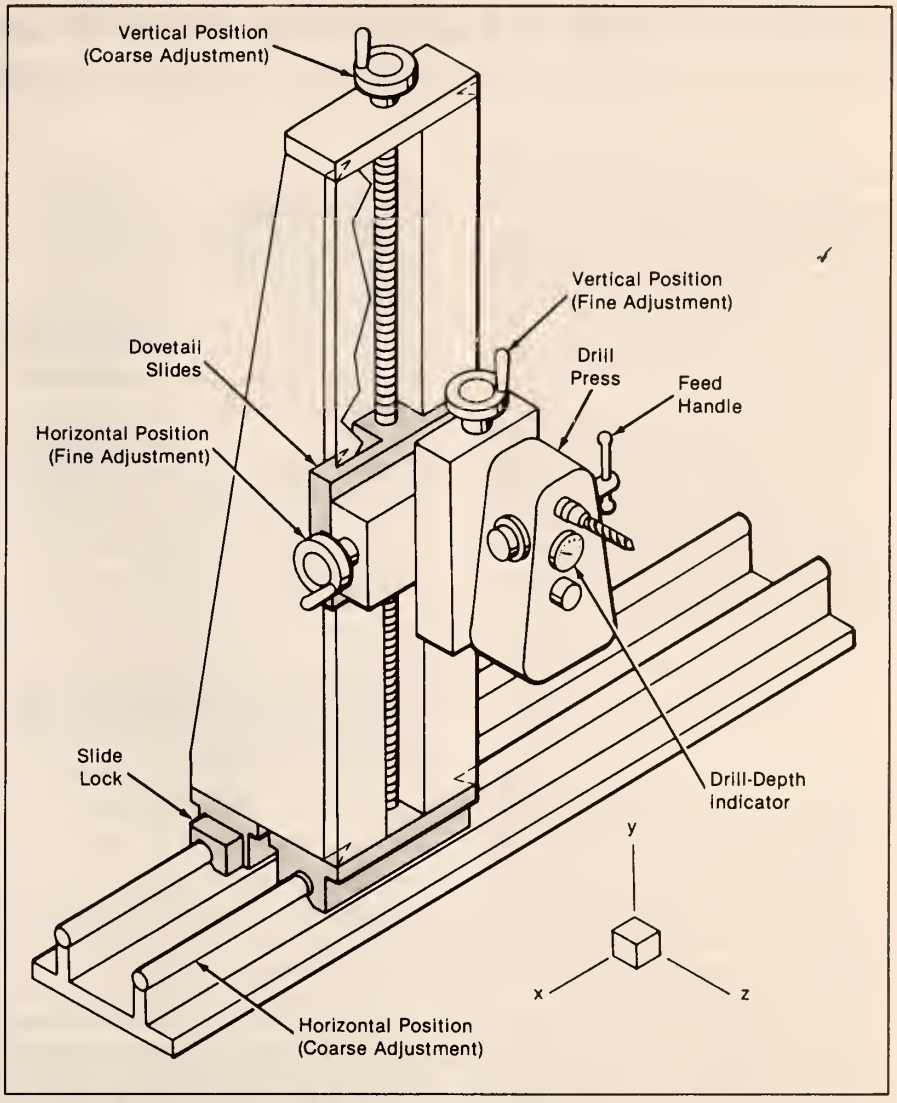

The **Portable Horizontal-Drilling Device**, constructed mainly of standard components, provides three axes of movement while maintaining the drill perpendicular to the workpiece.

This work was done by Edmund Smigocki and Clarence Johnson of **Goddard Space Flight Center**. *No further documentation is available.* GSC-13031

/TN

FOR ADDITIONAL INFORMATION: *Contact: Director, Technology Transfer Division, P.O. Box 8757, BWI Airport, MD 21240; (301) 621-0100 Ext. 241*
REFER TO THE NUMBER LISTED AT THE END OF THIS ARTICLE

NASA Tech Brief
National Aeronautics and Space Administration
NASA's Jet Propulsion Laboratory, Pasadena, California

Licensing Opportunity

Rotation Control in a Cylindrical Acoustic Levitator

A second driver introduces net circulation around the levitated sample.

The addition of a second acoustical transducer enables a single-mode, cylindrical acoustic levitator to rotate a levitated sample about the cylinder axis in a controlled manner. The ability to control rotation will enhance the usefulness of acoustic levitation in containerless processing, studies of the effects of rotation on fluid flows, and heating of samples by focused beams of light.

In the unmodified levitator, the sample does not rotate. The physical principle is easily visualized for a typical levitating acoustic field using the lowest-order nonplane wave made of the cylinder. In this mode, the acoustic pressure, P_1, varies about the axis and is given by

$$P_1 = a_1 \cos\phi \cos\omega t = \frac{a_1}{2}[\cos(\phi + \omega t) + \cos(\phi - \omega t)]$$

where a_1 contains the drive amplitude as well as the radial and axial dependences, ϕ is the azimuthal angle, ω is the angular frequency of the levitating sound, and t is time. The term in brackets represents two counterrotating acoustic fields that are equal and consequently impart no net torque or rotation to the sample.

in the modified levitator (see figure), a second transducer is orthogonal to the levitating transducer and excited at the same frequency but at a different amplitude or phase or both. In one scheme, the phase in the second transducer is shifted 90° from that in the first transducer, and the amplitude is different, resulting in an acoustic pressure, P_2, given by

$$P_2 = a_2 \sin\phi \sin\omega t = \frac{-a_2}{2}[\cos(\phi + \omega t) - \cos(\phi - \omega t)]$$

where a_2 is an amplitude factor similar to a_1. This equation also represents two additional equal counterrotating acoustic fields. However, the total acoustic field is expressed by

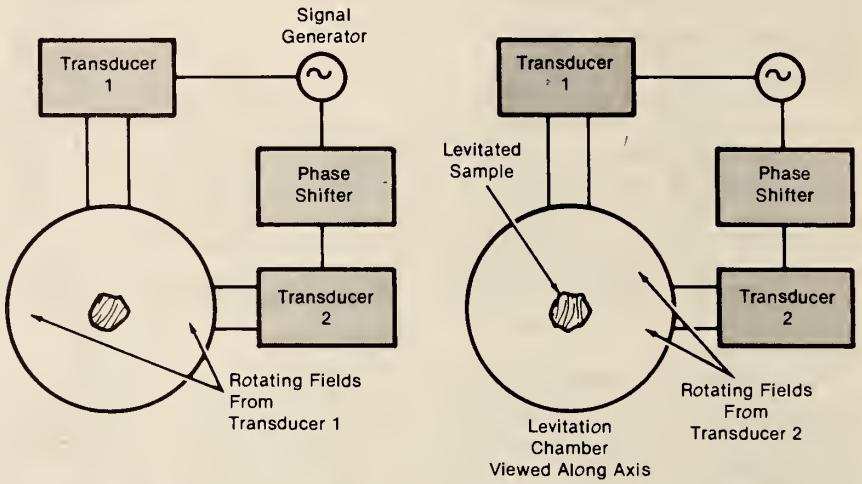

Two Transducers produce two sets of equal counterrotating acoustic fields. By appropriate adjustment of the amplitudes and phases in the two transducers, the total acoustic field can be made to consist of two unequal counterrotating fields, therefore producing a net torque on the levitated sample.

$$P_1 + P_2 = \tfrac{1}{2}[(a_1 - a_2)\cos(\phi + \omega t) + (a_1 + a_2)\cos(\phi - \omega t)]$$

This represents two unequal counterrotating fields, which produce a net torque. The torque is increased by increasing the amplitude in the second transducer.

In an alternative scheme, both transducers are excited at the same amplitude. If no rotation is desired, both are excited at the same phase to produce equal counterrotating acoustic fields. The introduction of a phase shift between the two transducers makes the counterrotating fields unequal. The degree of inequality, and therefore the torque, can be increased by raising the phase shift.

In both schemes, it is necessary to apply a starting acoustic torque in excess of a critical minimum to make the sample turn; less torque is needed to keep it turning. Thus, the sample begins to turn rapidly. If slower rotation is desired, the torque must then be reduced. This behavior is analogous to the decrease in frictional force between two objects when they begin to slide on each other.

This work was done by M. B. Barmatz and J. L. Allen of Caltech for **NASA's Jet Propulsion Laboratory**.

Inquiries concerning rights for the commercial use of this invention should be addressed to the Patent Counsel, NASA Resident Office-JPL Refer to NPO-16995 /TN

Jet Propulsion Lab.
NASA Resident Office
Technology Utilization Officer: Gordon S. Chapman
Mail Stop 180-801
4800 Oak Grove Drive
Pasadena, CA 91109
(818) 354-4849
Patent Counsel: Paul F. McCaul
Mail Code 180-801
4800 Oak Grove Drive
Pasadena, CA 91109
(818) 354-2734
Technology Utilization Mgr. for JPL Norman L. Chalfin
Mail Stop 156-211
4800 Oak Grove Drive
Pasadena, CA 91109
(818) 354-2240

FOR ADDITIONAL INFORMATION: *Contact: Director, Technology Transfer Division, P.O. Box 8757, BWI Airport, MD 21240; (301) 621-0100 Ext. 241*
REFER TO THE NUMBER LISTED AT THE END OF THIS ARTICLE

NASA Tech Brief
National Aeronautics and Space Administration

Licensing Opportunity

Checking Fits With Digital Image Processing

Computer-aided video inspection of mechanical and electrical connectors is feasible.

A report discusses work done on digital image processing for computer-aided interface verification (CAIV). The goal was to develop ways to assure that a component at any level of assembly will fit the mating part(s) of its intended interface. Two kinds of components were examined: a mechanical mating flange and an electrical plug.

The work encompassed the following tasks:

- Identification of ground rules and guidelines;
- Definition of CAIV requirements;
- Choice of a technological approach;
- Formulation of a technology implementation;
- Demonstration of the concept; and
- Delivery of equipment, computer programs, and documents.

The reference-image/image-subtraction method was selected for pattern recognition. In this technique, a reference image of the interface in question stored in memory is subtracted, one picture element at a time, from the image of the interface being viewed. The absolute values of the differences between the two images are retained. If the interfaces are identical, there will be no differences. If the interfaces are dissimilar, the differences will be highlighted.

One of the major components of the image-processing system is a charge-coupled photodiode array in a solid-state digital camera. The unit produces digital image-intensity values. A special sample-and-hold processing filter was developed to preserve the light-intensity values in the output video signal. In contrast, most charge-coupled-device cameras include filters that average intensity values across groups of picture elements. The averaging introduces an error of 10 to 12 percent into the light-intensity values.

The work showed that a CAIV system can be built with a resolution of 0.001 inch (25 μm) per picture element and an overall accuracy of ± 2 percent or ± 0.005 inch (127 μm). In 3 to 4 years, it should be possible to improve these performance figures to ± 1 percent and ± 0.0015 inch (38 μm), respectively.

This work was done by R. M. Davis of **Kennedy Space Center** *and W. D. Geaslen of EG&G Space Systems. "Computer Aided Interface Verification,"*

Inquiries concerning rights for the commercial use of this invention should be addressed to the Patent Counsel, Kennedy Space Center Refer to KSC-11367. /TN

John F. Kennedy Space Center
Technology Utilization Officer Thomas M Hammond
Mail Stop PT-TPO-A
Kennedy Space Center, FL 32899
(305) 867-3017
Patent Counsel James O. Harrell
Mail Code PT-PAT
Kennedy Space Center, FL 32899
(305) 867-2544

FOR ADDITIONAL INFORMATION: *Contact: Director, Technology Transfer Division, P.O. Box 8757, BWI Airport, MD 21240; (301) 621-0100 Ext. 241*

REFER TO THE NUMBER LISTED AT THE END OF THIS ARTICLE

NASA Tech Brief
National Aeronautics and Space Administration
Marshall Space Flight Center, Alabama

Licensing Opportunity

Optical-Fiber Temperature Sensor

Temperature could be measured in rotating machinery without speed-limiting mechanical sliprings.

Signals from a proposed fiber-optic temperature sensor would be transmitted across a rotary interface without electromechanical sliprings. The optical signal would be carried across a noncontacting optical slipring from the sensor on a rotating shaft to a stationary measuring circuit. The noncontacting optical connection would accommodate rotational speeds (in turbomachinery, for example) much higher than the limiting speeds of the contacting connections needed for electrical signals from thermocouples and other electrical temperature sensors.

In the sensor, the tip of an optical-fiber bundle would be inserted in a slotted hollow cylinder (see figure). A piston would sit in the hollow core of the cylinder with one end fixed in the cylinder and the other end — facing the fiber bundle ends — free to move longitudinally. The fluid, the temperature of which is to be measured, would enter the core through the slot and flow around the piston.

The cylinder would be made of a material having a coefficient of thermal expansion greater than that of the piston material. Thus, when the fluid temperature rises, the gap between piston and fiber bundle would increase; and when the temperature falls, the gap would narrow. The piston would reflect less light back into the bundle when the gap is wide than when it is narrow. The amount of reflected light carried by the fiber to a light detector would therefore vary inversely with the temperature of the fluid.

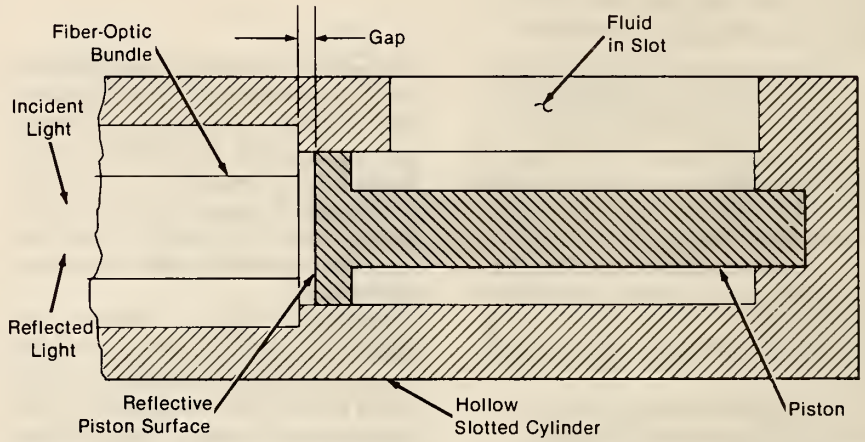

The **Gap Widens as the Temperature Rises** and narrows as the temperature falls. The light reflected from the piston face and recaptured by the fiber bundle varies accordingly.

This work was done by Edmund J. Roschak of Rockwell International Corp. for **Marshall Space Flight Center**. *No further documentation is available.*

Inquiries concerning rights for the commercial use of this invention should be addressed to the Patent Counsel, Marshall Space Flight Center Refer to MFS-29279. /TN

George C. Marshall Space Flight Center
Technology Utilization Officer: Ismail Akbay
Code AT01
Marshall Space Flight Center,
AL 35812
(205) 544-2223
Patent Counsel:
Leon D. Wofford, Jr
Mail Code CC01
Marshall Space Flight Center,
AL 35812
(205) 544-0024

FOR ADDITIONAL INFORMATION: *Contact: Director, Technology Transfer Division, P.O. Box 8757, BWI Airport, MD 21240; (301) 621-0100 Ext. 241*
REFER TO THE NUMBER LISTED AT THE END OF THIS ARTICLE

NASA Tech Brief
National Aeronautics and Space Administration
Marshall Space Flight Center, Alabama

Licensing Opportunity

Real-Time X-Ray Inspection

An x-ray imaging instrument is adapted to continuous scanning.

A modern version of the fluoroscope enables the rapid x-ray inspection of parts. The instrument was developed for the detection of buckling in insulated ducts. It replaced a large 160-kV x-ray machine that required time-consuming exposures of many small sections of a duct with the aid of cumbersome positioning fixtures and slow film-processing facilities.

The fluoroscope uses radiation from a radioactive gadolinium or thallium source. The instrument weighs only 6½ lb (2.9 kg). It can be quickly scanned by hand along the duct surface, providing a real-time image.

The instrument is based on the Lixiscope, a low-intensity x-ray imaging scope developed at Goddard Space Flight Center. In the Lixiscope, the pattern of x rays transmitted through the specimen is converted into a visible-light image in a scintillator. This image is intensified by a factor of 10^5 or more in a microchannel-plate device. The intensified image can be viewed directly, photographed, recorded on videotape, or coupled to other imaging devices.

The standard Lixiscope was modified so that it can be placed around the cylindrical duct. More shielding was added to the source holder so that a radioactive source with higher-than-usual energy could be used to penetrate the duct layers. The resulting image clearly shows buckled parts of the inner wall (see figure).

This work was done by Ronald V. Bulthuis of Rockwell International Corp. for **Marshall Space Flight Center**.

Inquiries concerning rights for the commercial use of this invention should be addressed to the Patent Counsel, Marshall Space Flight Center Refer to MFS-29217/TN

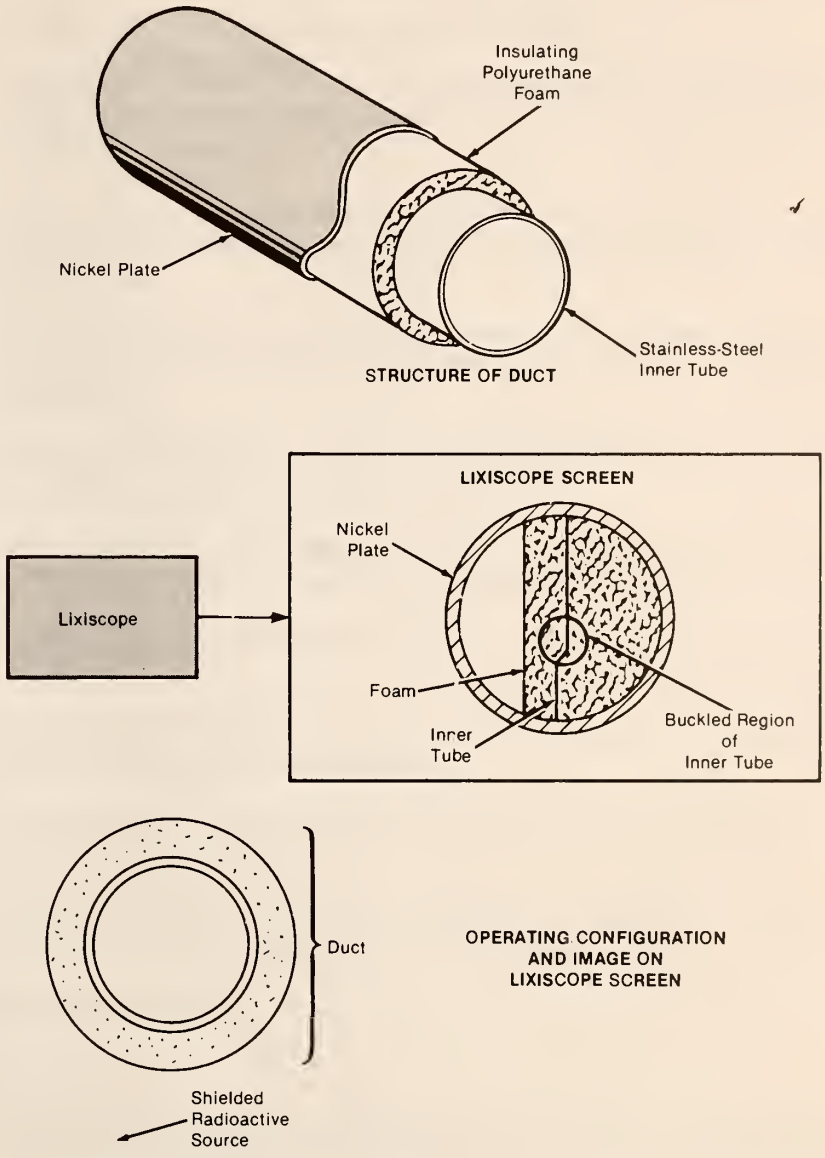

X Rays Show Inner Details of a plated, insulated duct. A buckled section of the inner steel wall of the duct appears as a bump on the vertical line at the center of the display. In an inspection, the duct is rotated and translated past the x-ray source so that it can be inspected completely.

George C. Marshall Space Flight Center

Technology Utilization Officer: Ismail Akbay
Code AT01
Marshall Space Flight Center,
AL 35812
(205) 544-2223

Patent Counsel: Leon D. Wofford, Jr
Mail Code CC01
Marshall Space Flight Center,
AL 35812
(205) 544-0024

FOR ADDITIONAL INFORMATION: *Contact: Director, Technology Transfer Division, P.O. Box 8757, BWI Airport, MD 21240; (301) 621-0100 Ext. 241*
REFER TO THE NUMBER LISTED AT THE END OF THIS ARTICLE

Materials

595 Bainite Hardenability of ASTM A723 Steel

596 Properties of Pulse-Electrodeposited Alloys

597 Ultralow-Loss Infrared Optical Fibers Developed

598 Contamination Barrier for Contour-Molding Material — A release agent prevents the molding compound from adhering to or contaminating the surface.

599 Carboranylmethylene-Substituted Cyclophosphazene Polymers — A new synthesis produces unusual electrical and chemical properties. (Licensing Opportunity)

600 Calculating Percent Gel for Process Control — The reaction state of a thermosetting resin is tracked to assure desired properties. (Licensing Opportunity)

601 Evaluating Solid-Lubricant Films — The pin-on-disk tribometer provides valuable information when used properly.

602 Investigation of Epoxy Curing — A kinetic model describes major features of the curing process. (Licensing Opportunity)

603 Microstructure of MnBi/Bi Eutectic Alloy — The effect of convection is examined.

604 Molding Compound for Inspection of Internal Contours — This material is clean, sets rapidly, and is easy to use.

605 Nonisothermal Crystallization in PEEK/Fiber Composite — Several features of the crystallization process are attributable to the fibers.

606 Stress-and-Strain Analysis of Hot Metal/Fiber Composites — Macroscopic mechanical properties are derived from micromechanics.

Testing & Instrumentation

607 Super Grip

608 Automatically Inspecting Thin Ceramics for Pinholes — Flaws would be located and marked.

609 Checking Nickel Plate for Porosity — A porosity test goes for a free ride with a cryogenic adhesion test.

610 Fast Measurements of Thermal Diffusivities of Ceramics — The tempera ture rises of samples are compared with that of a reference sample. (Licensing Opportunity)

Other Items of Interest

586 Transpiration Cooled Combustor Liner

US Army Fact Sheet

Bainite Hardenability of ASTM A723 Steel

ASTM Specification A723 covers high-strength, quenched-and-tempered Cr-Ni-Mo-V steel forgings used for pressure vessels, isostatic presses, shock tubes, and similar components. These high-hardenability materials are not intended for welded applications. The specification includes three grades of Cr-Ni-Mo-V steel and six classes of increasing strength. The strength class, section size, and configuration of the forging will largely dictate the applicable grade and class of steel.

The austenite transformation of A723 steels frequently is assumed to be described by the time-temperature-transformation (TTT) diagram for AISI 4340 steel. This may be a reasonable assumption for the Grade 1 version of A723. A key transformation characteristic for the A723 steels, which often are used in heavy sections, is the bainite hardenability, which is a measure of the ability of the sample or workpiece to avoid bainite formation on quenching. Because the three grades differ significantly in nickel and molybdenum contents, it is important to ascertain the extent to which the composition differences have altered the transformation behavior in order to design the heat treatments for large components made of these steels. However, because of the high hardenability of the A723 steels, the standard laboratory test for hardenability, the Jominy end-quench test, is not suitable for distinguishing those differences.

Cote, Meisel and Sheldon of the U.S. Army Armament Research, Development and Engineering Center Benet Weapons Laboratory studied the austenite transformation of A723 steel using a method that they developed for studying transformations in ferrous alloys. The method employs simultaneous thermal analysis and thermomagnetic analysis; it is especially useful when transformations are accompanied by changes in magnetic state.

In this study of ASTM A723 steel, lots were examined that had been prepared by various refining techniques, including conventional refining, calcium injection, electroslag remelting (ESR), and vacuum-arc remelting (VAR), although data for the VAR material were not included in the present report. The lots were similar in composition except for the nickel contents. Two of the lots had nominally Grade 1 compositions and had nickel contents of about 2.1 percent, a value approaching the upper limit for Grade 1, but the molybdenum contents were higher than that specified for Grade 1 (0.20 to 0.40 percent). These were the conventionally refined and the calcium-treated lots. The ESR lot contained 2.99 percent nickel, so it was Grade 2 material except that the molybdenum content was slightly higher than the upper limit for Grade 2 (0.50 percent).

The results of the special hardenability tests were surprising in that a large variation in hardenability was found among the various lots of A723 steel. The variations appeared to be the result of differences in nickel content of less than 1 percent. The ESR steel with 2.99 percent nickel had appreciably higher bainite hardenability than did the conventionally refined and calcium-treated materials with 2.12 and 2.15 percent nickel, respectively.

The mechanical properties were determined for parts of different size made from steel of different hardenability subjected to different cooling rates so as to be able to relate hardenability-test results to manufacturing variables. In particular, the investigators compared the properties of thick (approximately 3 to 4-inch wall thickness) and thin (approximately 1.7-inch wall thickness) sections of a given component that had been quenched by water spraying and then tempered. The Charpy V-notch impact energy absorption determined at -40 F was the property most sensitive to the presence of bainite. For given tempering conditions and approximately the same yield strength, the Charpy values of tempered lower bainite were about half those of tempered martensite.

Comparison of Charpy values and quench times showed a correlation with hardenability. For the very high hardenability ESR high-nickel material, little bainite would be expected, even for the very low quench rates, so the similar Charpy values observed for the thick and thin sections would be expected. On the other hand, for the lower hardenability calcium-treated steel with its lower nickel content, the tendency to form bainite was so high that a substantial amount was expected; the large difference in Charpy V-notch energy-absorption values observed for the thick and thin sections of this lot of steel reflect the dominant role of bainite hardenability in this heat.

The implication for manufacturing is that components of this steel made from a lot with low nickel content and, hence, lower bainite hardenability should be quenched rapidly so as to optimize mechanical properties, especially the low-temperature impact behavior. This would include Grade 1 material or Grade 2 material with a nickel content on the low side of the specified range. The Charpy data for the conventionally refined lot of A723 steel with its higher sulfur content and lack of inclusion-shape control exhibited relatively low Charpy values even for the more rapidly quenched thin section. This result indicated that impurity effects and the form of the nonmetallic inclusions played a greater role in limited Charpy V-notch impact values than did the presence of bainite. When a sufficiently high quenching rate was used, the calcium-treated steel, which had the lowest bainite hardenability, exhibited higher impact-energy absorption than did the conventionally treated heat.

FOR ADDITIONAL INFORMATION:

A full description of this activity is contained in a backup report which may be purchased from NTIS, Springfield, VA 22161; (703) 487-4650.

NTIS order number: AD-A181905/NAC
Price code: A02

US Army Fact Sheet

Properties of Pulse-Electrodeposited Alloys

A comprehensive investigation over more than a 3-year period was carried out by R. Weil and W. Kim (Stevens Institute of Technology, Hoboken, New Jersey) for the U.S. Army Research Office on the use of pulse plating to improve the properties of electro-deposits and electroforms and also to develop new materials. As part of this study, it was necessary to design and build a minitensile device capable of measuring elastic and plastic properties of thin foils over a wide range of strain rates and which used a specimen with the width and gage length scaled to the thickness. Such a unit was built and used successfully. A detailed description and schematic of the overall operation of the minitensile-testing device, along with photographs of the unit and a minitensile specimen, are presented in the report. Also, for this study it was necessary to build and use a cell for determining hydrogen permeation through electrodeposits. A detailed schematic of the overall hydrogen permeation cell unit is shown in the report. Some of the studies covered in this final report by R. Weil and W. Kim are essentially a continuation of earlier investigations carried out under a previous contract (DAAG-27-80-C-0056) and covered in a final report dated September 1, 1983.

The specific investigations covered in the current final report (March, 1987) involve studies of pulse-plated Ni-Mo and Cu-Zn alloys and nickel. The previously reported reduction of the internal stress in Ni-Mo alloy deposits was investigated further as was that in nickel. The observed compressive stress which developed each time that the current was turned on and which then changed to tensile was explained in terms of hydrogen expanding the surface layer. Hydrogen was also thought to be responsible for a decreasing stress with increasing pulse frequency when nickel was plated on palladium substrates. The reduction of Mo by hydrogen, also during the time the pulsed current was off, was considered the probable cause of the higher Mo content in the Ni-Mo alloy deposits and the lower stress. A comprehensive table, showing the alloy composition and mechanical properties (i.e., Young's modulus, yield strength, tensile strength, and percent elongation) of Ni-Mo deposits produced at various current densities and pulse frequencies, is included in the report.

Property enhancement of nickel electrodeposits by anodic current pulses to promote grain refinement was also investigated. The effects of the periodic imposition of anodic pulses on the mechanical and tribological properties of electrodeposited nickel were evaluated. However, the pulses, employed in this study, differed from those generally used in periodic reverse plating in that the duty cycles were much larger and the frequencies much smaller. Nickel was plated from an all-sulfate bath containing 112 g/l nickel sulfate hexahydrate and 30 g/l boric acid. Nickel was plated at a cathodic current density of 5 mA/sq cm. The anodic current during the pulses was 100 mA/sq cm. The durations of the anodic pulses were 10, 100, and 1000 msec. The cathodic charge between anodic pulses was such that about 0.5 microns of nickel plate was deposited in each interval. The total plate thickness in all experiments was about 10 microns. Both yield strength and tensile strength of nickel deposits reached a maximum at an

anodic pulse duration of 100 msec. With anodic pulses of 100-msec duration, the strengths were about three times higher than those of nickel deposits plated without anodic pulses which had a yield strength of 39 ksi (270 MPa) and a tensile strength of 64 ksi (440 MPa). However, the ductility (as manifested by percent elongation) of the nickel deposit plated with anodic pulses was lower (about 0.5 percent) than that of the nickel deposit plated without pulses which was 3.1 percent. The authors attributed the substantial three-fold increase in the yield and tensile strengths as being attained by the reduction of grain size in nickel deposits produced using the anodic pulses. The grain size reduction apparently resulted from the passivation of the nickel surface during the anodic pulse. It had been observed, in other preliminary experiments in this study, that grain size reduction was not attained in a Watts bath (nickel chloride-nickel sulfate-boric acid) or air all-chloride bath. Evidently, nickel does not tend to passivate in the presence of chloride ions. The authors further indicated that it was doubtful that there was any appreciable dissolution during the anodic pulse in the all-sulfate plating bath, used in this study, and that it was much more likely that an oxide formed.

The effect of anodic pulses and their duration on the coefficient of friction of nickel deposits was also investigated. At 100 msec a reduction of the coefficient of friction to a value of about 0.4 was achieved as compared to a value of 0.6 for a nickel deposit plated without the use of anodic pulses. The reduction in the coefficient of friction was also attributed to the grain size reduction achieved in the deposits produced using the anodic pulses.

FOR ADDITIONAL INFORMATION:

A full description of this activity is contained in a backup report which may be purchased from NTIS, Springfield, VA 22161; (703) 487-4650.

NTIS order number: AD-A178596/NAC
Price code: A03

Ultralow-Loss Infrared Optical Fibers Developed

The development of the first fluoride optical fiber with losses less than 1 decibel/kilometer (dB/km) that could revolutionize long-distance data transfer technology has been announced by the Naval Research Laboratory.

Fluoride glass optical fibers with potential propagation losses as low as 10 3 dB/km for repeaterless transoceanic optical fiber transmission systems have been intensively studied worldwide for the past several years in major laboratories conducting research in fiber optics. This represents a major break-through since the 1 dB/km mark, long recognized as the first major milestone to realizing ultralow-loss propagation. It also represents a major goal of many laboratories that are competitively developing ultralow-loss fiber technology.

Using the standard cutback measurement technique, NRL scientists measured losses at 2.55 microns of 9.0 dB/km. This figure was independently confirmed by separate scattering of the absorption measurements made in the infrared with a color-center laser. The average scattering was less than 0.2 dB/km and was as low as 0.12 dB/km. This scattering represented a considerable improvement over the previous low-scattering fiber result of l dB/km. The absorption component, measured by calorimetry, was found to be 0.75 dB/km.

The core was a ZrF_4-BAF_2-LaF_3-AlF_3-NaF composition; the cladding was similar except that HfF_4 was partially substituted for ZrF_4 to reduce the refractive index. The core diameter was 100 microns, and the overall diameter was 142 microns. The numerical aperture was 0.12.

For Additional Information:

Backup material on this effort is available from:

Navy Domestic Technology Fact Sheet
Reader Reply Service
Code E211
Naval Surface Weapons Center
Dahlgren, VA 22448-5000
(703) 663-8921

Refer to 120804/TN

NASA Tech Brief
National Aeronautics and Space Administration
Marshall Space Flight Center, Alabama

Contamination Barrier for Contour-Molding Material

A release agent prevents the molding compound from adhering to or contaminating the surface.

A soap-based cleaning agent enables the making of contamination-free molds of surface contours. The cleaning agent, Turco 4215 NCLT, forms a barrier that prevents the silicone molding compound from sticking to the surface and leaving a contaminating residue [see the companion article, "Molding Compound for Inspection of Internal Contours" (MFS-29243)]. It is no longer necessary to grind or polish the surface to remove the residue.

The cleaning agent is applied to the surface and allowed to dry completely to form a film. The molding compound is applied to the surface and allowed to cure. When the molding compound has been removed, the film is easily wiped away with deionized water.

This work was done by James F. Adams of Rockwell International Corp. for **Marshall Space Flight Center**. *No further documentation is available.*
MFS-29240 /TN

FOR ADDITIONAL INFORMATION: *Contact: Director, Technology Transfer Division, P.O. Box 8757, BWI Airport, MD 21240; (301) 621-0100 Ext. 241*
REFER TO THE NUMBER LISTED AT THE END OF THIS ARTICLE

NASA Tech Brief
National Aeronautics and Space Administration
Ames Research Center, Moffett Field, California

Licensing Opportunity

Carboranylmethylene-Substituted Cyclophosphazene Polymers

A new synthesis produces unusual electrical and chemical properties.

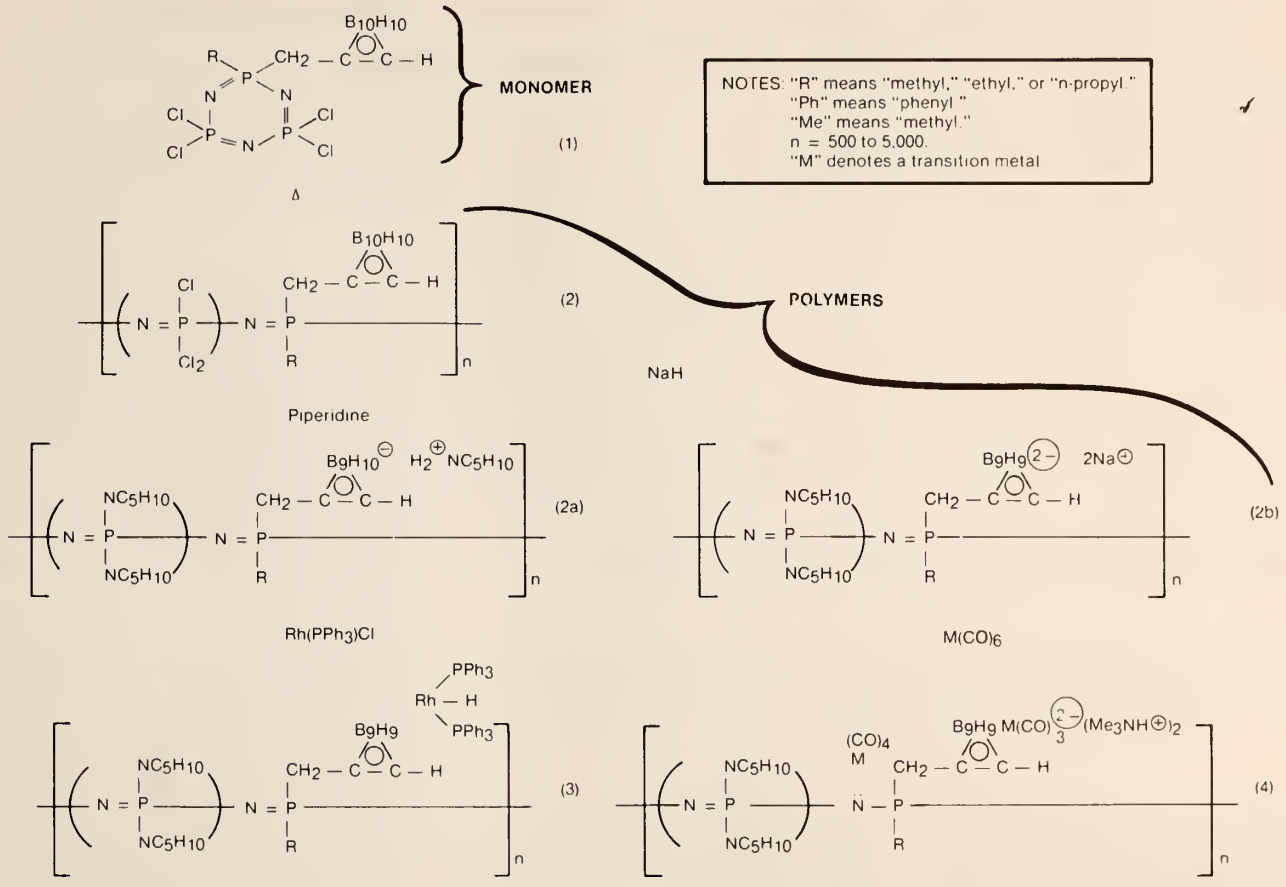

These Polymers are formed from the monomer (compound 1) in the sequence indicated here. The polymers have unique catalytic properties and are thermally stable.

A new class of polymers is based on cyclophosphazene monomers substituted with carboranylmethylene groups. The monomers are thermally polymerizable to carboranylmethylene-substituted phosphazene polymers, which are useful as thermally stable coatings. Since these compounds act as ligands for transition metals, metallocarboranylmethylene phosphazene polymers have also been synthesized and can act as immobilized-catalyst systems. Other useful forms of the polymers (both with and without metals) include fibers, films, moldings, and solvent-swelled gels.

The starting material is commercially available hexachlorocyclophosphazene. This compound is reacted with $[Bu_3PCuI]_4$ (where "Bu" means "butyl") in the presence of RMgCl (where "R" means "methyl," "ethyl," or "n-propyl"). It is then treated with isopropyl alcohol, followed by propargyl bromide in the presence of methyllithium, followed next by decaborane in acetonitrile and benzene. The resulting compound is the carboranylmethylene-substituted cyclotriphosphazene monomer.

The figure shows the sequence in which the polymers are formed from the monomer. The first step is to thermally polymerize the monomer (compound 1) by raising it to a temperature in the range of 225 to 300 °C. The polymer thus formed (compound 2) can be used as is or converted to less-reactive compound 2a by treating it with piperidine or another cyclic amine to remove the relatively reactive chlorine

atoms attached to the phosphorus atoms. When treated with a rhodium complex [for example, $Rh(PPh_3)Cl$, as in the figure], compound 2a becomes compound 3, which is useful as a catalyst for the hydrogenation of butenes to butanes at about 30 °C.

Compound 2a can also be treated with sodium hydride to produce compound 2b, which is useful as an intermediate in the production of polymers containing metallocarbonyl groups. Compound 2b is treated with the carbonyl compound of the metal to be complexed with the polymer, along with trimethylammonium chloride, while the reacting mixture is irradiated with ultraviolet light.

This work was done by Harry R. Allcock and Angelo G. Scopelianos of Pennsylvania State University for **Ames Research Center**.

Inquiries concerning rights for the commercial use of this invention should be addressed to the Patent Counsel, Ames Research Center Refer to ARC-11370 /TN

Ames Research Ctr.
Technology Utilization Officer: Laurance Milov
Mail Code 223-3
Moffett Field, CA 94035
(415) 694-6471
Patent Counsel:
Darrell G. Brekke
Mail Code 200-11
Moffett Field, CA 94035
(415) 694-5104

FOR ADDITIONAL INFORMATION: *Contact: Director, Technology Transfer Division, P.O. Box 8757, BWI Airport, MD 21240; (301) 621-0100 Ext. 241*
REFER TO THE NUMBER LISTED AT THE END OF THIS ARTICLE

NASA Tech Brief
National Aeronautics and Space Administration
Lyndon B. Johnson Space Center, Houston, Texas

Licensing Opportunity

Calculating Percent Gel for Process Control

The reaction state of a thermosetting resin is tracked to assure desired properties.

The percent gel has been found to be an important parameter for monitoring the progress toward cure of thermosetting resins. The only measurement required to track the accumulated progress in a given sample is its history of temperature versus time. The percent gel is particularly useful in adjusting the process conditions to achieve desired properties in resin-impregnated laminates.

In a typical process, a laminate or other composite part is impregnated with a reacting resin in the "B stage," which is an intermediate chemical state in which the resin softens while hot, allowing the part to be molded. The reaction rate increases with temperature, and the reaction proceeds until the resin is no longer plastic while hot. This state of reaction completion is defined as 100-percent gel, and intermediate states are characterized by smaller percentages.

Because of the temperature dependence of the reaction rate, the condition of the resin at the time of processing depends on the previous temperature history. Experiments with a representative phenolic resin show that the percent gel (that is, the amount of advancement toward cure) at a given moment is simply the sum of gel percentages accumulated during previous exposures to various temperatures, and that at an absolute temperature T, the rate of gel r_g follows an Arrhenius equation of the form

$$r_g = k \exp(-E/RT)$$

where k = the specific reactivity in percent per unit time, E = the activation energy per mole of reactant, and R = the ideal-gas constant (see figure). The percent gel G reached after exposure to a series of temperatures T_i for intervals of time t_i since initial preparation is thus given by

$$G = k\Sigma t_i \exp(-E/RT_i)$$

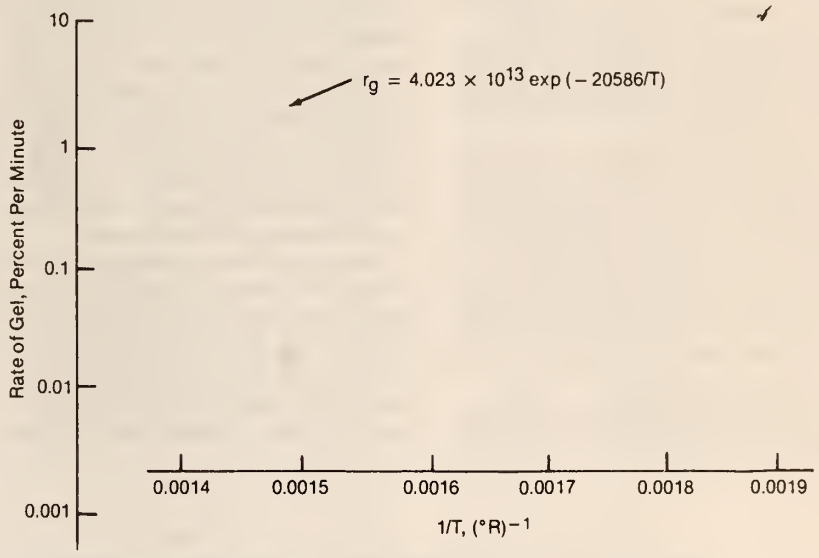

The **Rate of Gel** was determined as a function of temperature by measuring the time to gel of a part of graphite fabric impregnated with Hexcel R120 (or equivalent) phenolic resin.

Experiments have shown that such properties as the flexural strength, porosity, and thickness of a laminated part depend on the percent gel at the moment of application of pressure in an autoclave at the final high-pressure, high-temperature molding step. Thus the properties of the finished part can be controlled somewhat by controlling the times at various temperatures during the earlier stages of resin storage and part preparation. Since parts often arrive at the autoclave at different degrees of cure, each can be heated in the autoclave for the time needed to achieve the specified percent gel before the application of final pressure, thereby assuring uniformity from part to part.

This work was done by Charles Neal Webster and Robert O. Scott of LTV Aerospace Corp. for **Johnson Space Center**.

Inquiries concerning rights for the commercial use of this invention should be addressed to the Patent Counsel, Johnson Space Center Refer to MSC-21169/TN

Lyndon B. Johnson Space Center
Technology Utilization Officer: Dean C Glenn
Mail Code EA4
Houston, TX 77058
(713) 483-3809
Patent Counsel: Edward K Fein
Mail Code AL3
Houston, TX 77058
(713) 483-4871

FOR ADDITIONAL INFORMATION: *Contact: Director, Technology Transfer Division, P.O. Box 8757, BWI Airport, MD 21240; (301) 621-0100 Ext. 241*
REFER TO THE NUMBER LISTED AT THE END OF THIS ARTICLE

NASA Tech Brief
National Aeronautics and Space Administration

Evaluating Solid-Lubricant Films

The pin-on-disk tribometer provides valuable information when used properly.

A report describes experimental techniques for measuring the properties of solid-lubricant films. In addition, it discusses experimental parameters that are important in evaluating and developing new solid-lubricant materials.

The techniques are based on a pin-on-disk tribometer — a stationary, hemispherically tipped pin that slides against the flat surface of a rotating disk to which a specimen lubricant has been applied. The friction force on the pin is measured with a strain gauge. The measurement is made under varying loads. The temperature can be held constant or varied.

The report reviews the basic pin-on-disk configurations and methods of preparing disks and applying solid lubricants. Application methods range from quite simple (rubbing with a polishing cloth) to complex (plasma spraying, ion plating, and sputtering). The report describes factors that affect the performances of films; for example, the types of materials in sliding contact, sizes and shapes of the sliding parts, temperature, speed, and the presence or absence of liquids or dirt.

Techniques for constant-temperature testing, low-contact-stress testing, and temperature-versus-time testing are presented. Finally, the report suggests methods of measuring pin-wear volume and recommends ways of presenting data. In particular, plots of friction versus time and pin wear or film wear as functions of sliding distance are found useful.

This work was done by Robert L. Fusaro of **Lewis Research Center**. *Further information may be found in NASA TM-87236 [N86-19465/NSP], "How to Evaluate Solid Lubricant Films Using a Pin-on-Disk Tribometer." [A02]*

Copies may be purchased [prepayment required] from the National Technical Information Service, Springfield, Virginia 22161, Telephone No. (703) 487-4650. Rush orders may be placed for an extra fee by calling (800) 336-4700. LEW-14610

FOR ADDITIONAL INFORMATION: *Contact: Director, Technology Transfer Division, P.O. Box 8757, BWI Airport, MD 21240; (301) 621-0100 Ext. 241*
REFER TO THE NUMBER LISTED AT THE END OF THIS ARTICLE

NASA Tech Brief
National Aeronautics and Space Administration

Licensing Opportunity

Investigation of Epoxy Curing

A kinetic model describes major features of the curing process.

A report describes an investigation of the curing of an epoxy resin to be used in a carbon-fiber/epoxy version of the cases of the Space Shuttle booster rockets. The purpose of the investigation was to develop a physical and chemical kinetic model of the curing reaction for use in the control, verification, and optimization of the curing process to satisfy engineering objectives.

The resin studied was a mixture of a commercial epoxy and a reactive diluent. The curing agent was a commercial mixture of aromatic amines. The rocket case is to be made by winding carbon filaments impregnated with the mixture of resin and curing agent, partially curing the epoxy at room temperature, and completing the cure in an oven.

During the cure at room temperature, the resin gels and/or vitrifies, constraining the motion of the reacting molecules and thereby decreasing the rate of reaction to a value low on the time scale of the 2 to 3 weeks required for winding. Consequently, about 30 percent of the epoxy functional groups remain unreacted after the room-temperature cure. During the subsequent cure at higher temperatures, the resin may alternately soften and harden, allowing the curing reaction to continue.

A differential scanning calorimeter was used to determine the onset and extent of hardening as a function of temperature and time. Hardening and softening were considered to occur at the same rate and temperature. The transition temperature was defined as the temperature at which hardening begins. The extent of hardening was defined as the ratio of energy absorbed at a given point in a transition during a differential-scanning-calorimetry run to the total energy absorbed during that transition. The extent of reaction of the epoxy functional groups was also studied by Fourier-transform infrared spectroscopy. The transition temperature was correlated with the number average molecular weight. The number average molecular weight of the reacting mixture was measured as a function of time by dissolving the mixture in chloroform and measuring the resulting decrease in the vapor pressure.

The experimental data were interpreted in terms of an engineering model that accounts for the chemical and physical kinetics of the curing reaction. The chemical model includes the formation of an amine/water complex that reacts with the epoxy. The formation of an amine/epoxy complex and its decomposition into linear and cross-linked polymers are the steps that determine the reaction rate in the regime controlled by chemical kinetics.

Hardening is considered a zero-order reaction that begins when the transition temperature equals the actual temperature of the reacting mixture. As determined by differential scanning calorimetry, the hardening reaction has an activation energy typical of values associated with hydrogen bonding. An empirical correlation was developed to predict the transition temperature as a logarithmic function of the number average molecular weight during the room-temperature cure, when little cross-linking occurs.

The model predicts well the conversion of epoxy during the room-temperature and oven curing stages. However, the model needs to be improved to account for any reaction that may continue in the solid state and to predict the transition temperature more accurately, especially when cross-linking occurs at high temperatures.

This work was done by D. E. Cagliostro and A. Islas of **Ames Research Center** *and Ming-Ta Hsu of H C Chem. Corp. "A Cure-Rate Model for the Shuttle Filament-Wound Case,"*

Inquiries concerning rights for the commercial use of this invention should be addressed to the Patent Counsel, Ames Research Center Refer to ARC-11810 /TN

Ames Research Ctr.
Technology Utilization Officer. Laurance Milov
Mail Code 223-3
Moffett Field, CA 94035
(415) 694-6471
Patent Counsel:
Darrell G Brekke
Mail Code 200-11
Moffett Field, CA 94035
(415) 694-5104

FOR ADDITIONAL INFORMATION: *Contact: Director, Technology Transfer Division, P.O. Box 8757, BWI Airport, MD 21240; (301) 621-0100 Ext. 241*

REFER TO THE NUMBER LISTED AT THE END OF THIS ARTICLE

NASA Tech Brief
National Aeronautics and Space Administration

Microstructure of MnBi/Bi Eutectic Alloy

The effect of convection is examined.

A collection of three reports describes studies of the directional solidification of MnBi/Bi eutectic alloy. Fibers of MnBi are formed in a Bi matrix, with fiber dimensions and spacing that depend upon the conditions at and around the advancing solidification front. Prompted by the observation that the fibers formed on Earth are coarser than fibers formed in outer space (where there is no gravitationally driven convection) under otherwise identical conditions, the authors have engaged theoretical and experimental techniques to elucidate the effect of convection and other phenomena on the MnBi/Bi microstructure.

Two of the reports, "Influence of Convection on Lamellar Spacing of Eutectics" and "Influence of Convection on Eutectic Microstructure," establish the theoretical foundation for the remaining document. These reports seek to quantify the effect of convection on the concentration field of a growing lamellar eutectic. Numerical simulations lead to a number of conclusions regarding the coarsening effect of convection, including the following:

- The lamellar spacing, λ, increases with the square of the convective mixing.
- The influence of convection on λ decreases with an increase in the speed of the solidification front.
- The maximum increase of λ occurs where the lamellae are perpendicular to the flow.
- The lamellae tend to grow in the upstream direction.
- The increase in λ depends weakly on the eutectic composition and is a maximum in a 50:50-volume-percent eutectic.
- In a cylindrical ampoule held with its axis vertical, either not rotating or in alternating rotation about the axis, and with solidification proceeding along the axis, λ should increase with radial distance from the axis, both for gravitationally driven and rotationally driven convection.

The remaining report, "Study of Eutectic Formation," begins by continuing the theoretical developments. It notes that the effect, in the foregoing theory, of gravitation/buoyancy-driven convection alone is insufficient to explain the twofold increase in λ from solidification in space to solidification on Earth. The authors advance a partial explanation by discarding a previous simplistic assumption regarding the degree of undercooling and deriving equations that take account of the effect, upon undercooling, of the decrease in the eutectic mass fraction at the solidification interface and of the curvature of the interface. They also note that, although the theory was developed for lamellar eutectics, the increase in λ might be much larger in fibrous eutectics like MnBi/Bi, especially if the MnBi fibers extend out from the Bi matrix into the melt.

In alternating-spin, directional-solidification experiments, stirring affected the microstructure profoundly, even at high freezing rates: this contradicted the theoretical prediction that the effect of convection should die out at high freezing rates. At low freezing rates with 200-r/min stirring, no MnBi was found at the center of the ingot; there is no theoretical explanation for this.

A new technique under development by one of the authors will help to reveal the three-dimensional microstructures of alloys. The alloy specimen is etched in an electrochemical cell while it is monitored by time-lapse videotaping through a zoom microscope. The best candidate etching solution to date has been a mixture of sulfuric and phosphoric acids with water. This solution remains optically clear and etches the surface uniformly.

This work was done by William R. Wilcox, G. F. Eisa, B. Baskaran, and Donald C. Richardson of Clarkson University for **Marshall Space Flight Center.**
MFS-27174 /TN

FOR ADDITIONAL INFORMATION: *Contact: Director, Technology Transfer Division, P.O. Box 8757, BWI Airport, MD 21240; (301) 621-0100 Ext. 241*
REFER TO THE NUMBER LISTED AT THE END OF THIS ARTICLE

NASA Tech Brief
National Aeronautics and Space Administration
Marshall Space Flight Center, Alabama

Molding Compound for Inspection of Internal Contours

This material is clean, sets rapidly, and is easy to use.

A silicone elastomer, Citrocon (or equivalent), commonly used in dentistry, in combination with a mold-release agent [see the companion article, "Contamination Barrier for Contour-Molding Materials" (MFS-29240)], speeds and facilitates the making of impressions of interior surfaces so that the surface contours can be examined. A pliable semisolid material, the elastomer does not have to be contained by temporary dams or walls as do the viscous liquid room-temperature-vulcanizing (RTV) compounds previously used to mold internal contours. The elastomer also cures faster than do the RTV compounds — in about one-fourth the time.

The elastomer can easily be moved around in a cavity until the required location is found. An impression of the surface is then made by applying a small force to the elastomer and waiting for it to cure.

This work was done by Jim Adams and Steve Ricklefs of Rockwell International Corp. for **Marshall Space Flight Center**. *No further documentation is available.*
MFS-29243 /TN

FOR ADDITIONAL INFORMATION: *Contact: Director, Technology Transfer Division, P.O. Box 8757, BWI Airport, MD 21240; (301) 621-0100 Ext. 241*
REFER TO THE NUMBER LISTED AT THE END OF THIS ARTICLE

NASA Tech Brief
National Aeronautics and Space Administration

Nonisothermal Crystallization in PEEK/Fiber Composite

Several features of the crystallization process are attributable to the fibers.

A report describes experiments in the nonisothermal crystallization of poly(ether-etherketone)(PEEK) in APC-2, a composite of PEEK matrix reinforced with carbon fibers. PEEK is a high-performance, semicrystalline thermoplastic with properties that make it attractive for use in composites. Such properties as toughness and resistance to impact depend on the degree of crystallinity and the microstructure, which are very sensitive to processing conditions. Consequently, to understand the relation between processing and properties, it is necessary to study the kinetics of crystallization of the neat PEEK resin and of composites. Previous studies had addressed the related issues of isothermal crystallization of the neat resin and the ultimate degree of crystallinity achieved as a function of the rate of cooling.

In the experiments, pieces of the composite weighing less than 5 mg were placed in aluminum differential-scanning-calorimeter (DSC) pans and heated to 400 ° for 10 minutes to assure complete melting. The specimens were then cooled in the DSC at various constant rates ranging from 1 to 20 °C/min. The relative degrees of crystallinity as functions of time were inferred by integration of the rates of flow of heat from the specimens measured in the DSC. The ultimate degrees of crystallinity were estimated from wide-angle x-ray scattering and from areas under DSC exotherms of similarly treated specimens.

The kinetics of crystallization were studied with the help of a modified Avrami analysis, in which the relative degree of crystallinity is approximated by

$$X_c(t)/X_c(\infty) = 1 - \exp(-Kt^N)$$

where $X_c(t)$ = the degree of crystallinity at time t, $X_c(\infty)$ = the ultimate crystallinity, and K and N are related via the crystallization-rate parameter, $K^{1/N}$, which has the dimension of the reciprocal of time. This parameter was used in an equation for the rate as a function of temperature to determine the activation energy for crystallization.

The kinetics of crystallization in the composite were found to be significantly different from those of the neat resin. Such features as higher initiation temperature, higher temperature of maximum heat flow, and greater relative conversion to crystallinity via primary processes can be attributed to the presence of the carbon fibers. The fibers act as nucleation sites, which contribute to greater overall crystallinity. The fibers initiate the crystallization earlier (at higher temperature) and thereby also decrease the rate parameter compared to that of the neat resin.

For the composite material, the change from the primary kinetics of free crystal growth to slower secondary kinetics occurred at about 50 percent relative conversion. The activation energy for the primary process of crystallization was found to be larger than that of the neat PEEK resin; the reasons for this are still under investigation.

This work was done by Peggy Cebe of Caltech for **NASA's Jet Propulsion Laboratory**.

"Non-Isothermal Crystallization of Poly (etheretherketone) Aromatic Polymer Composite," NPO-17226 /TN

FOR ADDITIONAL INFORMATION: *Contact: Director, Technology Transfer Division, P.O. Box 8757, BWI Airport, MD 21240; (301) 621-0100 Ext. 241*

REFER TO THE NUMBER LISTED AT THE END OF THIS ARTICLE

NASA Tech Brief
National Aeronautics and Space Administration
Lewis Research Center, Cleveland, Ohio

Stress-and-Strain Analysis of Hot Metal/Fiber Composites

Macroscopic mechanical properties are derived from micromechanics.

Stress-and-strain equations have been developed to express the microscopic and macroscopic mechanical properties of metals reinforced by unidirectional fibers, over a range of temperatures. An object made of such a composite material can be treated mathematically by modeling the constituent materials discretely in finite-element analysis, but this treatment requires excessive computing time if the object has a complicated shape. The new equations reduce the computational load by providing approximate, closed-form expressions for the microscopic and the pseudohomogeneous anisotropic properties of a single ply reinforced by unidirectional fibers. These properties include the elastic moduli, Poisson's ratios, uniaxial strengths, thermal conductivities, coefficients of thermal expansion, heat capacities, and stresses in the microscopic constituents.

The micromechanical equations are derived by applying a mechanics-of-materials formulation to the mathematical model of the unidirectional ply, which is a planar array of square-cross-section unit cells. Each cell contains a fiber, the surrounding matrix material, and an interphase material generated by the chemical reaction between the fiber and the matrix (see Figure 1). The usual compatibility-of-displacement and equilibrium-of-forces conditions are imposed. For simplicity, it is pretended that the fibers are continuous, parallel, and equally spaced; that the fibers all have the same properties; and that the fibers, interphases, and matrix are all perfectly bonded to each other. Thermal effects are propagated by Fourier's law of heat conduction.

The resulting set of equations includes expressions for the properties of the ply as functions of the properties of the constituents. For example, the modulus of elasticity of the ply along the 1 axis is given by

$$E_{11} = k_m E_{m11} + k_f\{[1-(D/D_o)^2]\,E_{d11} + (D/D_o)^2 E_{f11}\}$$

where E denotes a modulus of elasticity; k denotes a volume fraction; the subscripts m, f, and d denote the matrix, fiber, and interphase, respectively; and D and D_o are as shown in Figure 1. The numerical results of this and the other micromechanical equations agree closely with the results of a finite-element analysis of a similar model.

Because the behavior of each constituent material is taken to be thermoviscoplastic and three-dimensionally anisotropic, the history of each constituent can be tracked independently as a function of time and represented as a state of stress and strain. A typical application of this capability would be the calculation of residual stress in a newly manufactured article (see Figure 2).

This work was done by Dale A. Hopkins and Christos C. Chamis of **Lewis Research Center**. *Further information may be found in NASA TM-87154 [N86-24757/NSP], "A Unique Set of Micromechanics Equations for High Temperature Metal Matrix Composites." [A03]*

Copies may be purchased [prepayment required] from the National Technical Information Service, Springfield, Virginia 22161, Telephone No. (703) 487-4650. Rush orders may be placed for an extra fee by calling (800) 336-4700.
LEW-14591 /TN

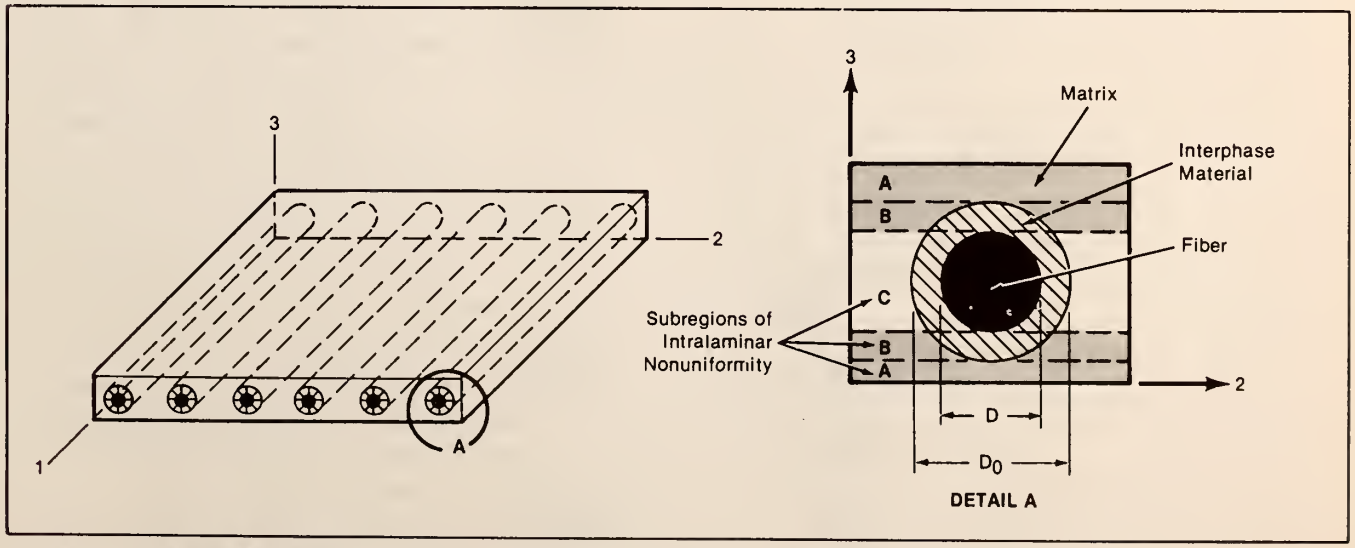

Figure 1. A **Unidirectional-Fiber Ply** in a metal/fiber composite material is modeled as an array of equally spaced fibers in square unit cells. The classical mechanics-of-materials formulation is applied to this model to obtain the micromechanical equations.

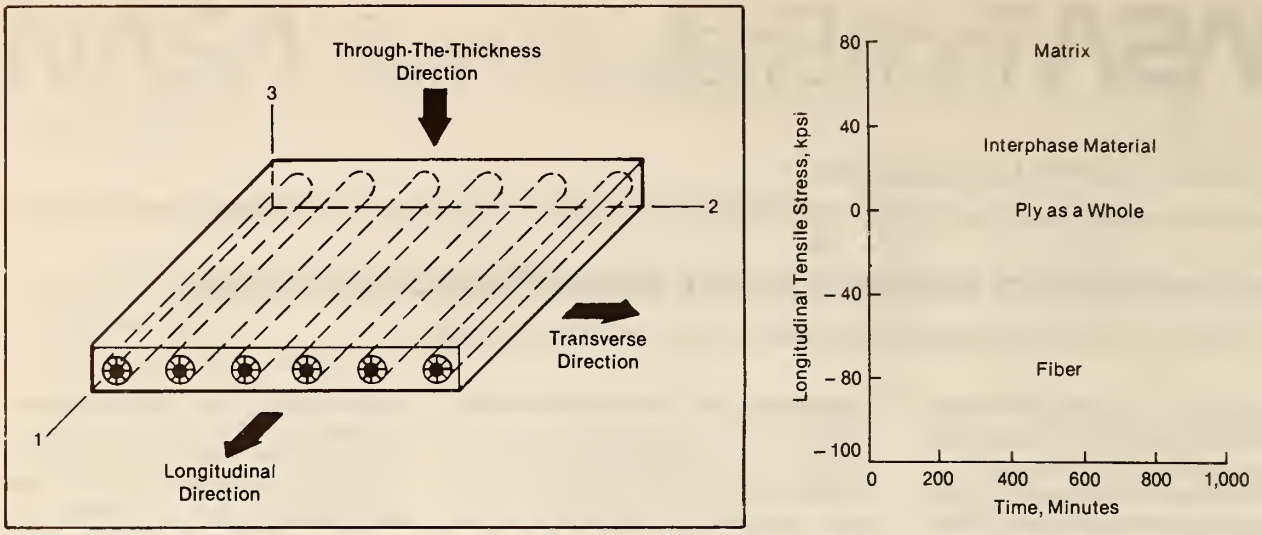

Figure 2. As a **Metal/Fiber Composite Cools** below the fabrication temperature, stresses develop in the constituents because each constituent has a different coefficient of thermal expansion.

FOR ADDITIONAL INFORMATION: *Contact: Director, Technology Transfer Division, P.O. Box 8757, BWI Airport, MD 21240; (301) 621-0100 Ext. 241*

REFER TO THE NUMBER LISTED AT THE END OF THIS ARTICLE

Oak Ridge National Laboratory

SUPER GRIP

Key words: Ceramics; bend-free tension testing; tension cyclic fatigue testing; hydraulic self-aligning grip; high temperature

Mechanical-property characterization of emerging advanced ceramics is important to their future use as structural components of advanced heat engines. Intrinsic tensile and fatigue properties are particularly needed in order to set stress allowable and to predict component lifetime. Unlike metal alloys, ceramics and many other brittle materials are inherently very difficult to test in tension because they contain many internal microdefects that are sensitive to testing methods. The difficulties include the gripping and alignment of a specimen so as to produce a concentric loading condition.

For years, many techniques and devices have been developed in attempts to improve the stress uniformity in tensile testing of ceramics. Although limited success has been made using sophisticated equipment and complicated procedures, none appears to offer any significant advantages over the others in terms of simplicity, reliability, and economy for routine testing.

Super Grip, the self-aligning grip system (Fig. 1) developed recently at ORNL, is operated hydraulically. It is a unique device that is capable of conducting pure static tensile and dynamic tension/tension cyclic fatigue testing of ceramics at elevated temperatures as high as 1400°C (Fig. 2).

The grip system is designed based on the principle of hydrostatics and the basic theorems of mechanics. Therefore, the device can perform precisely and reliably without the influence of operational skills. The grip system consists of

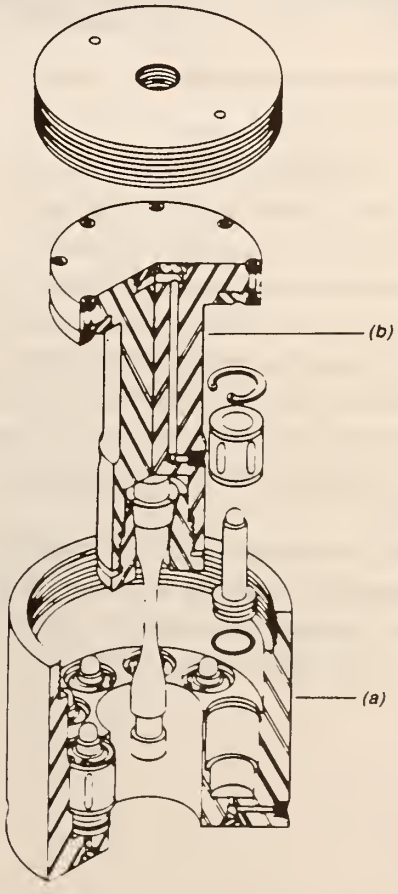

Fig. 1. The ORNL-developed Super Grip system is capable of performing bend-free tension-tension cyclic fatigue testing ($\Delta\sigma < 0.5\%$ of σ_{max}).

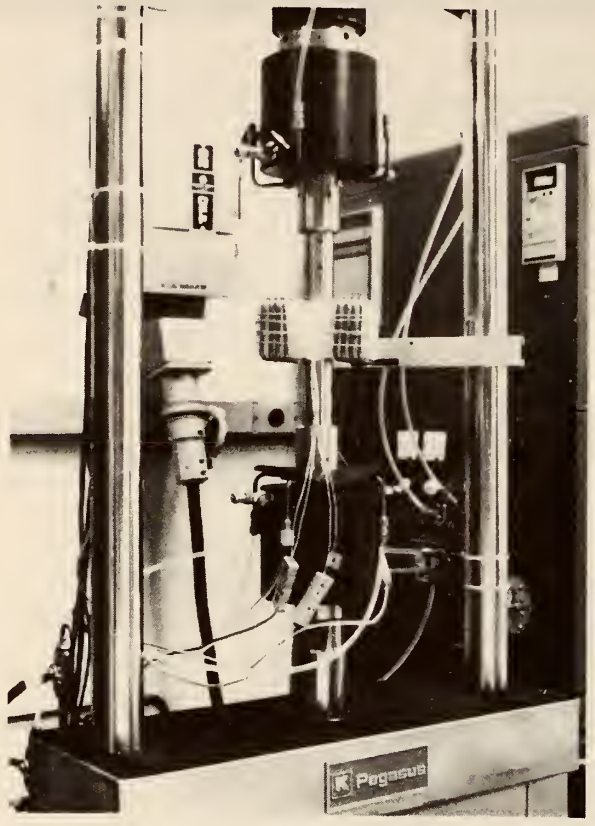

Fig. 2. The Super Grip system with a sample.

two major components: a hydraulic housing [Fig. 1(*a*)] and a pull-rod assembly (*b*). Built inside the housing unit are eight miniature hydraulic piston assemblies interconnected by a hydraulic manifold and equally spaced in a circle. The system works like an automobile brake system when the specimen load falls on the pistons. This design controls the force so that it passes through the center of the specimen automatically.

A number of tensile and cyclic fatigue tests were successfully completed, and meaningful results were obtained for commercial grades of aluminum oxide, silicon nitride, toughened ceramics, and ceramic composites. A summary of detailed examinations on test data and tested specimens suggests that the device and test method are reliable and that the data are indicative of material performance.

This grip system is now available from a commercial vendor under an exclusive licensing agreement with ORNL. U.S. patent No. 4,686,860 was issued to this invention on August 18, 1987.

Additional Information:

For a description of the technology, contact:

Office of Technology Applications
Information Service
Martin Marietta Energy Systems, Inc.
P.O. Box X
Oak Ridge, TN 37831
Telephone: (615) 574-4192; FTS 624-4192

References

K. C. Liu and C. R. Brinkman, "Tensile Cyclic Fatigue of Structural Ceramics," pp. 279-84 in *Proceedings of the 23rd Automotive Technology Development Contractors' Coordination Meeting, Dearborn, Mich., October 21-24, 1985, P-165,* Society of Automotive Engineers, Inc., Warrendale, Pa., March 1986.

K. C. Liu and C. R. Brinkman, "Tensile Cyclic Fatigue of Alumina at Room and Elevated Temperatures," pp. 191-200 in *Proceedings of the 24th Automotive Technology Development Contractors' Coordination Meeting, Dearborn, Mich., October 27-30, 1986, P-197,* Society of Automotive Engineers, Inc., Warrendale, Pa., April 1987.

For information about the availability of this technology, contact:

Instron Corporation
100 Royall Street
Canton, MA 02021

NASA Tech Brief
National Aeronautics and Space Administration
Lyndon B. Johnson Space Center, Houston, Texas

Automatically Inspecting Thin Ceramics for Pinholes

Flaws would be located and marked.

A proposed apparatus for inspecting prefired ceramic materials would detect minute flaws that might escape ordinary visual inspections. The method would not only detect flaws but would also mark their locations. The method is intended for such thin ceramic parts as insulation in capacitors and some radio-frequency filters.

According to the concept, a neon lamp in a reflecting chamber would direct intense light through a narrow slot onto the surface of the prefired ceramic. A row of photoelectric cells on the opposite side of the ceramic would sense light transmitted through flaws (see figure).

If a photocell sensed light as the ceramic was moved under the illuminated slot, the photocell output would be amplified and applied to a logic circuit. The circuit would activate an electromechanical marker, which would push a felt-tip pen onto the ceramic to mark the site of the flaw.

The method would enable the automatic nondestructive testing of ceramic parts. It could be made of inexpensive, off-the-shelf components.

This work was done by James R. Honaker of Rockwell International Corp. **Johnson Space Center**.
MSC-21091 /TN

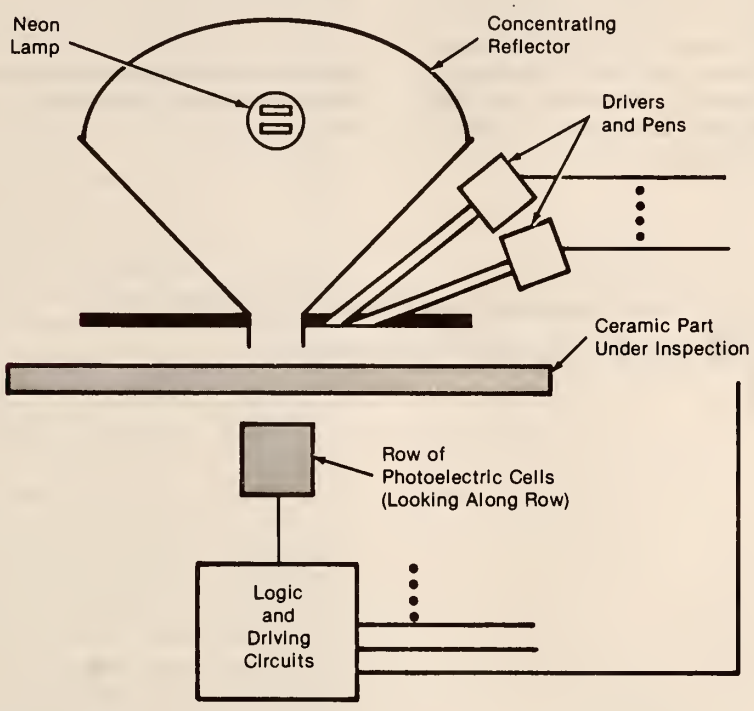

A **Ceramic Wafer** would be inspected optoelectronically for pinholes. The pinholes would be marked by felt-tipped pens.

FOR ADDITIONAL INFORMATION: *Contact: Director, Technology Transfer Division, P.O. Box 8757, BWI Airport, MD. 21240; (301) 621-0100 Ext. 241*
REFER TO THE NUMBER LISTED AT THE END OF THE ARTICLE

NASA Tech Brief
National Aeronautics and Space Administration
Marshall Space Flight Center, Alabama

Checking Nickel Plate for Porosity

A porosity test goes for a free ride with a cryogenic adhesion test.

Porosity in nickel plating on thermally insulated components can be readily detected as a side effect of an adhesion test for the plating. The combined adhesion/porosity test makes it unnecessary to subject the plated layer to a tedious, time-consuming inspection through a magnifying glass or microscope.

The adhesion of the nickel plating is checked by immersing the plated, thermally insulated part in liquid nitrogen, then withdrawing it and examining it for separation of the plated layer. A side effect of the immersion is that as soon as the part is removed from the cryogenic bath and for several minutes afterward, outgassing occurs at pores in the form of small gas jets. At each pore, the jet causes a rapid buildup of white frost that can be seen easily with the unaided eye.

The frosted areas can be marked so that the pores can be found after the frost disappears. A plating stylus can then be used for local repair of the nickel layer.

This work was done by Michael D. Roberts of Rockwell International Corp. for **Marshall Space Flight Center**. *No further documentation is available.*
MFS-29246 /TN

FOR ADDITIONAL INFORMATION: *Contact: Director, Technology Transfer Division, P.O. Box 8757, BWI Airport, MD. 21240; (301) 621-0100 Ext. 241*
REFER TO THE NUMBER LISTED AT THE END OF THE ARTICLE

NASA Tech Brief
National Aeronautics and Space Administration
Ames Research Center Moffett Field, California

Licensing Opportunity

Fast Measurements of Thermal Diffusivities of Ceramics

The temperature rises of samples are compared with that of a reference sample.

An apparatus quickly measures the thermal diffusivities of ceramics at high temperatures. The apparatus produces data on the relative thermal diffusivities of as many as six ceramic specimens per hour.

The apparatus includes a furnace box with quartz-lamp heating elements, a specimen holder, and a vacuum bell jar (see figure). The furnace box is made of blocks of fused silica and has a water-cooled aluminum floor. The specimen holder, made of rigid low-density silica, accommodates four ceramic samples, one of which is a reference sample. A hole at the center of each sample recess accommodates an aluminum calorimeter glued to the back of the sample. A thermal controller adjusts the power from a 440-V, 140-A supply to the quartz lamps according to the temperatures measured by two thermocouples at the top center of the sample holder.

The specimen holder, with its samples and calorimeters, is placed in the center of the furnace box. The tops of the holder and samples are coated with a black emittance-control coat. A bell jar is placed over the furnace box and is evacuated to a pressure of 20 millimeters of mercury (2.7 kPa).

The surfaces of the samples are heated by the lamps to 2,000 °F (1,093 °C) during 15 seconds and held at that temperature for 90 seconds. The lamps are then turned off. The temperatures of the calorimeters are measured during the last 18 seconds of the heat pulse. The apparatus records the maximum temperature and the rate of rise of temperature. The data are printed out in tables that show the rates of temperature rise or are plotted on graphs of temperature rise versus time during each heat pulse.

The ratio of the rate of temperature rise of an unknown sample to that of the reference sample, the thermal diffusivity of which is known, enables the determination of the relative thermal diffusivity of the unknown. If the densities of the unknown and reference ceramics are the same, the

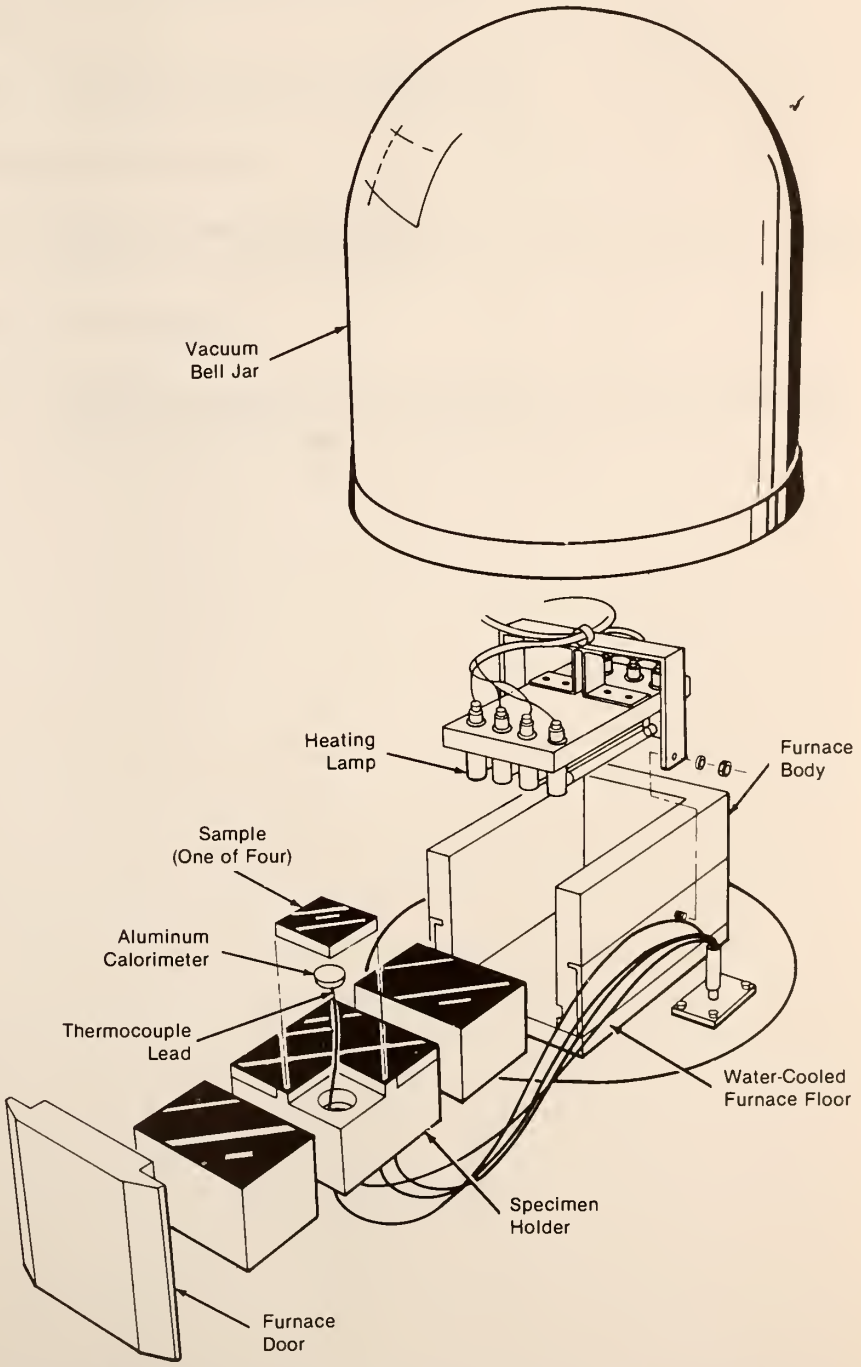

The **Thermal-Diffusivity Tester** makes it easy to determine the thermal diffusivities of ceramics. The pronounced effects of processing parameters on the thermal properties of the ceramics can therefore be evaluated quickly.

relative thermal conductivity is also obtained from the ratio.

This work was done by Marnell Smith and Howard E. Goldstein of **Ames Research Center.**

Inquiries concerning rights for the commercial use of this invention should be addressed to the Patent Counsel, Ames Research Center Refer to ARC-11705./TN

Ames Research Ctr.
Technology Utilization Officer: Laurance Milov
Mail Code 223-3
Moffett Field, CA 94035
(415) 694-6471
Patent Counsel:
Darrell G. Brekke
Mail Code 200-11
Moffett Field, CA 94035
(415) 694-5104

FOR ADDITIONAL INFORMATION: *Contact: Director, Technology Transfer Division, P.O. Box 8757, BWI Airport, MD 21240; (301) 621-0100 Ext. 241*

REFER TO THE NUMBER LISTED AT THE END OF THIS ARTICLE

Medicine & Biology

611 Protein in Diet Affects Excretion of Drugs

612 Heavy-Duty Rescue Straps for Coveralls — Straps enable rescuers to move injured people.

Software

613 Modeling Human Behavior During a Fire

Testing & Instrumentation

614 Blood Test Predicts Clinical Recurrence to Ovarian Cancer — The test uses CA125 radiometric assay.

Other Items of Interest

546 Screening for Alcohol-Producing Microbes — A dye reaction rapidly identifies alcohol-producing microbial colonies.

NIH
Research & Technology
U.S. Department of Health and Human Services Public Health Service National Institutes of Health

Protein in Diet Affects Excretion of Drugs

Scientists have long known that dietary protein affects the metabolism or breakdown of many drugs in the liver and other organs. Researchers at the General Clinical Research Center (GCRC) at the University of Iowa College of Medicine in Iowa City recently discovered that the amount of protein in the diet also profoundly affects the excretion of drugs — either by secretion or reabsorption.

A high protein diet increases the glomerular filtration rate, the speed at which urine is filtered in the glomeruli of the kidney. Since the rate of filtration affects the excretion of some drugs, there may be a 20 percent increase in the amount of drug excreted on a high-protein versus a low-protein diet.

In a study conducted at the University of Iowa GCRC, the drug oxipurinol — the active form of allopurinol — was used as a model to determine how the kidney handles drugs.

The renal clearance — the ability of the kidney to eliminate a substance from the body — of oxipurinol was markedly lower in subjects on a protein-restricted diet compared with subjects on a high-protein diet. Renal clearance of oxipurinol dropped by as much as 64 percent on a low-protein diet, resulting in a nearly threefold longer half-life of oxipurinol in the blood.

"A threefold difference in the half-life of any drug is a profound difference," says Dr. Reynold Spector, director of the University of Iowa GCRC and professor of internal medicine and pharmacology.

"Some drugs, if administered in full amounts to patients on protein-restricted diets, may be associated with toxicity because the drug accumulates in the patient's blood," he says, adding that if the reduced oxipurinol clearance lasted a period of weeks, causing the drug to remain in the body for an extended time, patients on protein-restricted diets or patients with poor nutrition might be at risk of developing severe reactions to the drug.

Dr. Spector and his colleague Dr. Glen D. Park, assistant professor of pharmacy at the University of Iowa, wanted to detect any long-term effects of protein or calorie restriction on the renal clearance of oxipurinol. They found that plasma oxipurinol concentrations rose in subjects after 2 and 4 weeks on a protein-restricted diet.

The renal clearance of uric acid, a substance produced as an end product of metabolism within the body, also decreased in the subjects on a protein-restricted diet. Because of the similarity between the breakdown of oxipurinol and uric acid, the researchers hypothesize that these compounds may share the same transport systems in the proximal tubule of the kidney. It appears then that oxipurinol and uric acid may be influenced by similar dietary factors such as protein.

The parallel between oxipurinol and uric acid is of substantial interest in medicine and physiology, according to Dr. Park.

"When excessive uric acid accumulates in the joints, causing the disease gout, allopurinol often is administered," Dr. Park says.

The study also showed an apparent dose-response relationship between the quantity of protein in the diet and the renal clearance of oxipurinol and uric acid, Dr. Spector says. A high-protein diet seems to increase the dose-response effect and a low-protein diet decreases the effect. In a previous study large or small amounts of protein intake resulted in correspondingly large or small oxipurinol renal clearance. In the current study, an intermediate protein intake resulted in an intermediate oxipurinol renal clearance.

Drs. Spector and Park have found very strong evidence that protein in the diet, not calories, is the major factor in the dose-response relationship. this effect was observed when the number of calories was standardized and the amount of protein in the diet was varied.

The results of this study of the effect of a 4-week restricted diet on the renal clearance of oxipurinol compared with a normal diet have two main implications, Dr. Spector says.

First, the effect of the diet on oxipurinol elimination is not readily reversed during continued protein restriction, so the risk of drug toxicity may remain as long as dietary restriction continues. Second, the effect of the diet on oxipurinol renal clearance may be applied to studies of other drugs that undergo active transport in the kidney.

The study also stresses the importance of the dosage of a drug. With such variables as amounts of protein in the diet, it may be extremely difficult to administer the proper dose of various drugs; for example, a hospitalized patient recovering from surgery who is being fed glucose intravenously would require a much smaller drug dose than an outpatient capable of eating a normal diet, Dr. Spector says.

The recent study was conducted with six healthy nonsmoking male volunteers between the ages of 20 and 35 years old, none of whom had a history of allergy, allergic skin rash, hyperuricacidemia or kidney or liver disease. The subjects received a normal diet for 10 days, followed by a protein- and calorie-restricted diet for 28 days.

"This study shows the impor-

tance of GCRC's. These kinds of studies are not easily conducted with outpatients or when there is a need for absolute control of such factors as drug dosing, smoking, caffeine, and activities," Dr. Spector says. "It is very important to control the diet to achieve constant results. If a vegetarian, who eats almost no protein, and an Iowan, who may consume two or three times the required daily amount of protein, were subjects in the same study, there would be considerable variability between the individuals in the half-life of the drug."

The control diet provided 100 grams of protein compared to only 19 grams of protein in the restricted diet. A normal-protein dinner consisted of baked chicken or roast beef, rice, peas, angelfood cake with strawberries, and apple juice. A typical low-protein dinner included low-protein spaghetti with tomato sauce, buttered corn, an apple, low-protein applesauce cookies, and orange juice.

Subjects lost an average of 7.7 kilograms of body weight during the 4 weeks on the restricted diet. During the restricted diet, significant reductions occurred in the renal oxipurinol clearance and were sustained for 4 weeks.

The change in the renal clearance of oxipurinol from the control diet through the second week of the restricted diet paralleled the change in the renal clearance of uric acid.

The current study shows strong but not conclusive evidence that oxipurinol is reabsorbed by the uric acid transport system, Dr. Spector says, but additional studies are necessary to investigate the mechanisms of uric acid and oxipurinol excretion related to changes in the diet.

The recent study has opened doors for future directions of research on the effect of protein restriction on the transport of drugs: what is the mechanism of the change in the renal clearance of oxipurinol; how quickly the change in oxipurinol renal clearance occurs; if renal clearance of other drugs might be similarly affected; and if the results of the studies on normal subjects can be generalized to malnourished patients.

"These studies also may serve as a model to explain changes in renal function during malnutrition," Dr. Spector says. "Although malnutrition is not a major problem in the United States, malnutrition due to calorie- and protein-restricted diets is an extreme problem in approximately 10 percent of the world."

Additional reading:

1. Park, G. D., Berlinger, W., G., Spector, R., Kitt, T. M., and Tsalikian, E., Sustained reduction in oxipurinol renal clearance during a restricted diet. *Clinical Pharmacology and Therapeutics* 41:616-621, 1987.
2. Berlinger, W. G., Park, G. D., and Spector, R., The effect of dietary protein on the clearance of allopurinol and oxipurinol. *New England Journal of Medicine* 313:771-776, 1985.
3. Hande, K. R., Noone, R. M., and Stone, W. J., Severe allopurinol toxicity: Description and guidelines for prevention in patients with renal insufficiency. *American Journal of Medicine* 76:47-56, 1984.
4. Fox, I. H., Halperin, M. L., Goldstein, M. B., and Marliss, E. B., Renal excretion of uric acid during prolonged fasting. *Metabolism* 25:551-559, 1976.
5. Bowering, J., Calloway, D. H., Margen, S., and Kauffmann, N. A., Dietary protein level and uric acid metabolism in normal man. *Journal of Nutrition* 100: 249-261, 1970.

The study of the effect of dietary protein restriction on the renal transport of oxipurinol described in this article was supported in part by the General Clinical Research Centers Program of the NIH Division of Research Resources, a Biomedical Resources Support Grant awarded to the College of Pharmacy by the NIH Division of Research Resources, and the Burroughs Wellcome Fund.

For Additional Information:

To locate information or professional contacts on this effort, contact:

Research Resources Information Center,
1601 Research Blvd.,
Rockville, MD 20850
(301) 984-2870

Refer to item XII, No. 02/TN

NASA Tech Brief
National Aeronautics and Space Administration
John F. Kennedy Space Center, Florida

Heavy-Duty Rescue Straps for Coveralls

Straps enable rescuers to move injured people.

A new type of strap on coveralls helps rescuers lift victims of industrial accidents. The new strap is made of heavy twill instead of the thin nylon previously used. The new material, which is 1 in. (2.54 cm) wide and has a breaking strength of 600 lb (2,670 N), is sewn to the coveralls with polyester thread in box "X" stitching. Reinforcing nylon webbing, 1¾ in. (4.4 cm) wide, is sewn with the strap at the attachment points.

Pairs of straps are placed at the back, shoulders, and hips, and a single strap is at the abdomen. They give rescuers a firm grip and enable them to carry the victim vertically or horizontally or by dragging. The bright-blue color of the straps makes them readily visible against white coveralls.

Normally, the straps are held flat against the coverall fabric by hook-and-pile patches. They are therefore less likely to snag on protruding equipment or otherwise impede wearers doing their work. However, the straps can be quickly detached by rescuers when they are needed. The patches replace metal fasteners.

This work was done by Henry M. Waddell of Rockwell International Corp. for **Kennedy Space Center**.

KSC-11295 /TN

A Dummy Is Used to illustrate one of the many possible ways in which an incapacitated worker can be moved by the heavy-duty straps on coveralls. When they are not being used, the straps are stored flat against the garment.

FOR ADDITIONAL INFORMATION: *Contact: Director, Technology Transfer Division, P.O. Box 8757, BWI Airport, MD. 21240; (301) 621-0100 Ext. 241*

REFER TO THE NUMBER LISTED AT THE END OF THE ARTICLE

NBS technology update
National Bureau of Standards
U.S. Department of Commerce
Gaithersburg, MD 20899

Modeling Human Behavior During a Fire

When the smoke alarm goes off, most people do predictable things: mother goes to get the children while father checks on the source of the smoke. Using such data from studies of residential fires and some controlled experiments, researchers in the NBS Center for Fire Research have developed a computer model that simulates the decisions and actions of occupants during a fire. Called EXITT, the model considers smoke conditions and the characteristics, capabilities, and locations of the occupants. It can be run on a personal computer using BASICA programming language. The user controls the model by answering simple questions that appear on the screen. EXITT also is part of a larger computer model developed by the center which takes into account the complex combination of variables, including human behavior, which influence the outcome of a residential fire.

FOR ADDITIONAL INFORMATION:

A report, EXITT - A Simulation Model of Occupant Decisions and Actions in Residential Fires: Users Guide and Program Description (NBSIR 87-3591), is available from the National Technical Information Service, Springfield, VA 22161 for $14.95 prepaid. Order by title and PB88-156088/NAC.

NIH
Research & Technology

U.S. Department of Health and Human Services Public Health Service National Institutes of Health

Blood Test Predicts Clinical Recurrence to Ovarian Cancer

The test uses CA125 Radiometric Assay

A blood test, the CA 125 radiometric assay, can be used to help predict whether women are likely to have a clinical recurrence of ovarian cancer during the 4-month period following the test, report Dr. Jonathan Niloff and his associates.

Women who have had ovarian cancers removed by surgery run a significant risk of recurrence. Even when the primary tumor has been excised, remaining cancerous cells can spread to adjacent tissues. Because these tissues lie deep within the abdomen, recurrent life-threatening cancers can be hard to detect. Even more problematic is the fact that long-term survival doesn't always hinge on whether or not some malignant cells are still present.

The CA 125 radiometric assay was developed in 1984. It is a blood test that measures the concentration of a glycoprotein released by human epithelial ovarian carcinoma cells. This test was used in association with exploratory surgery to find out if cancer has recurred, says Dr. Niloff of the division of gynecologic oncology at the New England Deaconess Hospital of Harvard Medical School in Boston.

The predictive information the test gives can be used to plan treatment, if that is required, to maximize efficacy and minimize possible adverse effects of the potentially toxic drugs and radiation commonly employed in therapy. In many cases treatment can be begun before new tumors have had time to grow and spread.

Dr. Niloff and his colleagues studied 55 women at four institutions around the country: Harvard; the Mayo Clinic, Rochester, Minnesota; Pennsylvania State University, Hershey Medical Center; and the University of California, Los Angeles, School of Medicine. All the women had had ovarian cancers removed surgically and had completed a primary course of chemotherapy. Their average age was 54; the range of age was 37 to 74 years.

Each patient had blood drawn for CA 125 levels just before a "second-look" operation was performed to see if malignant tissue was still present, and blood samples were drawn again several times thereafter. The women were monitored for approximately 1 year.

A clear cutoff point in the CA 125 level was discovered that proved to have strong predictive power for the subsequent probability of cancer recurrence, Dr. Niloff says.

If the concentration of CA 125 was 35 units per milliliter or higher, the woman had a 60 percent risk that there would be a clinical recurrence of cancer within the ensuing 4 months. If the level was less than 35, however, the chance of a recurrence dropped to 5 percent. Again, this prediction seemed to hold true for about 4 months, he reports.

When the researchers looked at the relationship between CA 125 levels and recurrence of cancer over an extended period, they were able to detect certain significant patterns. Gradually rising levels of CA 125 were found in women who eventually had a recurrence. Conversely, in patients who remained free of disease, CA 125 levels tended to fall over the 12 months of the study.

For the study period as a whole, 35 of the 55 women eventually had a clinical recurrence of cancer. In 94 percent of these 35 women, the CA 125 level had risen significantly approximately 3 months before the recurrence could have been detected by other means. In contrast, only 20 percent of the patients whose CA 125 levels always stayed low developed a new episode of disease.

Dr. Niloff notes that on some occasions surgeons are not able to remove all of the cancerous ovarian tissue. Here, too, there is an important threshold. If a tumor of 1.5 cm or more remains, the patients have a substantially greater risk of clinical recurrence.

The predictions of recurrence based on the CA 125 levels were found to be unrelated to this second predictor, he says, adding that having more cancerous tissue remaining after the initial surgery did not necessarily mean that the CA 125 level would be elevated correspondingly.

At the same time, it was also true that the CA 125 assay was most valuable in patients who still had malignant tissue remaining in their body after surgery, since these patients were most at risk of clinical recurrence. Early therapeutic intervention was therefore possible.

In studies just recently completed, Dr. Niloff has found that the CA 125 assay can also be used to make predictions about patient survival. "If we do the assays right away, just after the primary chemotherapy has been completed, the CA 125 is predictive to some extent. But further down the road — by 1 year after therapy — the 35-units-per-milliliter level becomes an excellent prognostic indicator. You can divide the patients into two clear groups: those who will likely survive and those who won't," he says.

The usual technique of repeated surgical procedures to check for tumor recurrence has several limitations, including the potential for infection and surgical complications. The results of

the procedures may be inaccurate, and it is obviously impossible to do this kind of surgery very often; therefore it is hard to tell what is happening to a given patient over a period of time, Dr. Niloff comments.

The CA 125 assay provides the physician with a simple noninvasive tool for checking on the status of patients who have had surgery for ovarian cancer. Knowing several months ahead that a patient is likely to develop a recurrence of cancer allows the physician to begin therapy earlier, when it has the greatest chance of success.

Dr. Niloff says that, since the test has already been approved by the Food and Drug Administration, there's no reason more primary-care physicians can't use it.

In future research Dr. Niloff's group will expand these studies and try to learn whether performing CA 125 assays on a regular and frequent basis can extend the interval of predictability between assay and recurrence beyond the current 4 months. If this is possible, appropriate therapy could be begun that much sooner.

—Dana H. Murphy

Additional reading:

1. Piver, M. S., Ovarian carcinoma—a decade of progress. *Cancer* 54:2706-2715, 1987.

2. Niloff, J. M., Knapp, R. C., Lavin, P. T., Malkasian, G. D., Berek, J. S., Mortel, R., Whitney, C., Zurawski, V. R. Jr., and Bast, R. C. Jr., The CA 125 assay as a predictor of clinical recurrence in epithelial ovarian cancer. *American Journal of Obstetrics and Gynecology* 155:56-60, 1986.

3. Berek, J. S., Knapp, R. C., Malkasian, G. D., Lavin, P. T., Whitney, C., Niloff, J. M., and Bast, R. C. Jr., CA 125 serum levels correlated with second-look operations among ovarian cancer patients. *Obstetrics and Gynecology* 67:685-689, 1986.

4. Richardson, G. S., Scully, R. E., Nikrui, N., and Nelson, J. H., Common epithelial cancer of the ovary. *New England Journal of Medicine* 312:415-424, 1985.

5. Copeland, L. J., Gershenson, D. M., Wharton, J. I., Atkinson, E. N., Sneige, N., Edwards, C. L., and Rutledge, F. N., Microscopic disease at second-look procedures for ovarian cancer. *Cancer* 55:472-478, 1985.

6. Niloff, J. M., Bast, R. C. Jr., Schaetzl, E. M., and Knapp, R. C., Predictive value of CA 125 antigen levels in second-look procedures for ovarian cancer. *American Journal of Obstetrics and Gynecology* 151:981-986, 1985.

7. Berek, J. S., Hacker, N. F., Legasse, L. D., Poth, T., Resnick, B., and Nieberg, R. K., Second-look laparotomy in stage III epithelial ovarian cancer: Clinical variables associated with disease status. *Obstetrics and Gynecology* 64:207-212, 1984.

8. Wharton, J. T., Edwards, C. L., and Rutledge, F. N., Long-term survival after chemotherapy for advanced epithelial ovarian carcinoma. *American Journal of Obstetrics and Gynecology* 148: 997-1005, 1984.

9. Klug, T. L., Bast, R. C. Jr., Niloff, J. M., Knapp, R. C., and Zurawski, V. R. Jr., A monoclonal antibody immunoradiometric assay for an antigenic determinant (CA 125) asssociated with human epithelial ovarian carcinomas. *Cancer Research* 44: 1048-1053, 1984.

10. Bast, R. C. Jr., Klug, T. L., St. John, E., Jenison, E., Niloff, J. M., Lazarus, H., Berkowitz, R. S., Leavitt, T., Griffiths, C. T., Parker, L., Zurawski, V. R. Jr., and Knapp, R. C., A radioimmunoassay using a monoclonal antibody to monitor the course of epithelial ovarian cancer. *New England Journal of Medicine* 309:883-887, 1983.

11. Schwartz, P. E. and Smith, J. P., Second-look operations in ovarian cancer. *American Journal of Obstetrics and Gynecology* 138:1124-1130, 1980.

Studies on the prediction power of the CA 125 assay were supported in part by the Biomedical Research Support Program of the NIH Division of Research Resources and the William P. Graves Ovarian Cancer Fund.

For Additional Information:

To locate information or professional contacts on this effort, contact:

Research Resources Information Center,
1601 Research Blvd.,
Rockville, MD 20850
(301) 984-2870

Refer to item XII, No. 03/TN

Natural Resources Technology & Engineering

615 Computer Architecture for Research in Meteorology and Atmospheric Chemistry

Testing & Instrumentation

616 Ultraviolet Lidar Would Measure Wind Velocity — Incoherent Doppler-shifted scattering from aerosols will reveal important weather data.

Other Items of Interest

568 Acoustical Measurement of Mine-Shaft Length — The length is calculated from the measured resonant frequency. (Licensing Opportunity)

United States
Environmental Protection
Agency

Atmospheric Sciences
Research Laboratory
Research Triangle Park NC 27711

Research and Development

EPA

Project Summary

A Computer Architecture for Research in Meteorology and Atmospheric Chemistry

This study examines the feasibility of constructing a peripheral hardware module that could be attached to a mini or midsized computer to accelerate the execution of large air pollution models, such as the EPA's Regional Oxidant Model (ROM). Crucial information necessary to design such an accelerator is acquired by running the ROM computer code under instrumentation which shows how the computational load is distributed within the model and the data transfer rates between each step of the model execution. These data reveal that a model such as the ROM is not amenable to acceleration using a vector-type architecture because the computational burden is too inhomogeneous in space and time. They also show that the most computationally intensive portions of the model involve little or no data communication with neighboring points in the grid mesh. Together, these facts suggest that the most efficient accelerator design is one that utilizes a system of loosely coupled processors. Two such designs are explored. In one, the host computer performs part of the model execution while the most computationally intensive portions are executed by a network of slave processors under control of the host machine. In the second design, called the tile machine, the spatial domain simulated by the model is subdivided into small pieces and a separate processor executes the full ROM code within each subdomain. Simulations show that an accelerator based on the tile machine architecture would be capable of executing the ROM up to 100 times faster than the host machine working alone.

This Project Summary was developed by EPA's Atmospheric Sciences Research Laboratory, Research Triangle Park, NC, to announce key findings of the research project that is fully documented in a separate report of the same title (see Project Report ordering information at back).

Introduction

In the mid 1970's the EPA began the development of the Regional Oxidant Model (ROM) as a state-of-the-science tool for both research and regulatory applications. In the early 1980's similar efforts were begun to develop regional scale acid deposition and particulate models. All of these models are very large and complex and as a result they require large computer resources to operate. For example, on the EPA's VAX 8600 computer, the ROM requires about 24 hours of CPU time to simulate a 24-hour day. The same simulation requires only 2 hours on the Agency's IBM 3090 computer, but time on this machine is expensive and it is not available on a demand basis. The acid rain and particulate models are expected to require even longer execution times. In short, increases in the scale and complexity of air pollution models have outpaced the growth in the available computing capability. One possible solution to this problem is to build computer hardware specifically designed to perform the computations that these models entail. This report describes a study conducted by the Research Triangle Institute for the EPA to determine the feasibility of constructing equipment of this type, capable of accelerating the execution of the ROM on the Agency's VAX 8600 and/or VAX 785 computers.

Procedure

The first step in this study was to understand the basic mathematical structure of the ROM. This model consists of 30 coupled nonlinear partial differential equations that are solved on a 3-dimensional grid containing some 7500 mesh points. Each equation describes the effects of winds, chemistry, sources, deposition and other physical processes on the concentration of each of 30 chemical species. The equations are solved as an initial value problem to simulate concentration patterns in space at 30 minute intervals over periods up

to 1 month in length.

The technique employed in the ROM to solve the governing equations splits each of the 30 dependent variables into two components. One of these, represented mathematically by the Greek letter, Γ, embodies the effects of the horizontal winds only. Each of the 30 Γ components is the solution of a single, linear, 2-dimensional differential equation. The simplicity of the Γ equations is offset somewhat by the fact that the value of Γ at each grid point is coupled to the corresponding values at 36 neighboring grid points. This is an important factor in the design of a model accelerator.

The second component of the dependent variables, represented mathematically by γ, embodies the effects of chemistry, sources, deposition and other processes. Unlike Γ, the γ components are governed by a system of nonlinear equations in which the γ's of all 30 species are coupled together. However, for the most part the value of any one of the γ components at any given grid point is independent of the γ values at neighboring grid points. This fact suggests that the γ equations would be amenable to treatment by parallel processors.

The second stage of the feasibility study was to run the ROM code under instrumented conditions to determine how much machine time is spent on the Γ computations, how much is devoted to γ, and how these times vary from grid point to grid point and time step to time step during the model execution. These data, plus information on the data transfer rates within the model, provide the specifications for feasibile accelerator designs.

Conclusions

The analyses performed on the ROM computer code during an actual model run revealed a number of important features. First, the ROM is totally dominated by floating point computations. Consequently, an essential requirement of a model accelerator is high speed floating point capability. Second, an average 10 percent of the model execution time is used by the Γ computations and the remaining 90 percent is devoted to the γ calculations. This lopsided split reflects the heavy computational burden created by the nonlinear chemical processes represented by the γ equation. Third, the CPU time required to derive γ varies by more than a factor of seven from grid point to grid point and time step to time step.

Taken together these facts suggest that the most efficient design of a ROM accelerator would be one consisting of a set of loosely coupled processors. The investigators proposed and simulated two separate designs. In one system, referred to as the Γ/γ architecture, the host machine performs the Γ computations while the γ equations are solved by a set of slave processors which together comprise the accelerator module. Simulations of this design indicated that with an accelerator consisting of about 25 Micro VAX-II class processors, the VAX 8600 could execute the ROM about 10 times faster than it can acting alone. This would make the ROM run times on the VAX comparable to those achievable on the IBM 3090.

In the second proposed system, referred to as the tile machine, the spatial domain simulated by the ROM would be subdivided into a number of small areas, or tiles. In this system a separate processor would handle both the Γ and γ equations in each tile while the host machine would take care of data communication and load leveling chores. Analysis of this design indicated that with a large enough number of processors, an accelerator based on this architecture could potentially increase ROM execution speeds by a factor of 100. Computing capacity of this magnitude would open up new areas of model applications and research that are presently infeasible due to prohibitive computer time requirements.

The report also addresses the issues of fault tolerance, the use of array processors, hardware interfaces, cost vs performance trade-offs, and other topics

J McHugh, J Pierce, D Rich, J Dunham, D McLin, and N Kanopoulos are with Research Triangle Institute, Research Triangle Park, NC 17709
***Robert G. Lamb** is the EPA Project Officer (see below)*
The complete report, entitled "A Computer Architecture for Research in Meteorology and Atmospheric Chemistry," (Order No PB 88 145 313 AS, Cost $19 95, subject to change) will be available only from
National Technical Information Service
5285 Port Royal Road
Springfield, VA 22161
Telephone, 703-487-4650
The EPA Project Officer can be contacted at
Atmospheric Sciences Research Laboratory
U S Environmental Protection Agency
Research Triangle Park, NC 27711

NASA Tech Brief
National Aeronautics and Space Administration
NASA's Jet Propulsion Laboratory, Pasadena, California

Ultraviolet Lidar Would Measure Wind Velocity

Incoherent Doppler-shifted scattering from aerosols will reveal important weather data.

A remote-sensing system now in an early stage of development could make global measurements of wind velocities along a probing beam of ultraviolet light. The ability to measure wind velocities remotely is necessary for a better understanding of atmospheric physics and to improve weather prediction. In aviation, a remote wind-measuring system could promote safety through the detection of wind shears and clear-air turbulence.

The system under development will include a range-gated (pulsed) ultraviolet-excimer laser operating at 308 or 353 nm. From an orbit around the Earth, the laser would illuminate the portion of the atmosphere to be probed. A portion of the incident radiation would undergo Mie scattering from aerosol particles entrained in the wind and would be reflected back to the orbiting station with a Doppler-shifted spectrum representative of the distribution of aerosol-particle velocities along the line of sight.

An earlier proposal for such a system was based on the use of infrared radiation from a CO_2 laser. The ultraviolet system was proposed subsequently because the ultraviolet radiation is scattered more effectively by the aerosol particles — an important consideration in measurements at high altitudes and in the southern hemisphere where aerosol concentrations are low.

The processing of the scattered light in the receiving portion of the system will be complicated somewhat by the strong component of thermally broadened Rayleigh scattering from nitrogen and oxygen molecules. In the developmental system, the receiver will contain a wavelength filter composed of multiple Fabry-Perot etalons to discriminate between the broad air spectrum and the relatively narrow aerosol spectrum (see figure).

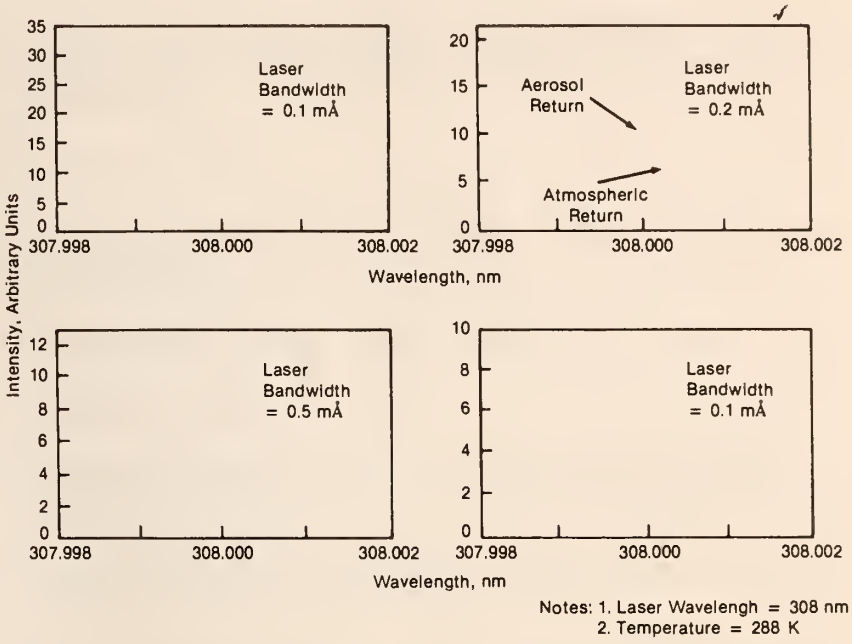

Backscattering Spectra were calculated for air based on a standard atmosphere and continental haze-type aerosol distribution. These spectra show that it is advantageous to operate at the minimum possible laser bandwidth to increase the height of the narrow aerosol return above the broad molecular return.

A small fraction of the transmitted laser pulse will be diverted to the wavelength meter in the receiver to provide a measurement of the output wavelength and the wavelength reference with which the return pulse is compared. Because the comparison will be made for each transmitted/received pulse pair, mode hops between laser pulses will not affect the measurement of the wind velocity. Furthermore, even in the presence of mode hopping, the differential-wavelength measurements can still be averaged to increase the accuracy.

Several experimental units have demonstrated the feasibility of the XeCl excimer type of laser that will be used. One distinct advantage of the incoherent Doppler lidar is that on account of the differential measurement at each pulse, the absolute laser frequency does not have to be controlled: it is necessary only to keep the bandwidth narrow. This places the emphasis in the stabilization of frequency on the passive wavemeter and the multiple Fabry-Perot filter, which are easier to control than is the laser.

This work was done by Iain Stuart McDermid and James B. Laudenslager for **NASA's Jet Propulsion Laboratory** *and David Rees of University College London.*
NPO-16756 /TN

FOR ADDITIONAL INFORMATION: *Contact: Director, Technology Transfer Division, P.O. Box 8757, BWI Airport, MD 21240; (301) 621-0100 Ext. 241*
REFER TO THE NUMBER LISTED AT THE END OF THIS ARTICLE

Physical Sciences

617 Electrochemical Growth of Crystals in Gels — Nucleation and growth rates are readily controlled. (Licensing Opportunity)

618 Equations for Fading-Memory Filters — Simplified solutions are based partly on the exponential decay of effects of previous states.

619 Mechanical Properties of Large Sodium Iodide Crystals — For the first time, data on large thallium-doped samples are available.

620 Slow Release of Reagent Chemicals from Gel Matrices — A simple technique enables the slow diffusion of chemicals into solutions. (Licensing Opportunity)

Testing & Instrumentation

621 Preconcentrating Air Sampler—PAS-100 — Enhancing analysis with a simple first step.

622 Portable, Surface-Enhanced Raman Spectroscopy System

623 Crystal Laser Monitor

624 Measuring Incorporation of Arsenic in Molecular-Beam Expitaxy — Changes in surface layers cause oscillations in RHEED measurements.

625 Pressure-Sealing Optical Coupling — Light signals are passed out of a high-pressure cryogenic environment.

626 Optical Temperature Sensor for Gas Turbines — The new design promises accuracy even in the presence of contamination. (Licensing Opportunity)

627 Probing Polymer-Segment Motions by ESR — Molecular origins of mechanical properties and aging processes can be studied.

Other Items of Interest

599 Carboranylmethylene-Substituted Cyclophosphazene Polymers — A new synthesis produces unusual electrical and chemical properties. (Licensing Opportunity)

NASA Tech Brief
National Aeronautics and Space Administration
Langley Research Center, Hampton, Virginia

Licensing Opportunity

Electrochemical Growth of Crystals in Gels

Nucleation and growth rates are readily controlled.

A technique has been developed to grow crystals by controlling the rate of transfer of one component into the crystallization volume. This method involves the electrochemically controlled generation of one of the precipitation species, coupled with a diffusion barrier.

The new procedure, which can be extended to other crystals, was developed in connection with the formation of lead tin telluride by the reaction in gels of the metal ions with telluride ions. The principal difficulty in dealing with solutions of telluride ions is that the ions are easily oxidized by many impurities found in solutions. Consequently, in this new technique the telluride ions are formed in situ.

An electrically conductive gel is prepared by the use of potassium acetate in place of the usual distilled water. While still fluid, the gel is poured into the bottom of an inverted sintered-glass Gooch crucible. When the gel sets, the crucible is inverted and mounted inside a beaker (see figure). If desired, sites of nucleation and subsequent crystal growth can be established by gently pricking the gel with a very thin platinum wire or glass fiber to form small holes. A lead sheet is fitted to the inside of the outer beaker, and a piece of tellurium is mounted on the inside of the Gooch crucible. A 1-M solution of lead (II) acetate is poured into the outer beaker, and a 50-percent solution of phosphoric acid is poured into the Gooch crucible.

A constant-voltage source is applied in such a way that the tellurium is the cathode. By regulation of the voltage and current, the telluride concentration and the subsequent extent of supersaturation can be regulated to provide the conditions most suitable for crystal growth. Voltages on the order of 2 to 3 Vdc with currents of

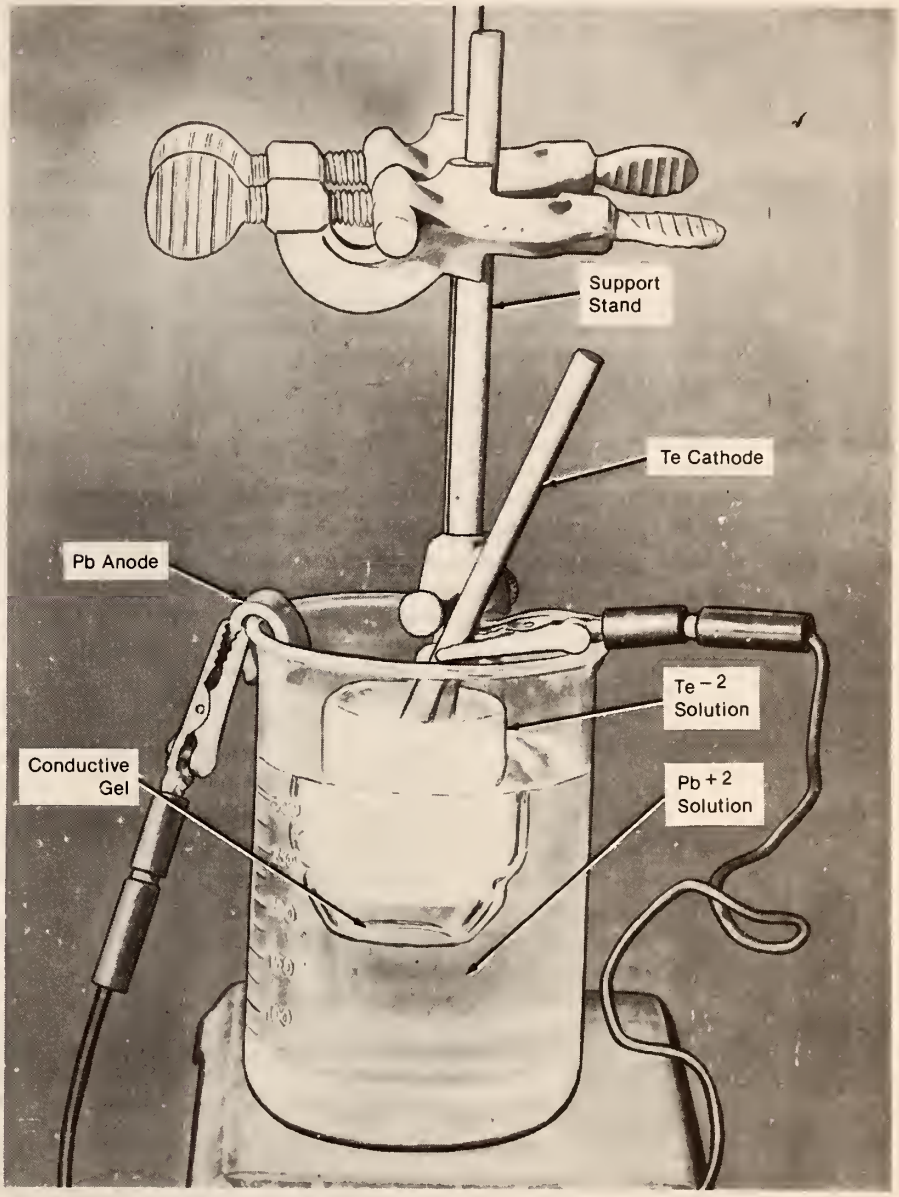

The **Electrochemical Gel Cell** is used for the control of mass flow.

10 to 15 mA have proved suitable.

Although this method was developed for lead telluride, it is generally applicable for the electrochemical growth of any crystals that are formed from the reaction of ionic species generated at cathodes and anodes. The greatest advantages of this method are the ease with which nucleation and growth rates can be controlled and the simplicity with which the concentrations of ions that are easily oxidized or reduced can be maintained.

This work was done by Patrick G. Barber and James Coleman of Longwood College for **Langley Research Center**.

Inquiries concerning rights for the commercial use of this invention should be addressed to the Patent Counsel, Langley Research Center Refer to LAR-13608/TN

Langley Research Ctr.
Technology Utilization Officer: John Samos
Mail Stop 139A
Hampton, VA 23665
(804) 865-3281
Patent Counsel: George F. Helfrich
Mail Code 279
Hampton, VA 23665
(804) 865-3725

FOR ADDITIONAL INFORMATION: *Contact: Director, Technology Transfer Division, P.O. Box 8757, BWI Airport, MD 21240; (301) 621-0100 Ext. 241*

REFER TO THE NUMBER LISTED AT THE END OF THIS ARTICLE

NASA Tech Brief
National Aeronautics and Space Administration

Equations for Fading-Memory Filters

Simplified solutions are based partly on the exponential decay of effects of previous states.

A report discusses simplified recursive solutions for the equations of a class of fading-memory filters. Under appropriate assumptions regarding noise and the exponential decay of the effects of previous states, the filter equations can be reduced to analytic formulas in closed form.

The general filter problem involves a linear system that passes through a sequence of discrete states, each of which depends on the previous state. The filter is not a piece of equipment but rather a set of equations that provides a sequence of estimates of the states that fit the measurements of the states and the mathematical model of the system as closely as possible according to a weighted-least-squares criterion. Transitions between, and measurements of, the states include state-independent white noise. The filter calculations are complicated matrix and matrix-inverse operations at each discrete time.

The choice of weighting matrices for the least-squares calculation determines the filter equations. One such choice results in Kalman filtering, which offers recursive solutions for state estimates and for a state-estimate-covariance matrix. However, Kalman filters attempt to fit all past data into a single model, a disadvantage when the system varies with time. When the model is in error, large errors occur in the state estimates.

In this study, a weight that decays exponentially with time is applied to older measurements. This approach entails the loss of information as past measurements are discounted but compensates by overcoming most of the mismodeling and instability associated with Kalman filters. The fading-memory filter has the added advantage that an exponential decay of past data is intuitively comprehensive to most users.

A simplification is achieved by assuming that the state-noise-covariance matrix is proportional to the time-propagated state-estimate-covariance matrix. Even though this assumption departs from the modeling of the state noise in the physical system, it is useful in practical problems where the state noise is unknown, difficult to model, or not of the assumed constant-white-noise form. The equation for the filter-decay factor α_n then becomes

$$\alpha_n = \exp(-T/\tau_n)$$

where T is the filter sample time and τ_n is the filter time constant. The filter response to an input impulse is thus similar to the response of a resistor/capacitor combination to a step-voltage input.

Filter equations are derived for a system with time-invariant state-transition, measurement, measurement-noise-covariance, matrices and filter-decay factor. For the steady-state case, the filter is expressed as a z-transform transfer function in the form of a matrix between m inputs (measurements) and n outputs (states). As examples, closed-form analytic tracking-filter solutions are found for second- and third-order fading-memory filters used in a Global Positioning System receiver. In general, this class of fading-memory filters is computationally efficient, and the solutions are stable.

This work was done by J. I. Statman of Caltech for **NASA's Jet Propulsion Laboratory**. *To obtain a copy of the report, "Simplified Solution for a Class of Fading-Memory Filters," NPO-17089 /TN*

FOR ADDITIONAL INFORMATION: *Contact: Director, Technology Transfer Division, P.O. Box 8757, BWI Airport, MD 21240; (301) 621-0100 Ext. 241*

REFER TO THE NUMBER LISTED AT THE END OF THIS ARTICLE

NASA Tech Brief
National Aeronautics and Space Administration

Mechanical Properties of Large Sodium Iodide Crystals

For the first time, data on large thallium-doped samples are available.

A report presents data on mechanical properties of large crystals of thallium-doped sodium iodide [NaI(Tl)]. Previously, only data on small crystals were available. However, information was needed on large crystals so that a NaI(Tl) gamma-ray scintillator 20 in. in diameter and 0.5 in. thick (50.8 by 1.27 cm) could be built.

Accordingly, five specimens in the shape of circular flat plates were subjected to mechanical tests. The specimens, although not single-crystal, were composed of large multicrystals. A test fixture in a dry box applied a uniform pressure load across the surface of each specimen.

The report presents the test results for each specimen as plots of differential pressure versus center displacement and differential pressure versus stress at the center. It also tabulates the raw data.

The specimens were found to be plastic and to have a higher ultimate strength than expected. Although they were loaded to develop a stress of 500 lb/in.^{2} (3.5 MPa), only one specimen — an extremely hydrated one — failed. Specimens with many grain boundaries were less plastic, and therefore developed less permanent deformation, than those with fewer gain boundaries.

The test program also developed a procedure for screening candidate crystals for the gamma-ray sensor: specimens that acquire permanent deformations in excess of 0.0025 in. (0.064 mm) during the mechanical test are to be ranked as unacceptable. The procedure should eliminate potentially weak crystals before they are installed and should ensure that material yielding will be kept to a minimum.

This work was done by Henry M. Lee of **Marshall Space Flight Center**. *Further information may be found in NASA TM-86518 [N86-17187/NSP], "Mechanical Testing of Large Thallium Doped Sodium Iodide Single Crystals."*

Copies may be purchased [prepayment required] from the National Technical Information Service, Springfield, Virginia 22161, Telephone No. (703) 487-4650. [A04] MFS-28158 /TN

FOR ADDITIONAL INFORMATION: *Contact: Director, Technology Transfer Division, P.O. Box 8757, BWI Airport, MD 21240; (301) 621-0100 Ext. 241*
REFER TO THE NUMBER LISTED AT THE END OF THIS ARTICLE

NASA Tech Brief
National Aeronautics and Space Administration
Langley Research Center, Hampton, Virginia

Licensing Opportunity

Slow Release of Reagent Chemicals From Gel Matrices

A simple technique enables the slow diffusion of chemicals into solutions.

A procedure has been developed for the slow release of reagent chemicals into solutions. In a particular situation it was necessary to regulate the concentration of a reagent and to have it slowly released into the reaction solution over a period of days since too rapid an addition would have caused precipitation. The standard procedure for the slow, controlled addition of reagents involves expensive and sophisticated titration equipment, which requires operator attention and which may malfunction. The new procedure is simple and inexpensive and is not subject to failure of equipment.

A gel is prepared, and the desired amount of reagent is added to the gel while it is still fluid. Gelatin was used in this situation, but other gels are equally suitable; these include agar, carboxymethyl cellulose, and silica gel. While still fluid, the gel/reagent solution is poured into an ordinary plastic drinking straw that is sealed at one end. The gel is allowed to set and can keep for days or weeks.

For use, the gelled contents of the plastic straw are squeezed out into the reaction solution. The reagent slowly diffuses out of the gel matrix, which sits in the solution looking much like a transparent snake. The rate of diffusion can be regulated by control of the density of the gel; stiffer gels allow slower diffusion than do thinner gels. The use of a toothpaste-type tube or pump dispenser could conceivably provide a more controlled technique for the storage and dispensation of the gel matrix.

This simple and flexible procedure has many possible uses including controlled, slow release of the following:

1. Reagents in chemical reactions;
2. Reagents in crystal growth;
3. Reagents in space-flight experiments; e.g., on the Space Shuttle and Space Station, in which this technique may be especially important for the controlled addition of hazardous chemicals with minimum human attention; and
4. Preformed gel medications from packets, which may be sealed to prolong shelf life, for the dressing of wounds and burns, and for other medical treatments.

This work was done by William J. Debnam of **Langley Research Center** *and Patrick G. Barber and James Coleman of Longwood College. No further documentation is available.*

Inquiries concerning rights for the commercial use of this invention should be addressed to the Patent Counsel, Langley Research Center. Refer to LAR-13607/TN

Langley Research Ctr.
Technology Utilization Officer: John Samos
Mail Stop 139A
Hampton, VA 23665
(804) 865-3281
Patent Counsel:
George F. Helfrich
Mail Code 279
Hampton, VA 23665
(804) 865-3725

FOR ADDITIONAL INFORMATION: *Contact: Director, Technology Transfer Division, P.O. Box 8757, BWI Airport, MD 21240; (301) 621-0100 Ext. 241*
REFER TO THE NUMBER LISTED AT THE END OF THIS ARTICLE

02-02-0188

Preconcentrating Air Sampler--PAS-100

Enhancing analysis with a simple first step

The PAS-100 is a simple device for sampling and preconcentrating vapors of hazardous pollutants from a large volume of air into a small volume of liquid extractant for direct injection into an analytical instrument (e.g., liquid or gas chromatograph or mass spectrometer). It consists of an inner porous Teflon tubule containing the liquid extractant and an outer co-axial, impervious (polyethylene or glass) tube. The air is pumped between the co-axial tubes, and the vapors contained therein permeate the porous Teflon and are absorbed into the liquid extractant. This device should be interfaceable to automated analyzers and portable monitors. Alternatively, by use of specific indicator dye or other reagent, the sampler could serve as a self-contained monitor.

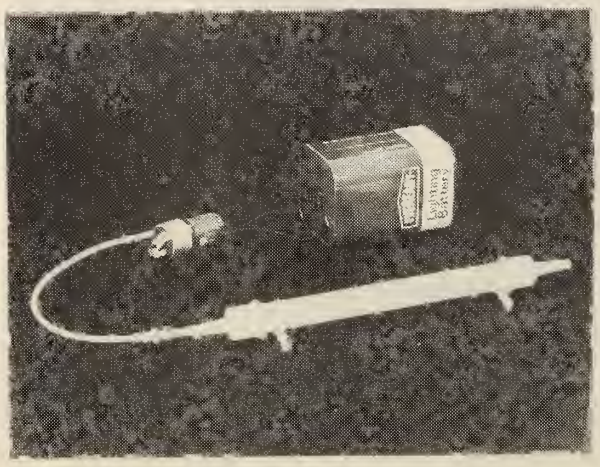

The PAS-100 is a fast preconcentrating air sampler that can be either interfaced to analytical instruments or, potentially, used with a detector kit or indicator dye.

The PAS-100 greatly enhances the detection of certain gaseous air contaminants. Sampling is faster, simpler, and neater--direct one-step absorption avoids time-consuming and somewhat involved desorption and sorbent-reconditioning steps or introduction of interfering contaminants from solvents and is not subject to problems of sorbent half-life or pollutant breakthrough. In addition, the PAS-100 should be adaptable to automated, repetitive sampling followed by direct injection into an analytical instrument. The device can be made highly selective to specific types of vapors by proper choice of liquid extractant (e.g., acidic or basic liquid for basic or acidic vapors), and can yield a high preconcentration ratio and hence a low detection level with a portable liquid or gas chromatograph.

Additional Information

Key Words: preconcentrator-sampler, permeation absorber, selective liquid extractant

Literature: S. Zaromb et al., A Simple Permeation Absorber for Sampling and Preconcentrating Hazardous Air Contaminants, J. Chromatography (in press). S. Zaromb and T. M. Beasley, Technique for Calibrating Air Samplers and Certain Other Analytical Devices, J. Chromatography (in press).

Patent Status: A patent application has been filed.

Potential Applications/Spinoffs: Neutral compounds eventually may be sampled by using appropriate extractants, possibly in conjunction with a fine cold finger that will enhance absorption of the neutral compounds. By use of an appropriate indicator dye or chemiluminescence reagent, the sample might serve as a self-contained visual or photometric monitor. These aplications are conceptually feasible, and will be possible when the proper liquid extractants and operating conditions are determined.

For More Information: Contact the Technology Transfer Center, 9700 S. Cass Ave., Argonne, IL 60439 (312/972-7694).

Oak Ridge National Laboratory

PORTABLE, SURFACE-ENHANCED RAMAN SPECTROSCOPY SYSTEM

Key words: Raman spectroscopy; surface-enhanced Raman scattering; He-Ne laser; monochrometer; light detection

Researchers in ORNL's Health and Safety Research Division have developed a portable, surface-enhanced Raman spectroscopy (SERS) system. Raman spectroscopy systems detect scattered monochromatic light from a sample surface through which a light beam has passed. Compounds on the surface can be identified by their characteristic Raman spectrum.

Most of these systems use expensive lasers as source beams so that sufficient scattered light will be produced. The SERS system provides a special sample-adsorption surface, a microbase, that enhances the scattered light signal. The microbase design uses the principle of stimulation of surface resonances on microparticulates by visible light. This unique microbase sufficiently increases the scattered light signal to permit the use of a portable, inexpensive helium-neon (He-Ne) laser source.

Because surface-enhanced Raman spectroscopy is a recent discovery (1978), it has not yet been used outside the research laboratory. This portable system is the first instrument of its kind designed for commercial applications. Its cost, including the laser, is one-eighth to one-tenth that of other currently available Raman spectroscopy systems.

The primary use of the SERS system is for identification. The microbase material, a thin aluminized Mylar sheet on which submicron-sized "microneedles" have been deposited, can be reliably mass produced (Fig. 1). This material can be used as a tag that the SERS system can identify. Tags only slightly larger than a period (approximately 0.1 mm) could be verified rapidly at checkpoints equipped with the SERS system. These tags can be laminated without significant signal loss (Fig. 2).

The SERS system can also be used to detect ultralow levels of chemicals. For example, it can be used for position-sensitive identification of protein components separated by gel

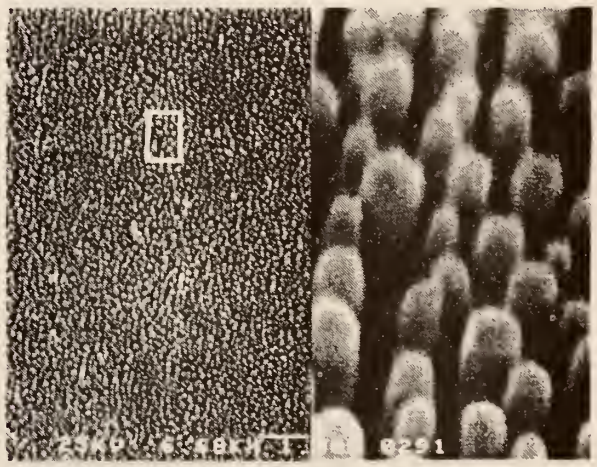

Fig. 1. Photomicrograph of the microbase material, a thin aluminized Mylar sheet on which submicron-sized "microneedles" have been deposited (not to scale).

Fig. 2. Prototype identification badge with two small SERS samples of the microbase material laminated onto its surface (one under the word "sample" and one in the radiation symbol). This material can be laminated without significant signal loss.

electrophoresis. Raman spectra of the four DNA bases can be obtained, and this possible application is currently being tested. This system can also detect trace amounts of other compounds, including contraband drugs, and could detect compounds of interest in forensics far more inexpensively than is now possible. It could also be incorporated into bar-code-reading cash registers for verification of name-brand commodities.

Additional information:

Office of Technology Applications
Information Service
Martin Marietta Energy Systems, Inc.
P.O. Box X
Oak Ridge, TN 37831
Telephone: (615) 574-4192; FTS 624-4192

J. P. Goudonnet et al., "Enhanced Raman Scattering from Benzoic Acid on Silver and Gold Prolate Spheroids on Large and Transparent Patterned Areas," *Chem. Phys.* **106**, 225-32 (1986).

CRYSTAL LASER MONITOR

Key words: Laser-beam monitor; ultraviolet; absorption

Ultraviolet laser beams, important for both industrial use and research, are invisible. The Crystal Laser Monitor is an improvement over conventional, disruptive methods of recording the size, shape, and divergence of these beams. It can make direct and inexpensive measurements of high-power ultraviolet or vacuum ultraviolet laser beams. Measurements could previously be made only indirectly or at the risk of damaging expensive equipment. The Crystal Laser Monitor has a greater dynamic range than conventional "laser footprint" photosensitive paper and can discriminate between ultraviolet and other wavelengths in a mixed beam.

The Crystal Laser Monitor is a polished halide crystal (KCl, NaCl, or CsBr), which is clear and colorless. This crystal undergoes a two-photon absorption when placed in the path of an ultraviolet laser beam, which causes color centers to form within it (Fig. 1). These color centers, visible to the unaided eye, indicate the size and shape of the beam. Color density indicates the relative intensity of regions within the beam. Because the color extends through the thickness of the crystal, it also has the unique ability to show an image of the beam's divergence. Stored properly, in a cool dark place, the crystal will retain its image indefinitely. Heat or light will erase the image; consequently, the same crystal can be used repeatedly. Because the beam passes through a clear crystal, it can be monitored intact while it is being used to perform a specific task.

Additional information:

Office of Technology Applications
Information Service
Martin Marietta Energy Systems, Inc.
P.O. Box X
Oak Ridge, TN 37831
Telephone: (615) 574-4192; FTS 624-4192

Fig. 1. This KCl(Tl) crystal contains a color center formed when an ultraviolet laser beam was passed through it.

M. P. McCann, C. H. Chen, and S. D. Kramer, "Ultraviolet Laser Beam Monitoring Using Alkali Halide Crystals," *Opt. Eng.* **25**(10), 1177-8 (October 1986).

C. H. Chen and M. P. McCann, "Luminescence of Alkali Crystals by Multiphoton Excitation," *Chem. Phys. Lett.* **126**, 54-57 (April 1986).

C. H. Chen, M. P. McCann, and J. C. Wang, "Room-Temperature Two-Photon Induced Luminescence in Pure CsI," *Solid State Commun.* **61**, 559-61 (1987).

C. H. Chen and M. P. McCann, "Threshold of F-Center Formation of Alkali Crystals by Two-Photon Absorption," *Opt. Commun.* **60**, 296 (1986).

NASA Tech Brief
National Aeronautics and Space Administration
NASA's Jet Propulsion Laboratory, Pasadena, California

Measuring Incorporation of Arsenic in Molecular-Beam Expitaxy

Changes in surface layers cause oscillations in RHEED measurements.

Reflection high-energy electron diffraction (RHEED) has been used to measure the rate of incorporation of arsenic into GaAs and InAs during growth by molecular-beam epitaxy. The measurement is sensitive only to the portion of arsenic incorporated into the growing film and not to the portion lost in splitting of the incident arsenic tetramers or by evaporation from the film. Because the measurements are independent of the characteristics of vacuum systems, pressure gauges, or flux monitors, they can be used to resolve ambiguities in the literature about absolute fluxes and flux ratios.

The measurement technique was demonstrated in a commercial molecular-beam-epitaxy system. The RHEED electron gun was operated at an energy of 8 keV and an emission current of 5 to 15 μA, aligned with the [110] axis of the growing GaAs or InAs sample. Most of the time, the samples were exposed to a flux of arsenic generated in a standard effusion cell by sublimation of As_4. The pressure of arsenic was measured by an ion gauge near the sample.

The basic measurements were made on buffer layers of GaAs that had been annealed at 600 to 620 °C and of InAs that had been annealed at 480 to 500 °C, both in the arsenic flux. Just before each measurement, the sample temperature was changed to the desired growth temperature and allowed to stabilize for 2 to 5 minutes. Typically, a burst of gallium or indium was deposited on the surface for 1.0 to 1.5 seconds at a rate of 5 to 7 monomolecular layers per second. The arsenic flux was maintained before, during, and after the deposition of metal.

The figure shows the RHEED intensities from GaAs samples at two temperatures. After the initial Ga transient, each oscillation represents the incorporation of about one monomolecular layer of arsenic into the sample from the steady arsenic flux. Once the inflowing arsenic has combined with the available deposited gallium, the oscillations stop, indicating the cessation of growth of GaAs and the return of the surface to the arsenic-stabilized condition.

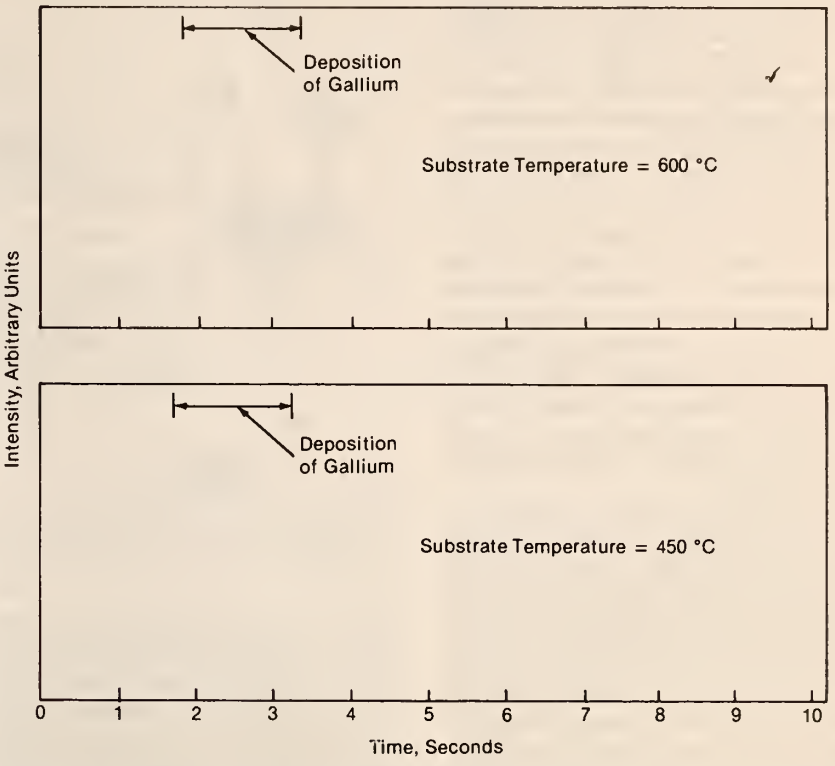

The **Specular RHEED Beam Intensity** was measured before, during, and after the deposition of seven to eight monomolecular layers of gallium during 1.5 seconds. The arsenic pressure was 1.7×10^{-7} torr (2.3×10^{-5} Pa) throughout the measurements.

The frequency of the arsenic-induced oscillations in the figure decreases with increasing temperature of the sample: this suggests that the rate of growth decreases with temperature, because of evaporation of arsenic from the sample. Except when the evaporation rate is high at high temperatures or low arsenic fluxes, the measured rate of incorporation of arsenic into GaAs follows the approximate equation

$$F = A P \exp(E/kT)$$

where F is the rate of incorporation in monomolecular layers per unit time, P is the pressure of the arsenic flux as measured by the ion gauge, A is a scale factor that depends on the particular equipment used, E is an empirical activation energy of 0.07 ± 0.02 eV, k is the ideal-gas constant, and T is the absolute temperature of the sample.

This work was done by Blair F. Lewis, Rouel F. Fernandez, Anupam Madhukar, and Frank J. Grunthaner of Caltech for **NASA's Jet Propulsion Laboratory**.
NPO-16821 /TN

FOR ADDITIONAL INFORMATION: *Contact: Director, Technology Transfer Division, P.O. Box 8757, BWI Airport, MD 21240; (301) 621-0100 Ext. 241*
REFER TO THE NUMBER LISTED AT THE END OF THIS ARTICLE

NASA Tech Brief
National Aeronautics and Space Administration
Marshall Space Flight Center, Alabama

Pressure-Sealing Optical Coupling

Light signals are passed out of a high-pressure cryogenic environment.

A design for a pressure-sealing coupling provides for the passage of optical signals between a laboratory environment and an environment filled with liquid oxygen at a pressure of 600 psi (4 MPa). In both environments, the signals are transmitted in two or more discrete light-conducting channels in fiber-optic cables. The coupling can be connected and disconnected quickly, is rugged, and resists vibration by providing a secure mount for the sensitive optical components that it contains. Designed as a feedthrough connector for a fiber-optic deflectometer in the high-pressure-oxygen turbopump of the Space Shuttle main engine, the coupling can be made in different configurations and modified to suit the requirements of other cryogenic instrumentation systems.

The coupling (see figure) maintains the alignment between an inner probe and an outer probe, both of which terminate their respective fiber-optic cables. The two probes face each other across an optical coupler, which is a rigid section of fused, coherent optical fibers. The coherent arrangement of fibers passes the discrete light channels undistorted through the coupler between the transmitting and receiving fiber ends on the facing ends of the two probes. The pressure-actuated seal around the periphery of the optical coupler constitutes the barrier to leakage between the two environments.

A nut serves as the mount for the outer probe. The outer probe is captured by a split ring at the inner end of the nut. Another split ring captures the inner probe. When the nut is threaded into the housing, the outer and inner probes are pressed against the optical coupler, spring-loaded against vibration by spring washers. The split rings enable the easy installation or removal of components and can be reached, if desired, through small access holes leading to the coupling.

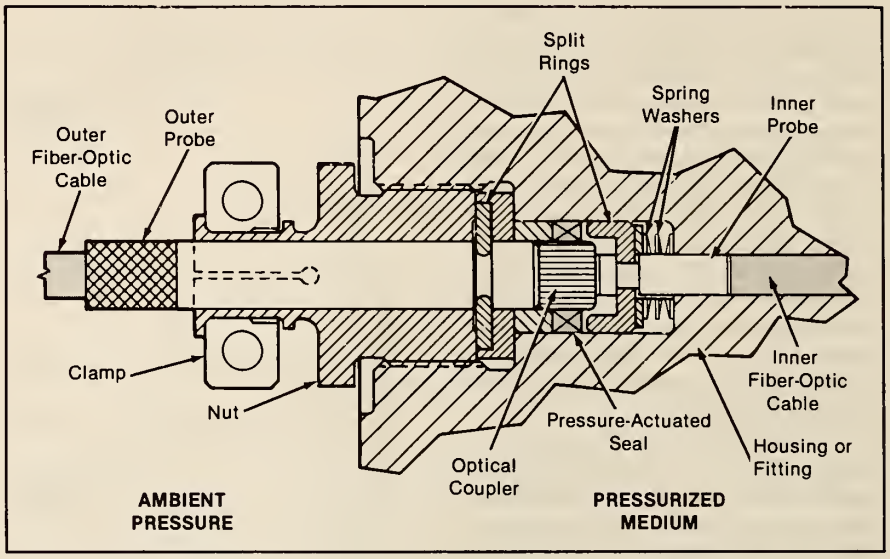

The **Optical Coupling** passes signals in fiber-optic channels across a pressure-and-temperature barrier.

The inner probe is kept from rotating by a key, slot, or half-circle shape (not shown). The outer probe is rotated in the nut until maximum signal output indicates that the optical channels in the two probes are aligned. A clamp is then tightened about the nut to fix the position of the outer probe.

This work was done by Timothy B. Irvin and Richard E. French of Rockwell International Corp. for **Marshall Space Flight Center**. *No further documentation is available.*

Inquiries concerning rights for the commercial use of this invention should be addressed to the Patent Counsel, Marshall Space Flight Center Refer to MFS-29348 /TN

FOR ADDITIONAL INFORMATION: *Contact: Director, Technology Transfer Division, P.O. Box 8757, BWI Airport, MD 21240; (301) 621-0100 Ext. 241*

REFER TO THE NUMBER LISTED AT THE END OF THIS ARTICLE

NASA Tech Brief
National Aeronautics and Space Administration
Lewis Research Center, Cleveland, Ohio

Licensing Opportunity

Optical Temperature Sensor for Gas Turbines

The new design promises accuracy even in the presence of contamination.

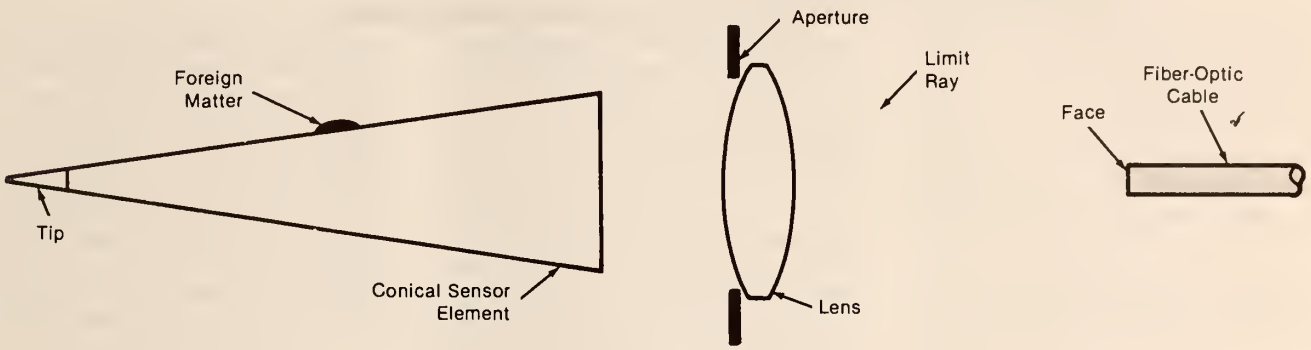

The **New Sensor** has a conical shape for mechanical strengths and an optical configuration that is insensitive to deposits of foreign matter on the sides of the cone.

An improved sensor is being developed to measure gas temperatures up to 1,700 °C in gas-turbine engines. The accurate measurement of gas temperatures within a gas-turbine engine is difficult because of the severe temperature, pressure, and vibration environment. The discharge gas of the turbine-engine combustor is particularly difficult to measure because the major constituents of the gas are hot, chemically active products of the combustion of a fossil fuel.

The sensing element of an existing optical thermometer (DILS, NBS) is a thin single crystal of sapphire, with a tip coated to form a blackbody cavity. When immersed in the gas stream, the sensing element eventually reaches the temperature of the stream and emits thermal radiation. The radiation is transmitted through a fiber-optic light pipe to a radiation detector.

In principle, this sensor will function reliably only if the thermal energy is transmitted to the detector without changes in intensity induced by the fiber-optic waveguide. It is known, however, that inside the gas-turbine engine, the combustor and turbine parts tend to accumulate a thin but optically absorbing deposit of various substances. In a modern engine, this deposit consists primarily of atmospheric dust that has been ingested by the engine and pyrolized. In engines of older designs, some carbon particles may also be present.

The existing sensing device, although having a blackbody cavity at the tip, has no protection against the formation of deposits on the uncoated portion, which is also exposed to the gas stream. It is expected that optically absorbing deposits will form on the exposed sensing element over an extended time. This will cause some of the light to be absorbed at the interface between the sapphire crystal and the deposit. Thus, the calibration will be shifted, and the displayed temperature will be in error. As an example of this effect, when a silicon diode detector of near-infrared radiation is used at a tip temperature of 1,000 °C, a drop in transmission of energy by 10 percent would result in an error of approximately 10 degrees.

Another deficiency of existing sensing elements is in the inherent weakness of a cylinder when loaded as a cantilever beam. This loading comes from the drag of the flowing gases acting on the cylinder to produce a bending moment that is greatest at the base of the cylinder.

The foregoing deficiencies should be overcome by a new sensor design. The new sensor element (see figure) is a cone of a solid, refractory, and optically transparent material; for example, single-crystal sapphire. The tip is coated with a durable and emissive material; for example, iridium. When the cone is heated by the combustion gas, radiant-energy rays are emitted. The limit (marginal) rays just pass by the aperture, are collected by the lens, and are brought to a focus at the face of the fiber-optic cable. Rays between the margins that originate at the tip also pass through the aperture and are focused onto the fiber-optic face. Rays that glance off the cone surface (where some of the ray energy is absorbed by foreign-matter deposits) continue on to be collected by the lens and focused away from the fiber-optic face.

It can be shown, then, that only the rays that are emitted from the tip and that do not intersect the cone will be collected and focused onto the fiber-optic face. All other rays — that is, all rays that intersect the cone surface — will not be focused onto the fiber-optic face. This design, therefore, makes the sensor respond only to the radiation emitted by the tip, and deposits of foreign matter on the sides of the cone have no effect on the measurement.

This work was done by P. W. Mossey of General Electric Co. for **Lewis Research Center**. *Further information may be found in NASA CR-175108 [N86-28729/NSP], "1700 °C Optical Temperature Sensor."*

Copies may be purchased from the National Technical Information Service, Springfield, Virginia 22161, [A08]

This invention is owned by NASA, and a patent application has been filed. Inquiries concerning nonexclusive or exclusive license for its commercial development should be addressed to the Patent Counsel, Lewis Research Center
Refer to LEW-14276. /TN

Lewis Research Center
21000 Brookpark Road
Cleveland, OH 44135
Technology Utilization Officer: Daniel G. Soltis
Mail Stop 7-3
(216) 433-5567
Patent Counsel: Gene E. Shook
Mail Code 301-6
(216) 433-5753

FOR ADDITIONAL INFORMATION: *Contact: Director, Technology Transfer Division, P.O. Box 8757, BWI Airport, MD 21240; (301) 621-0100 Ext. 241*
REFER TO THE NUMBER LISTED AT THE END OF THIS ARTICLE

NASA Tech Brief
National Aeronautics and Space Administration
NASA's Jet Propulsion Laboratory, Pasadena, California

Probing Polymer-Segment Motions by ESR

Molecular origins of mechanical properties and aging processes can be studied.

Electron-spin resonance (ESR) can now be used to study the motions of main-chain and side-chain segments of molecules in polymers. By enhancing the ability to determine the molecular origins of rotational and torsional relaxation modes, this extension of the ESR technique will contribute to our understanding of the degradation processes that take place as polymers age. The ESR indications of microscopic changes can be obtained long before the changes manifest themselves in changes of macroscopic physical properties.

The technique has been demonstrated in studies of poly(methyl methacrylate). For each measurement, tailored molecules of known molecular weight and size were either dispersed in the polymer to serve as spin probes or attached to the polymer to serve as spin labels. The molecular motions of the spin probes and labels were deduced from the changes in the widths and shapes of their ESR spectral lines as functions of temperature.

The motions of the main-chain and side-chain segments of the polymer were then deduced from the rotational motions of the probes and labels. From the temperature dependencies of the deduced motions, the activation energies of the motions of various molecular segments were also determined (see figure).

A correlation between the mobilities of molecular segments and the excess free volume in the polymer was found by studying the increases of the narrow components of the ESR spectra with increasing temperature. Because the sizes of the probes and labels were known, the size of the free volume was also determined as a function of temperature.

This work was done by Fun-Dow Tsay and Amitava Gupta of Caltech for **NASA's Jet Propulsion Laboratory**.

NPO-16970 /TN

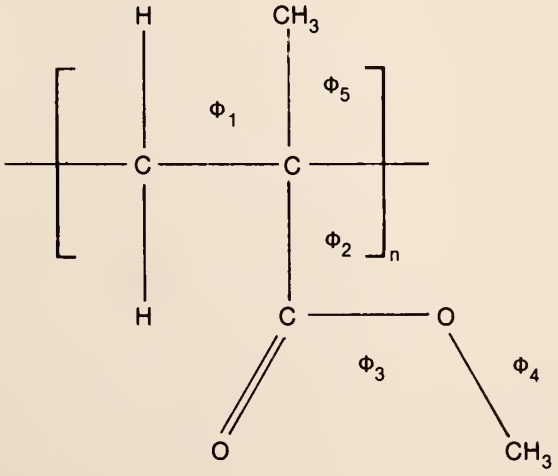

Rotation	Activation Energy, kcal/mole		
	Predicted by Theory	Measured by ESR Label	Measured by ESR Probe
Φ_1	6	6	7
Φ_2	4	5	4
Φ_3	20	18	19
Φ_4	1	1	1
Φ_5	3	2	2

Rotational Motions of Segments of poly(methyl methacrylate) molecules were studied theoretically and experimentally. The activation energies of these motions as determined from the temperature dependencies of ESR spectra agree closely with the predictions of theory.

FOR ADDITIONAL INFORMATION: *Contact: Director, Technology Transfer Division, P.O. Box 8757, BWI Airport, MD 21240; (301) 621-0100 Ext. 241*

REFER TO THE NUMBER LISTED AT THE END OF THIS ARTICLE

Transportation & Components

628 Landing-Time-Controlled Management of Air Traffic — A conceptual system would control aircraft with old and new guidance equipment. (Licensing Opportunity)

629 New Acoustic Treatment for Aircraft Sidewalls — Cabin noise is reduced with minimal addition of weight.

630 Study of Helicopter-Tail-Rotor Noise — Impulsive noise and blade loads in blade/vortex interactions are discussed.

631 Unducted-Fan Engine — Counterrotating propellers are directly connected to turbines. (Licensing Opportunity)

Software

632 Aerodynamic-Analysis Programs fr Microcomputers — Lifts, drags, and moments can be calculated for subsonic and supersonic speeds.

NASA Tech Brief
National Aeronautics and Space Administration

Licensing Opportunity

Landing-Time-Controlled Management of Air Traffic

A conceptual system would control aircraft with old and new guidance equipment.

A report describes a concept for air-traffic management that promises to increase efficiency at busy airports. The concept is based on controlling the landing time of all aircraft entering the terminal area — aircraft with only conventional guidance equipment as well as aircraft with advanced four-dimensional (space and time) guidance systems.

The report begins with an overview of the concept, then reviews controller-interactive simulations. It describes a fuel-conservative-trajectory algorithm, based on the equations of motion for controlling the landing time. Finally, it presents the results of piloted simulations.

The two major ground-based elements in the concept are (1) an electronic scheduler, which assigns conflict-free landing times to aircraft and (2) an electronic profile-descent advisor, which generates trajectory commands for aircraft without four-dimensional guidance. Assigned landing times are transmitted by data links to four-dimensional-equipped aircraft and are translated by the on-board flight-management system into trajectory commands. Meanwhile, a human controller relays descent advisories by voice link to unequipped aircraft.

Such a system would handle a range of aircraft, from high-performance jets to low-performance general-aviation airplanes. It would also give full authority to the human controller, who would monitor the time assignments of the scheduler on a graphics terminal and could override its decisions by using a small, but flexible, set of commands. For example, a controller could delay traffic feeding into the terminal area or increase the time separation between aircraft if there were landing delays at the airport. The controller could also overrule the built-in first-come, first-served rule to give landing priority to an aircraft that had missed an approach or was in an emergency.

The simulations of trajectories flown by pilots in a training apparatus have demonstrated that profile-descent advisories can control the descent time of unequipped aircraft. A landing-time accuracy of ±20 seconds, which a time-based system needs to be effective, appears attainable.

This work was done by Heinz Erzberger and Leonard Tobias of **Ames Research Center**. *Further information may be found in NASA TM-88243 [N86-28049/NSP], "A Time-Based Concept for Terminal-Area Traffic Management." [A02]*

Copies may be purchased [prepayment required] from the National Technical Information Service, Springfield, Virginia 22161, Telephone No. (703) 487-4650. Rush orders may be placed for an extra fee by calling (800) 336-4700.

Inquiries concerning rights for the commercial use of this invention should be addressed to the Patent Counsel, Ames Research Center
Refer to ARC-11713 /TN

Ames Research Ctr.
Technology Utilization Officer: Laurance Milov
Mail Code 223-3
Moffett Field, CA 94035
(415) 694-6471
Patent Counsel:
Darrell G Brekke
Mail Code 200-11
Moffett Field, CA 94035
(415) 694-5104

FOR ADDITIONAL INFORMATION: *Contact: Director, Technology Transfer Division, P.O. Box 8757, BWI Airport, MD 21240; (301) 621-0100 Ext. 241*
REFER TO THE NUMBER LISTED AT THE END OF THIS ARTICLE

NASA Tech Brief
National Aeronautics and Space Administration
Langley Research Center, Hampton, Virginia

New Acoustic Treatment for Aircraft Sidewalls

Cabin noise is reduced with minimal addition of weight.

There is a continuing need in the aircraft industry to control and reduce cabin noise and vibration. Conventional noise-reduction treatments are essentially additions of multilayered porous acoustic materials, impervious separating layers, and trim panels to the cabin walls. Additional noise reduction is usually achieved by increasing the weights of these layers. However, such increases in weight require more fuel and/or larger engines. The new aircraft-sidewall acoustic treatment reduces interior noise to acceptable levels and minimizes the addition of weight to an aircraft.

With the new technique, the transmission of noise through the aircraft sidewall is reduced by a stiffening device attached to the interior side of the aircraft skin, constrained-layer damping tape attached to the stiffening device, porous acoustic materials of high resistivity, and a relatively-soft trim panel isolated from the vibrations of the main fuselage structure.

The stiffening device is an aluminum honeycomb panel or an equivalent honeycomb panel made from other materials; the constrained-layer damping tape is effective at low temperatures; the resistivity factor of the porous acoustic material is significantly higher than that of present conventional acoustic/thermal materials used in the soundproofing of aircraft; and the trim panel is a relatively soft and impervious septum. To minimize the transmission of vibrations from the fuselage to the trim panel, soft isolators are installed when the trim panel is attached to the main frame of the fuselage. This treatment requires an increase in thickness of the exterior sheets of windows and increased stiffening of window supports.

The total increase of weight due to this acoustic treatment is approximately 2 percent of the gross takeoff weight of the aircraft. This increase is slightly lighter than that of standard acoustic/thermal treatment, and laboratory tests indicate that the new treatment will provide about 4 to 10 dB more of noise reduction than the standard treatment does. The average calculated overall noise levels of the untreated cabin will be reduced by about 17 dB with the new acoustic treatment.

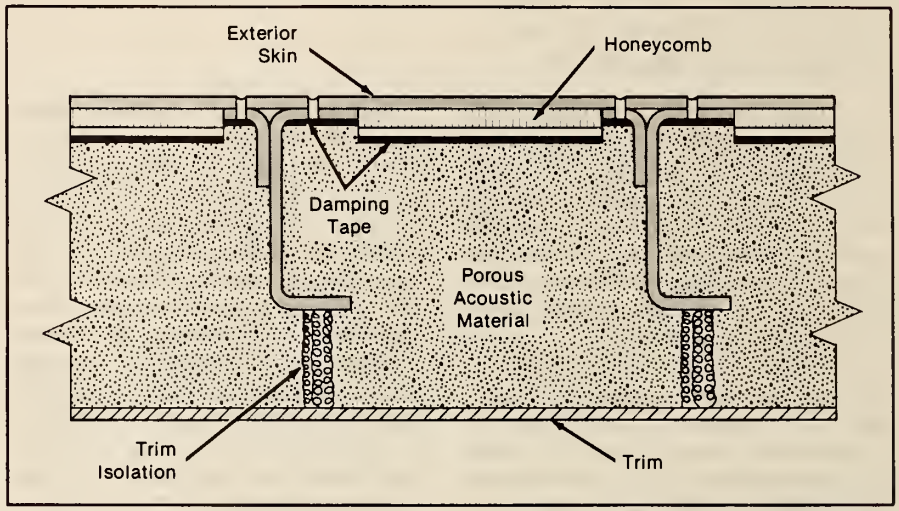

*A **Honeycomb Panel and a High-Resistivity Porous Material** are combined to decrease overall noise levels.*

This work was done by Rimas Vaicaitis of Columbia University for **Langley Research Center**. *Further information may be found in:*

NASA CR-172245 [N85-30771/NSP], "Design of Sidewall Treatments for Cabin Noise Control of a Twin Engine Turboprop Aircraft," and [A05]

NASA CR-17218 [N84-11884/NSP], "Study of Noise Transmission through Double Wall Aircraft Windows." [A05]

Copies may be purchased [prepayment required] from the National Technical Information Service, Springfield, Virginia 22161, Telephone No. (703) 487-4650. Rush orders may be placed for an extra fee by calling (800) 336-4700.

Further information may be found in AIAA Paper 84-2329 [A85-10873], "Noise Transmission through an Acoustically Treated and Honeycomb Stiffened Aircraft Sidewall."

Copies may be purchased [prepayment required] from AIAA Technical Information Service Library, 555 West 57th Street, New York, New York 10019, Telephone No. (212) 247-6500.

LAR-13545 /TN

FOR ADDITIONAL INFORMATION: *Contact: Director, Technology Transfer Division, P.O. Box 8757, BWI Airport, MD 21240; (301) 621-0100 Ext. 241*

REFER TO THE NUMBER LISTED AT THE END OF THIS ARTICLE

NASA Tech Brief
National Aeronautics and Space Administration

Study of Helicopter-Tail-Rotor Noise

Impulsive noise and blade loads in blade/vortex interactions are discussed.

A report describes the findings of an experiment in the generation of impulsive noise and fluctuating blade loads by a helicopter tail rotor interacting with the vortexes from the main rotor. The experiment used a model rotor and an isolated vortex and was designed to isolate the blade/vortex interaction (BVI) noise from other types of rotor noise.

It was found that BVI produces impulsive noise, which radiates primarily ahead of the blade. The interaction away from the blade tip demonstrated the dipole character of BVI radiation. Moreover, the direction of minimum noise radiation, previously found to be in the plane of the blade, was found to be shifted considerably downstream. The shift is believed to be due to unsteady drag radiation caused by the stronger BVI's in the present study.

For BVI close to the rotor tip, the three-dimensional relief effect reduced the intensity of the interaction, despite the larger BVI angle and higher local mach number. The radiation pattern was also more complex because of diffraction at, and pressure communication around, the tip.

Fluctuating blade pressures measured near the leading edge displayed impulsive features due to BVI. Away from the tip, the peak-to-peak amplitude of fluctuating pressure on the suction side of the blade was larger than that on the pressure side. However, this trend was reversed near the blade tip. Furthermore, the peak-to-peak amplitude of the fluctuating pressure on the pressure side near the tip was consistently the largest of all measured blade pressures for all conditions tested.

This work was done by Ali R. Ahmadi of Bolt Beranek and Newman Inc., for **Ames Research Center**. *Further information may be found in NASA CR-177338 [N85-23376/NSP], "An Experimental Investigation of the Chopping of Helicopter Main Rotor Tip Vortices by the Tail Rotor." [A06]*

Copies may be purchased [prepayment required] from the National Technical Information Service, Springfield, Virginia 22161, Telephone No. (703) 487-4650.

Inquiries concerning rights for the commercial use of this invention should be addressed to the Patent Counsel, Ames Research Center [see page 12]. Refer to ARC-11677. /TN

FOR ADDITIONAL INFORMATION: *Contact: Director, Technology Transfer Division, P.O. Box 8757, BWI Airport, MD 21240; (301) 621-0100 Ext. 241*

REFER TO THE NUMBER LISTED AT THE END OF THIS ARTICLE

NASA Tech Brief
National Aeronautics and Space Administration

Licensing Opportunity

Unducted-Fan Engine

Counterrotating propellers are directly connected to turbines.

Lewis Research Center, Cleveland, Ohio

The unducted-fan (UDF™) engine is an advanced counterrotating-pusher-propeller propulsion system for high-subsonic (mach 0.7 to 0.85) aircraft. The UDF combines a modern high-pressure-ratio gas-turbine engine with a multistage counterrotating power turbine that is directly coupled to counterrotating, advanced high-speed propellers called "unducted fans." A key feature of the system is the unique direct turbine drive that eliminates the need for a gearbox to transmit power to the propeller blades.

The two highly loaded, multiple-bladed, counterrotating propeller stages have swept, variable-pitch blades with thin, advanced airfoil sections for good high-speed performance. Counterrotation reduces propeller and turbine flow losses and, along with the large number of highly loaded blades, allows a relatively small propeller diameter.

First operated in August, 1985, this engine has achieved its design thrust of 25,000 lb (0.11 MN). Its measured specific fuel consumption (SFC) of 0.24 lb of fuel per hour per pound of thrust (6.8×10^{-6} kg/sN) is lower than the SFC of any previous turbofan-type engine. UDF-powered aircraft should consume 30 to 50 percent less fuel than do aircraft powered by conventional turbofan engines at comparable flight speeds.

This work was done by Edward T. Meleason of **Lewis Research Center** *and K. O. Johnson of General Electric Co. Further information may be found in AIAA Paper 85-3061, "Propulsion for Advanced Commercial Transports."*

Copies may be purchased [prepayment required] from AIAA Technical Information Service Library 555 West 57th Street New York, New York 10019, Telephone No. (212) 247-6500.

Inquiries concerning rights for the commercial use of this invention should be addressed to the Patent Counsel, Lewis Research Center.
Refer to LEW-14429/TN

Lewis Research Center
21000 Brookpark Road
Cleveland, OH 44135
Technology Utilization Officer: Daniel G. Soltis
Mail Stop 7-3
(216) 433-5567
Patent Counsel:
Gene E. Shook
Mail Code 301-6
(216) 433-5753

FOR ADDITIONAL INFORMATION: *Contact: Director, Technology Transfer Division, P.O. Box 8757, BWI Airport, MD. 21240; (301) 621-0100 Ext. 241*
REFER TO THE NUMBER LISTED AT THE END OF THE ARTICLE

Aerodynamic-Analysis Programs for Microcomputers

Lifts, drags, and moments can be calculated for subsonic and supersonic speeds.

A series of computer programs used for aerodynamic analysis at the NASA Langley Research Center has been modified for use on a microcomputer. The programs include an aerodynamic-analysis program for low-speed wing and flap systems (SUBAERF), a supersonic-wave-drag-analysis program (WDRAG2), and a supersonic-lifting-surface program (Lift Analysis). The programs are set up to run from a common geometry format with appropriate additional input data for each particular program.

SUBAERF provides estimates of the performances of wings, including the effects of attainable thrust and vortex lift, and analysis of simple leading- and trailing-edge flap systems. This low-speed wing/flap aerodynamic analysis is based on a lifting-surface solution from linearized theory.

WDRAG2 can be used to determine the wave drag of a configuration that may include a wing, a fuselage, and various combinations of nacelles, canards, horizontal tails, and vertical tails. The program uses the supersonic-area rule to determine the equivalent body-area distributions from which the wave drag is calculated. An optimization feature is included.

The Lift Analysis program determines distributions of lifting pressures, drag due to lift, pitching moment, and trimmed drag of a fuselage and wings with canard and/or horizontal tail configurations. The program employs modified methods of linearized theory to calculate lifting-surface pressures, both far-field and near-field methods to calculate forces due to configuration volume, and turbulent-flat-plate theory to calculate skin friction.

This package is written in FORTRAN 77 for interactive execution and has been implemented on the IBM PC series of computers operating under DOS with a central-memory requirement of approximately 256K of 8-bit bytes. The Lift Analysis program requires a hard disk. The SUBAERF and Lift Analysis programs require a math coprocessor and the commercial Lahey F77L compiler and Phoenix PLINK linker. (A Microsoft compiler and linker are not sufficient.) The package includes source, object, executable (except for Lift Analysis), and sample input/output files for each program. This collection of microcomputer programs was made available in 1986. The mainframe versions of these programs are available separately from COSMIC.

This program was written by Marie L. Knapp of PRC Kentron, Inc., for **Langley Research Center**. *LAR-13666 /TN*

FOR ADDITIONAL INFORMATION *CONTACT:*

COSMIC®
112 Barrow Hall
University of Georgia
Athens, GA 30602
(404) 542-3265

NTIS Order Form

NTIS Telephone Numbers

To Order Reports
(703) 487-4650

For Subscription Questions
(703) 487-4630

Other Information
(703) 487-4600

Editorial Questions
(703) 487-4805

Postage:
NTIS uses First Class Delivery, or equivalent service, on all shipping. For information about one day RUSH ordering, call (703) 487-4600.

NTIS PRICE CODE SCHEDULE *

This schedule gives the current values to the price codes cited in those Tech Notes having a backup report available from NTIS.

Microfiche	
A01	$6.95
Paper copy	
A02	9.95
A03	12.50
A04 through A05	14.95
A06 through A09	19.95
A10 through A13	25.95
A14 through A17	32.95
A18 through A21	38.95
A22 through A25	44.95
A99	Call for price

Customers in Canada, United States, and Mexico use this schedule. Other addresses should write for the price listing, number PR-360-4.

Prices effective January 1, 1988

Use this form ONLY to order reports designated as available from NTIS

MAIL ORDER TO: National Technical Information Service
U.S. DEPARTMENT OF COMMERCE
5265 Port Royal Road
Springfield, VA 22161

Send me the reports I have selected on this form. I have placed order numbers in appropriate blanks and have indicated the quantity. IF ADDRESS LABEL

Last Name: .....

Title: .....

Company/Organization: .....

Address: .....

.....

City/State/Zip: .....

Telephone Number: .....

METHOD OF PAYMENT

☐ Check enclosed payable to NTIS for $ .....

☐ Charge to my NTIS Deposit Account, No: ....-.....

☐ Purchase order number: .....

Charge to: ☐ American Express ☐ VISA ☐ MasterCard

Card Number: .....

Expation date: .....

Signature: .....
(Required to validate order)

NTIS ORDER NUMBER (Use only for backup reports stated as available from NTIS)

NTIS Order Number	*Price**	*Quantity*	*Total Price*
.....	.....	.....	.....
.....	.....	.....	.....
.....	.....	.....	.....
.....	.....	.....	.....
.....	.....	.....	.....
	Shipping and handling fee		$3.00 .....
	Total		.....

NTIS Order Form

NTIS Telephone Numbers

To Order Reports
(703) 487-4650

For Subscription Questions
(703) 487-4630

Other Information
(703) 487-4600

Editorial Questions
(703) 487-4805

Postage:
NTIS uses First Class Delivery, or equivalent service, on all shipping. For information about one day RUSH ordering, call (703) 487-4600.

NTIS PRICE CODE SCHEDULE *

This schedule gives the current values to the price codes cited in those Tech Notes having a backup report available from NTIS.

Microfiche	
A01	$6.95
Paper copy	
A02	9.95
A03	12.50
A04 through A05	14.95
A06 through A09	19.95
A10 through A13	25.95
A14 through A17	32.95
A18 through A21	38.95
A22 through A25	44.95
A99	Call for price

Customers in Canada, United States, and Mexico use this schedule. Other addresses should write for the price listing, number PR-360-4.

Prices effective January 1, 1988

Use this form ONLY to order reports designated as available from NTIS

MAIL ORDER TO: National Technical Information Service
U.S. DEPARTMENT OF COMMERCE
5265 Port Royal Road
Springfield, VA 22161

Send me the reports I have selected on this form. I have placed order numbers in appropriate blanks and have indicated the quantity. IF ADDRESS LABEL

Last Name: .....

Title: .....

Company/Organization: .....

Address: .....

.....

City/State/Zip: .....

Telephone Number: .....

METHOD OF PAYMENT

☐ Check enclosed payable to NTIS for $ .....

☐ Charge to my NTIS Deposit Account, No: ....-.....

☐ Purchase order number: .....

Charge to: ☐ American Express ☐ VISA ☐ MasterCard

Card Number: .....

Expation date: .....

Signature: .....
(Required to validate order)

NTIS ORDER NUMBER (Use only for backup reports stated as available from NTIS)

NTIS Order Number	*Price**	*Quantity*	*Total Price*
.....	.....	.....	.....
.....	.....	.....	.....
.....	.....	.....	.....
.....	.....	.....	.....
.....	.....	.....	.....

Shipping and handling fee $3.00 .....

Total .....

NTIS Order Form

NTIS Telephone Numbers

To Order Reports
(703) 487-4650

For Subscription Questions
(703) 487-4630

Other Information
(703) 487-4600

Editorial Questions
(703) 487-4805

Postage:
NTIS uses First Class Delivery, or equivalent service, on all shipping. For information about one day RUSH ordering, call (703) 487-4600.

NTIS PRICE CODE SCHEDULE *

This schedule gives the current values to the price codes cited in those Tech Notes having a backup report available from NTIS.

Microfiche	
A01	$6.95
Paper copy	
A02	9.95
A03	12.50
A04 through A05	14.95
A06 through A09	19.95
A10 through A13	25.95
A14 through A17	32.95
A18 through A21	38.95
A22 through A25	44.95
A99	Call for price

Customers in Canada, United States, and Mexico use this schedule. Other addresses should write for the price listing, number PR-360-4.

Prices effective January 1, 1988

Use this form ONLY to order reports designated as available from NTIS

MAIL ORDER TO: National Technical Information Service
U.S. DEPARTMENT OF COMMERCE
5265 Port Royal Road
Springfield, VA 22161

Send me the reports I have selected on this form. I have placed order numbers in appropriate blanks and have indicated the quantity. IF ADDRESS LABEL

Last Name: .....

Title: .....

Company/Organization: .....

Address: .....

.....

City/State/Zip: .....

Telephone Number: .....

METHOD OF PAYMENT

☐ Check enclosed payable to NTIS for $ .....

☐ Charge to my NTIS Deposit Account, No: ....

☐ Purchase order number: .....

Charge to: ☐ American Express ☐ VISA ☐ MasterCard

Card Number: .....

Expation date: .....

Signature: .....
(Required to validate order)

NTIS ORDER NUMBER (Use only for backup reports stated as available from NTIS)

NTIS Order Number	*Price**	*Quantity*	*Total Price*
.....	.....	.....	.....
.....	.....	.....	.....
.....	.....	.....	.....
.....	.....	.....	.....
.....	.....	.....	.....

Shipping and handling fee $3.00 .....

Total .....

- Agriculture & Food
- Computers
- Electrotechnology
- Energy
- Engineering
- Environmental Science & Technology
- Manufacturing, Machinery, & Tools
- Materials
- Medicine & Biology
- Natural Resources Technology & Engineering
- Physical Sciences
- Transportation & Components

Route To:

PENN STATE UNIVERSITY LIBRARIES
A0000720099B7

PARTMENT OF COMMERCE
l Technical Information Service
d, Va. 22161

BUSINESS
r Private Use, $300

UNITED STATES · DEPARTMENT OF COMMERCE ·

Stimulating America's Progress
1913-1988

AN EQUAL OPPORTUNITY EMPLOYER

BULK RATE
POSTAGE & FEES PAID
NTIS
Permit No. G-292